

STYRELSEN FÖR
VINTERSJÖFARTSFORSKNING

WINTER NAVIGATION RESEARCH BOARD

Research Report No 42

J. Koskikivi & P. Kujala

LONG-TERM MEASUREMENTS OF ICE INDUCED LOADS ON THE
PROPULSION MACHINERY OF PRODUCT TANKER SOTKA

Sjöfartsstyrelsen
Finland

Finnish Board of Navigation

Sjöfartsverket
Sverige

Swedish Administration
of Shipping and Navigation

J. Koskikivi & P. Kujala

LONG-TERM MEASUREMENTS OF ICE INDUCED LOADS ON THE
PROPULSION MACHINERY OF PRODUCT TANKER SOTKA

TECHNICAL RESEARCH CENTRE OF FINLAND (VTT)
Ship Laboratory

Espoo, October 1985

THE UNIVERSITY OF CHICAGO

1961

UNIVERSITY OF CHICAGO

CONTENTS

	page
1 INTRODUCTION	1
2 SHIP PARTICULARS	2
2.1 Main characteristics	2
2.2 Propulsion machinery	3
2.3 Dynamic properties of the propulsion machinery	5
3 MEASURING SYSTEM	11
3.1 Measuring pick-ups	11
3.2 Recording devices	16
4 MEASUREMENTS	18
4.1 Long-term measurements	18
4.2 Short-term measurements	19
5 RESULTS OF THE MEASUREMENTS	22
5.1 Results of the short-term measurements	22
5.1.1 Analysis of the results	22
5.1.2 Discussion of the results	44
5.2 Results of the long-term measurements	46
5.2.1 Analysis of the results	46
5.2.2 Discussion of the results	51
5.3 Extrapolation of extreme values	57
6 CONCLUSIONS	69
7 ACKNOWLEDGEMENT	70
REFERENCES	71
APPENDICES	

1 INTRODUCTION

The present knowledge about the ice loads of propulsion machinery and the phenomena connected with propeller-ice interaction is rather incomplete. In the dimensioning of propulsion machinery ice loads are usually approximated only roughly and the uncertainty in calculations is compensated by using high values for safety factors. To improve the dimensioning methods more accurate knowledge about ice loads is needed.

The ice loads of a propulsion machinery have a clear statistical nature. Due to varying ice conditions and influence of several parameters, such as ship speed, propeller pitch and power, variations in ice loads are quite extensive. The magnitudes and distributions of ice load peaks can best be studied through long-term measurements. Short-term measurements are conducted to study the basic phenomena associated with the ice loads.

An automatic data gathering system was installed on board the icebreaking product tanker Sotka in autumn 1982 by VTT Ship laboratory to achieve long-term data of the behaviour of the propulsion machinery when navigating in ice. The measuring system and the results of the long-term measurements carried out on Sotka during winters 1983 and 1984 are described in this report together with the results of the short term measurements conducted in March 1983.

Firstly in this report main characteristics of the studied ship and propulsion machinery are presented. Then the measuring system and results of the short and long-term measurements are described. Finally the long-term results are analysed applying some statistical methods and long-term estimates for the measured quantities are evaluated.

2 SHIP PARTICULARS

2.1 Main characteristics

The measurements were carried out on an ice-breaking product tanker Sotka (Fig. 1) owned by the Finnish oil company Neste Oy. Sotka is the second ship in the series of four tankers known as the Lunni-class. She operates mainly along the Finnish coast distributing oil products from refineries to stores in coastal ports. The main characteristics of the ship are listed in Table 1.

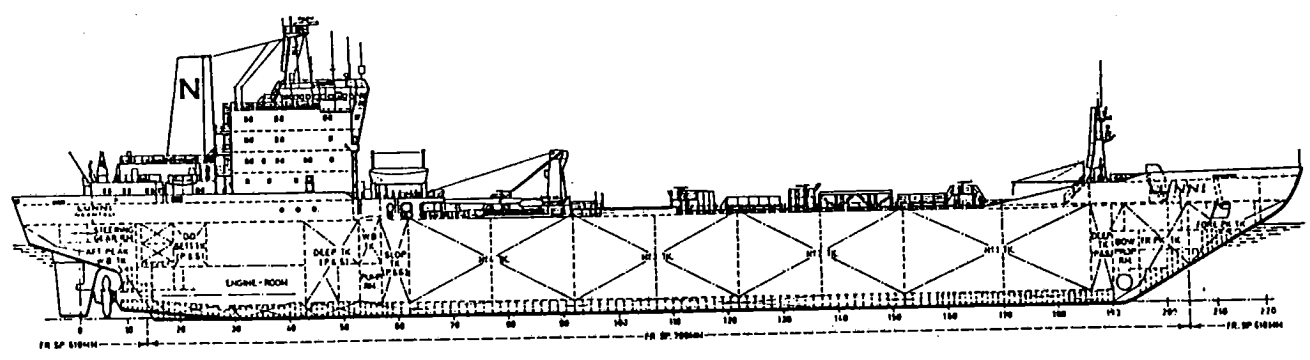


Fig. 1. Lunni-class product tanker.

The Lunni-class tankers have been specially designed for operating without icebreaker assistance in normal ice conditions throughout the Baltic. These ice-breaking requirements have above all had an effect on the hull form and strength, and on design of the propulsion system. The Finnish-Swedish ice class of the Lunni-class ships is 1 A Super.

Table 1. Main characteristics /2/.

Length, o.a.	164.45 m
Length, b.p.	150.00 m
Breadth moulded (wl)	21.50 m
Breadth moulded (main deck)	22.20 m
Depth moulded	12.00 m
Draft, summer	9.50 m
Deadweight	15 995 tonnes
Gross Register	10 975 tons
Net Register	5 951 tons
Propulsion	2xMaK 12M551AK
Output	2 x 5740 kW at 425 rev/min
Speed	14.5 knots

2.2 Propulsion machinery

The propulsion machinery of the Sotka consists of two main engines, which drive one controllable pitch propeller through a reduction gear. In ice-free and in light ice conditions only one engine is required, but in heavier ice conditions, when more power is required both engines are driven simultaneously. The main components of the propulsion machinery can be seen in Fig. 2.

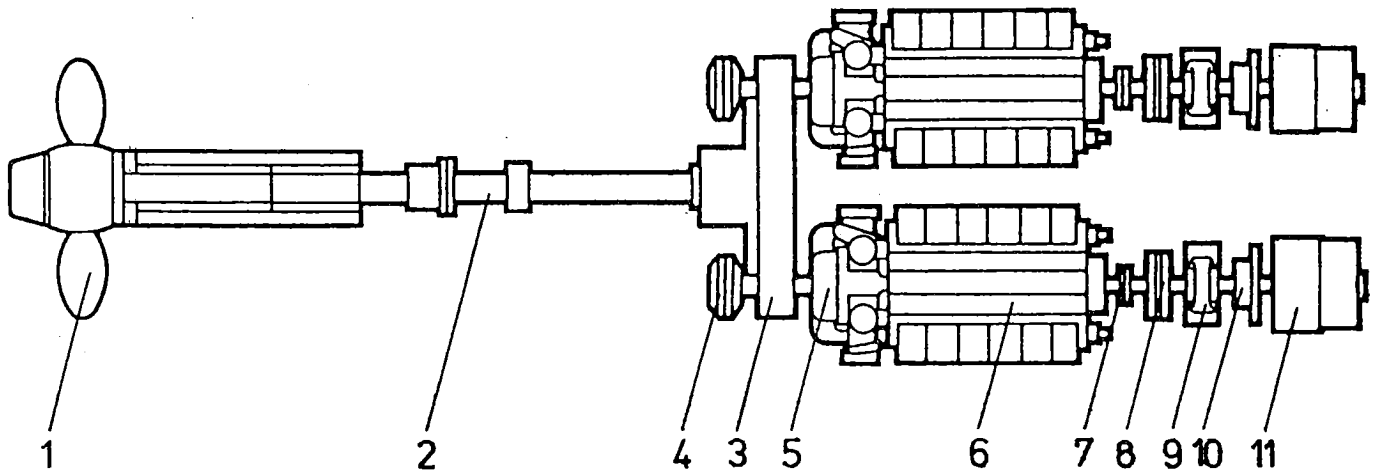


Fig. 2. Propulsion machinery /1/.

1. Ice-strengthened CP-propeller, KaMeWa: 4 blades, diameter $D_p = 5450$ mm, design pitch ratio $P/D = 1.077$, nominal rotational speed $n = 120$ r/min
2. Propeller shaft, KaMeWa: outside diameter varies between 616 - 500 mm, inside diameter 180 mm.
3. Reduction gear, Lohmann & Stolterfoht Navilus GVQ 2050: reduction ratio $i = 3.5102:1$.
4. Clutch coupling, Pneumaster KUG 370.
5. Flexible coupling, Geislinger BC 90/20/13.
6. Main engine, MaK 12 M 55 1 AK: 12-cylinders, four-stroke V-engine, power $P = 5740$ kW, nominal speed $n = 425$ r/min
7. Flexible coupling, Geislinger BE 72/15/13.
8. Clutch coupling, Airflex 38 VC 1200.
9. Step-up drive gear, Lohmann & Stolterfoht Motilus GAA 560. Transmission ratio 1:2.344
10. Flexible coupling, Lohmann & Stolterfoht Spiroflex KJR 220 M.
11. Shaft alternator, AEG PKL 712/06 (3500 kVA, 6 kV, 50 Hz): nominal speed $n = 1000$ r/min. (Only one of the shaft alternators is used at a time).

2.3 Dynamic properties of the propulsion machinery

The study is concentrated on torsional vibrations because they have caused major dynamical difficulties in our previous investigations. The dynamical properties of the shafting of the Lunni type tanker were studied in two stages. The first stage was an undamped free vibration analysis where the lowest natural frequencies and corresponding vibration modes were solved. The second one was a forced vibration analysis where the total damping and the transient propeller excitation were taken into the consideration. The needed inertia and stiffness values for the lumped mass model were obtained from the document of torsional vibration calculations, delivered by the engine manufacturer (MaK). Natural frequencies and corresponding mode vectors are presented in Table 2 and in figures 3 and 4.

Table 2. Natural frequencies

Mode number	Natural frequencies (Hz)			
	one engine		two engines	
1	2.56	(2.61)	2.49	(2.49)
2	6.15	(6.25)	5.51	(5.62)
3	8.89	(9.55)	6.21	(6.32)
4	11.20	(11.64)	9.68	(9.95)
5	52.35	(52.69)	11.23	(11.31)
6			16.46	(16.47)
7			52.34	

Natural frequencies and modes are calculated for the system where the stiffnesses of the couplings are supposed to be constant. In reality they are related to the vibration frequency. When this effect on the stiffness of the main flexible couplings is included in the calculations, the natural frequencies of the lowest modes will be somewhat higher as shown by the numbers in parenthesis in Table 2.

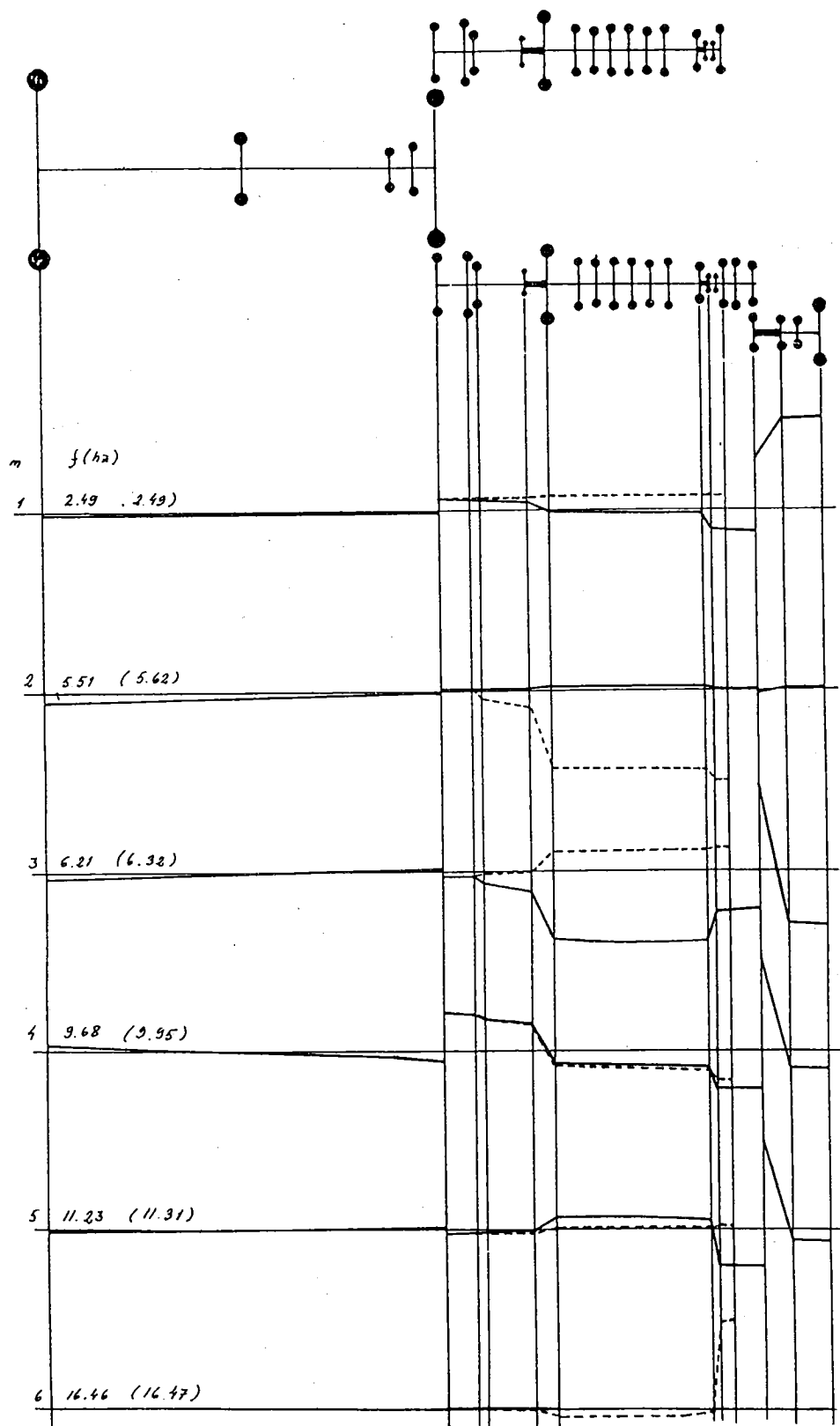


Fig. 3. Lumped mass model of propulsion shafting for twin engine running mode and the shapes of the lowest vibration modes.

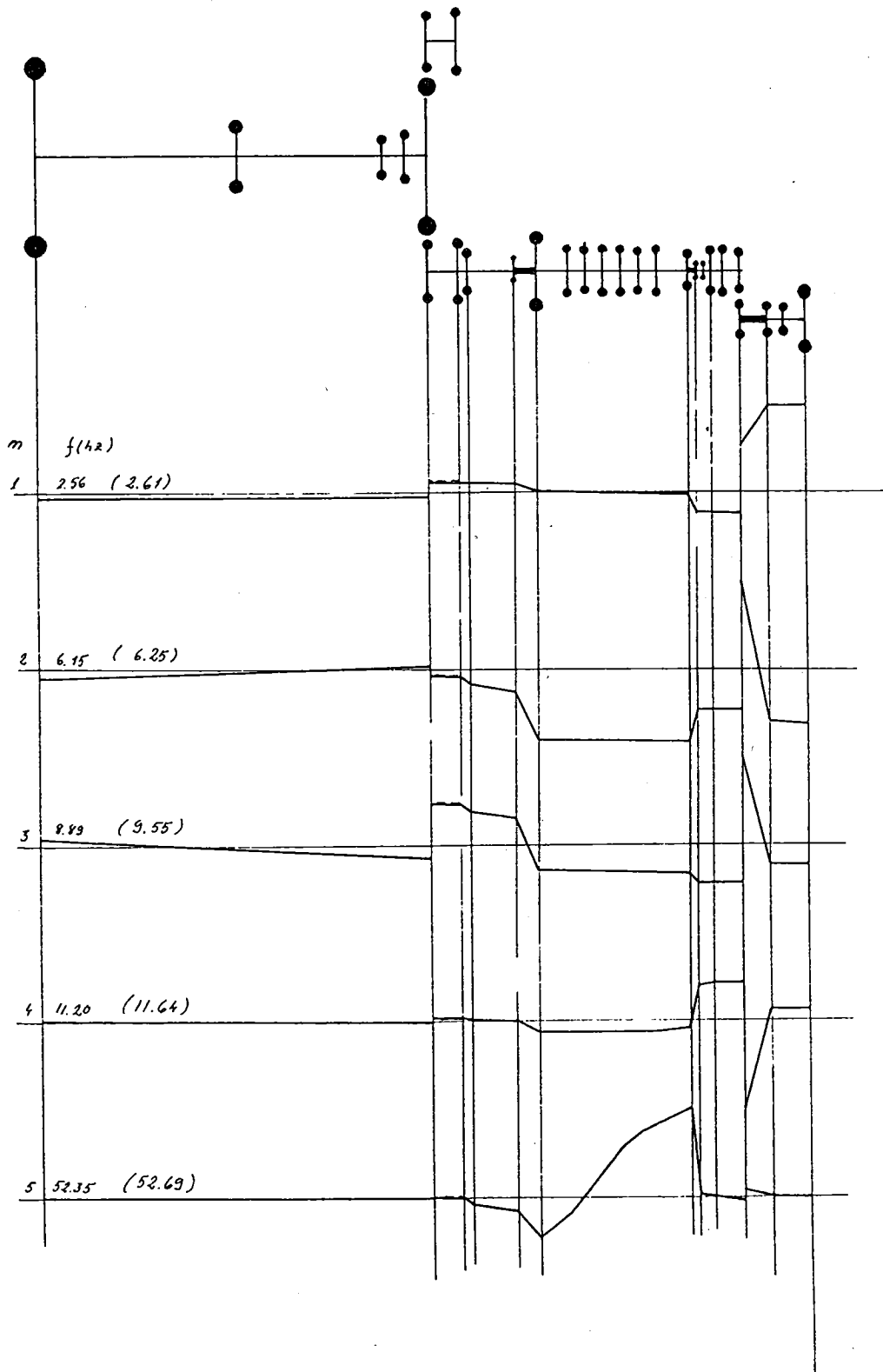


Fig. 4. Lumped mass model of propulsion shafting for single engine running mode and the shapes of the lowest vibration modes.

Natural frequencies and the shape of the corresponding modes will give information about possible vibration resonances and the effectiveness of the excitation. In this case the frequencies of the main excitations are

- propeller shaft speed	2 Hz	(121 1/min)
- blade frequency	8.1 Hz	(4x121 1/min)
- engine speed	7.1 Hz	(425 1/min)
- first order of engine excitation	3.5 Hz	($\frac{1}{2}$ x425 1/min)
- first main order of engine excitation	21.3 Hz	(3x425 1/min)
- shaft generator speed	16.7 Hz	(1000 1/min)

The most significant excitation source in ice conditions is the propeller. Although the engine speed and the blade frequency are rather close, it does not normally cause major difficulties because the level of engine excitation is low comparing to transient propeller excitation due to the ice.

It can be seen from the mode shapes (figures 3 and 4) that the torsional amplitude of the propeller is significant in the modes with natural frequencies under 11 Hz. This means that resonances with these frequencies will cause considerable vibratory loads at the point of the propeller shaft, where the torque measuring devices are installed. Furthermore it can be concluded from the previous results that the propeller ice loads will excite modes 3 and 4 ($f=6.32$ Hz and 9.95 Hz) with twin engine run and modes 2 and 3 ($f=6.25$ Hz and 9.55 Hz) with one engine run.

In order to get information from the responses of the measuring point, the transient forced vibration calculations were made for both twin engine and single engine engaged. The used idealized ice load excitations with two different frequencies correspond a short milling situation. The results of these calculations are given in Fig. 5.

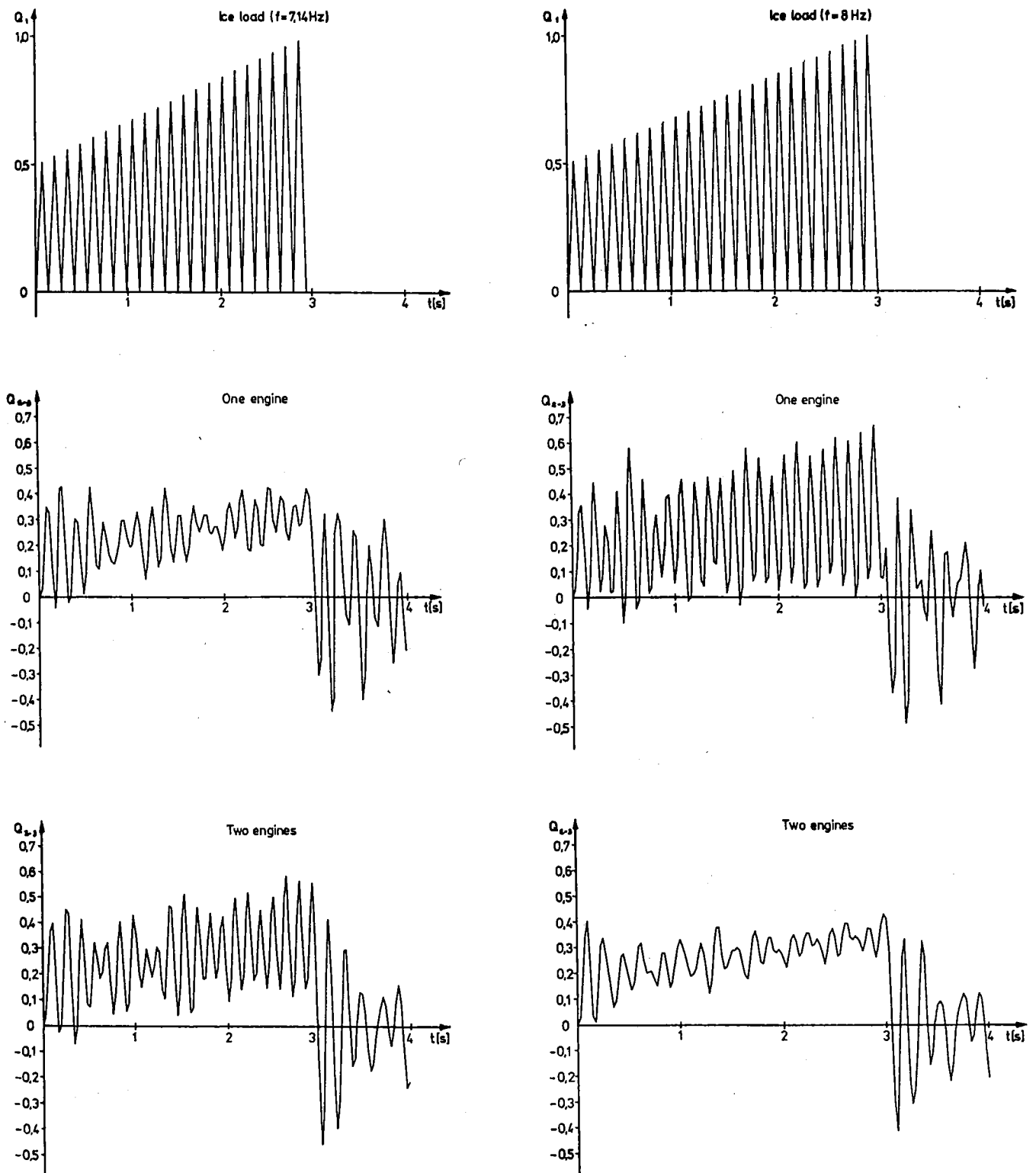


Fig. 5. Idealized excitation force and corresponding response at the propeller shaft with single engine and twin engine running mode.

The form of response signal is greatly influenced by the relation between the natural and excitation frequencies. As a conclusion from the calculated results it can be noted that the torque amplitude is mainly the sum of the neighbouring vibration modes. The dominating mode is certainly the nearest one. For example the excitation frequency ($f=8$ Hz) is almost the arithmetic mean of the natural frequencies of third and fourth modes ($f=6.21$ Hz and 9.68 Hz) when two engines are running together. The response in this case differs much from the case where only one engine is running, because in the latter case the excitation frequency is rather near the third natural frequency ($f=8.89$ Hz).

In practice durations of ice load sequences are normally rather short and greatly influenced by ice conditions and the size of the ship. This means that ice floes can induce free vibration responses which differ from the blade frequency. Another reason for this kind of deviation can be the orientation of the incoming ice floes and the entraining of smaller floes with propeller.

It has to be noted here that the lowest and thus the most significant natural frequencies are strongly influenced by the stiffness of flexible couplings, which is, in several cases, rather poorly known and can even be changed with time. On this ground the actual frequencies can differ considerably from calculated ones.

On the basis of calculations it can be said that dynamical properties of the shafting have a great influence on the measured results. If there are not any natural frequencies in the close vicinity of the blade frequency, the inertia of the propeller can reduce considerably the amplitude of the measured torque fluctuation. If on the contrary the shafting is near the resonance condition with the excitation the measured torque can be considerably magnified.

3 MEASURING SYSTEM

3.1 Measuring pick-ups

A block diagram of the measuring system is presented in Fig. 6.

The measurements included the following pick-ups.

- propeller thrust (T) and torque (Q)
- propeller shaft speed
- power on the propeller shaft
- propeller pitch
- ship speed
- rudder angle and torque (RQ)

Thrust and torque were measured with strain gauges attached on the propeller shaft and on the shaft between flexible coupling and reduction gear. Their location can be seen in Fig. 7. Strain gauges Q3 and Q4 were used only in short term measurements. The strain gauges received their power through a wireless power supply system (Q3 and Q4 from a voltage battery) and the signals were transmitted from the rotating shaft with telemetric devices.

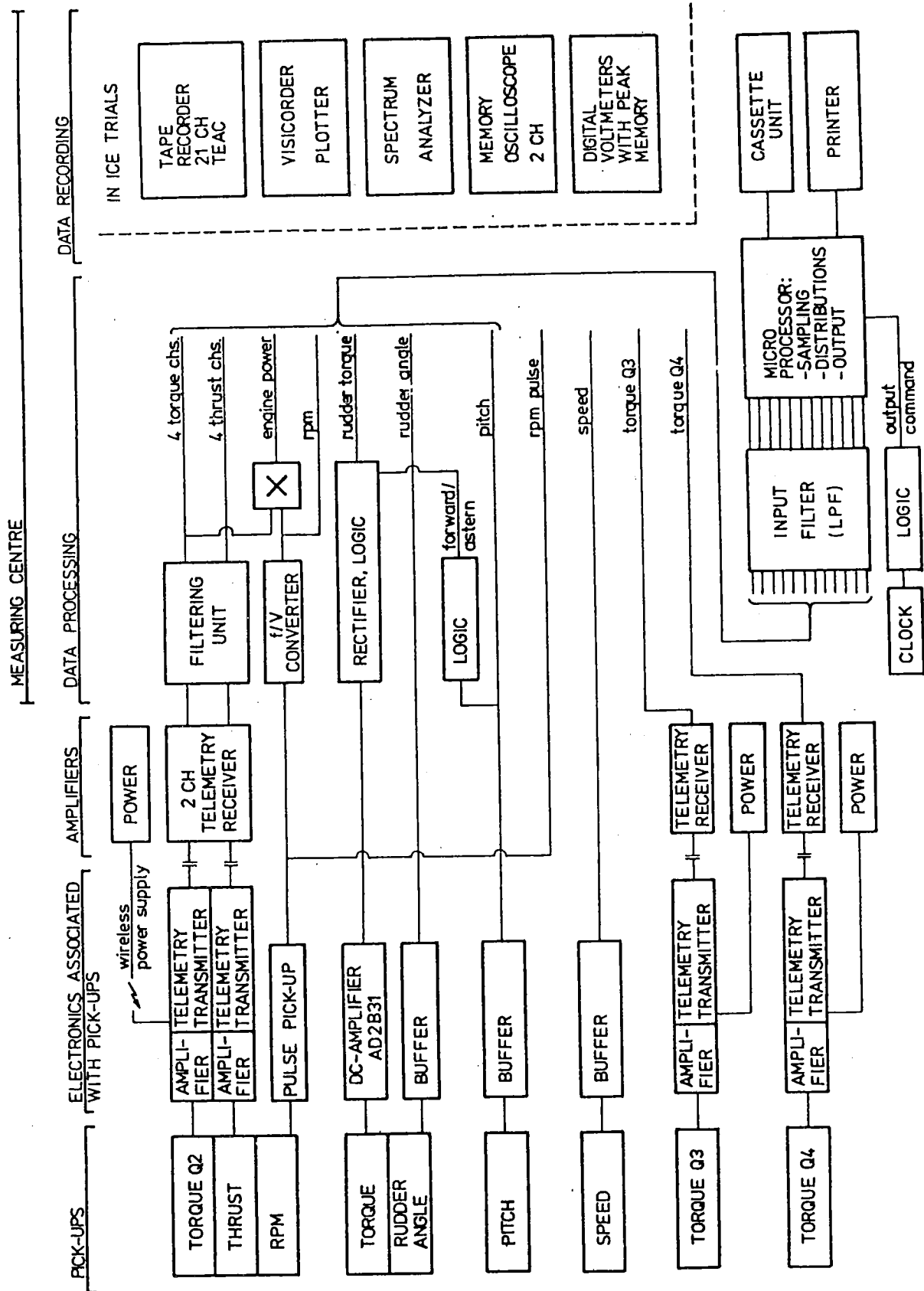


Fig. 6. Measuring system.

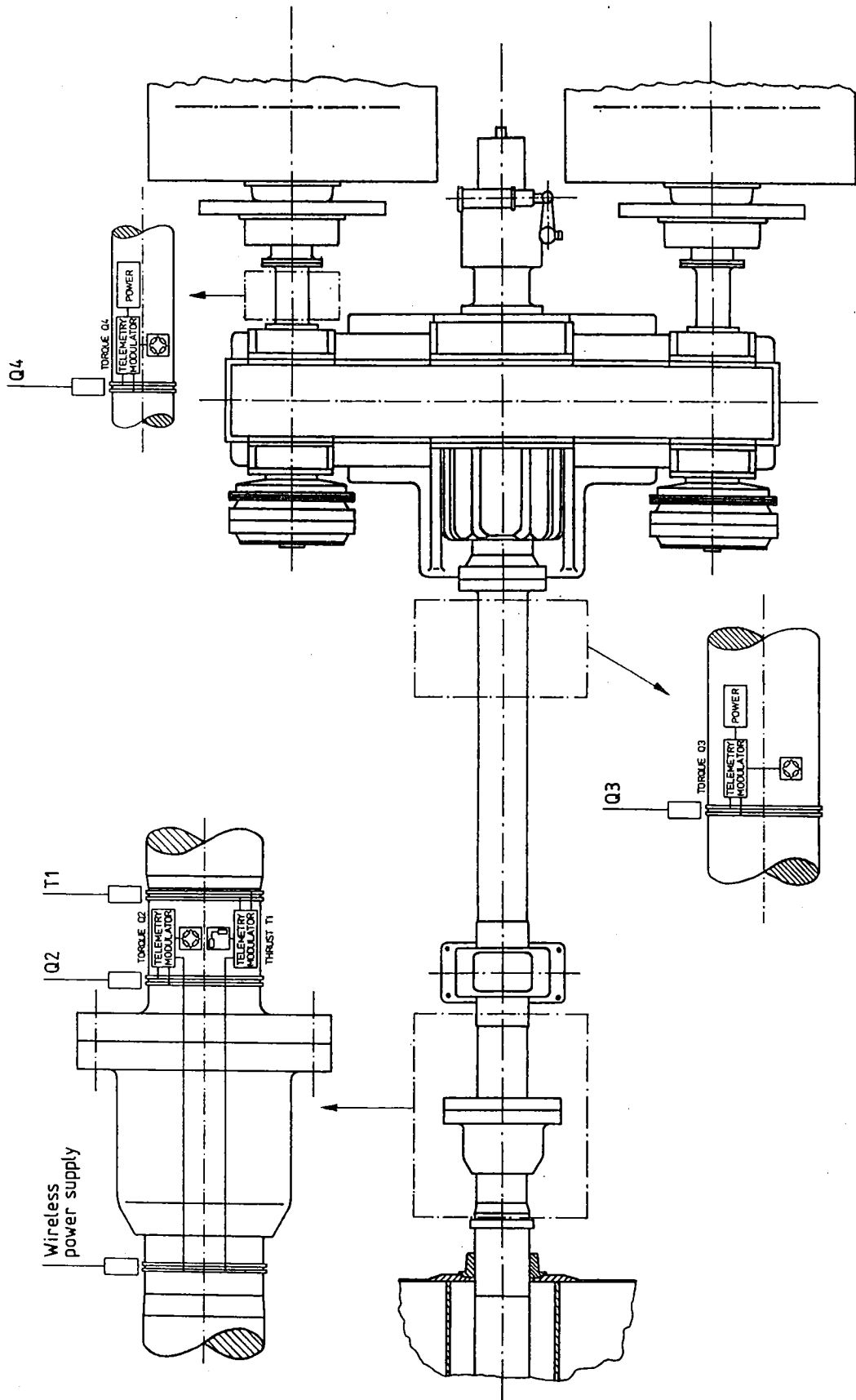


Fig. 7. Location of thrust and torque strain gauges.

Thrust and torque (only Q2) signals were divided into four frequency bands. The filtration was carried out to distinguish the oscillatory ice loads from the slower changes of the mean load. Another goal was to separate some of the machinery excitations from the typical ice load frequencies. The limits of these bands are drawn in the typical frequency spectra in ice conditions shown in Fig. 8. The lowest frequency band (DC-0.5 Hz) was used to find out the mean torque and thrust during short term measurements. The mean torque was also needed for evaluation of power on the propeller shaft.

The zero point of the thrust signal was continuously drifting due to temperature variations. In short-term measurements the creep of the zero-point could be compensated by regular zero-value checkings. In long-term measurements this kind of checkings weren't possible and therefore nominal thrust values cannot be obtained from long-term recordings. In winter 1983 the thrust strain gauge was also slightly dispositioned, what caused to the thrust signal an irrelevant vibration (2 Hz) coming from shaft rotation. The thrust strain gauge was changed in 1984.

Shaft rotation speed was obtained with a frequency/voltage converter from a pulse signal coming once in a cycle from the propeller shaft. Power was obtained from measured shaft revolutions and mean torque (Q2).

Ship speed was measured with a doppler radar specially designed for ice going vessels. In ice-free conditions at open sea the signals of the doppler radar is inaccurate, because there are no solid surfaces to reflect back the radar signals. Ship speed was measured only in short-term measurements.

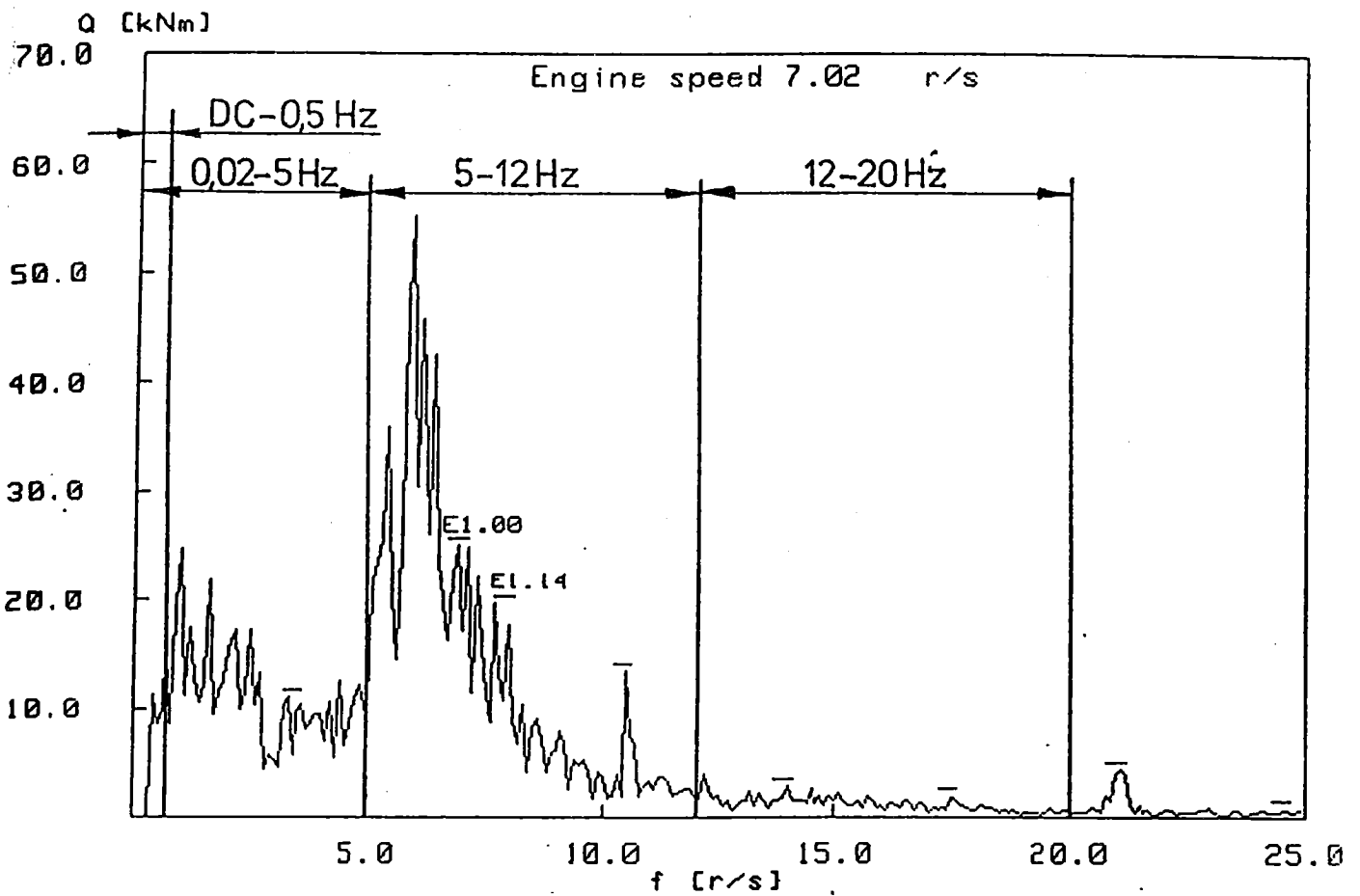


Fig. 8a. The limits of torque (Q) frequency bands.

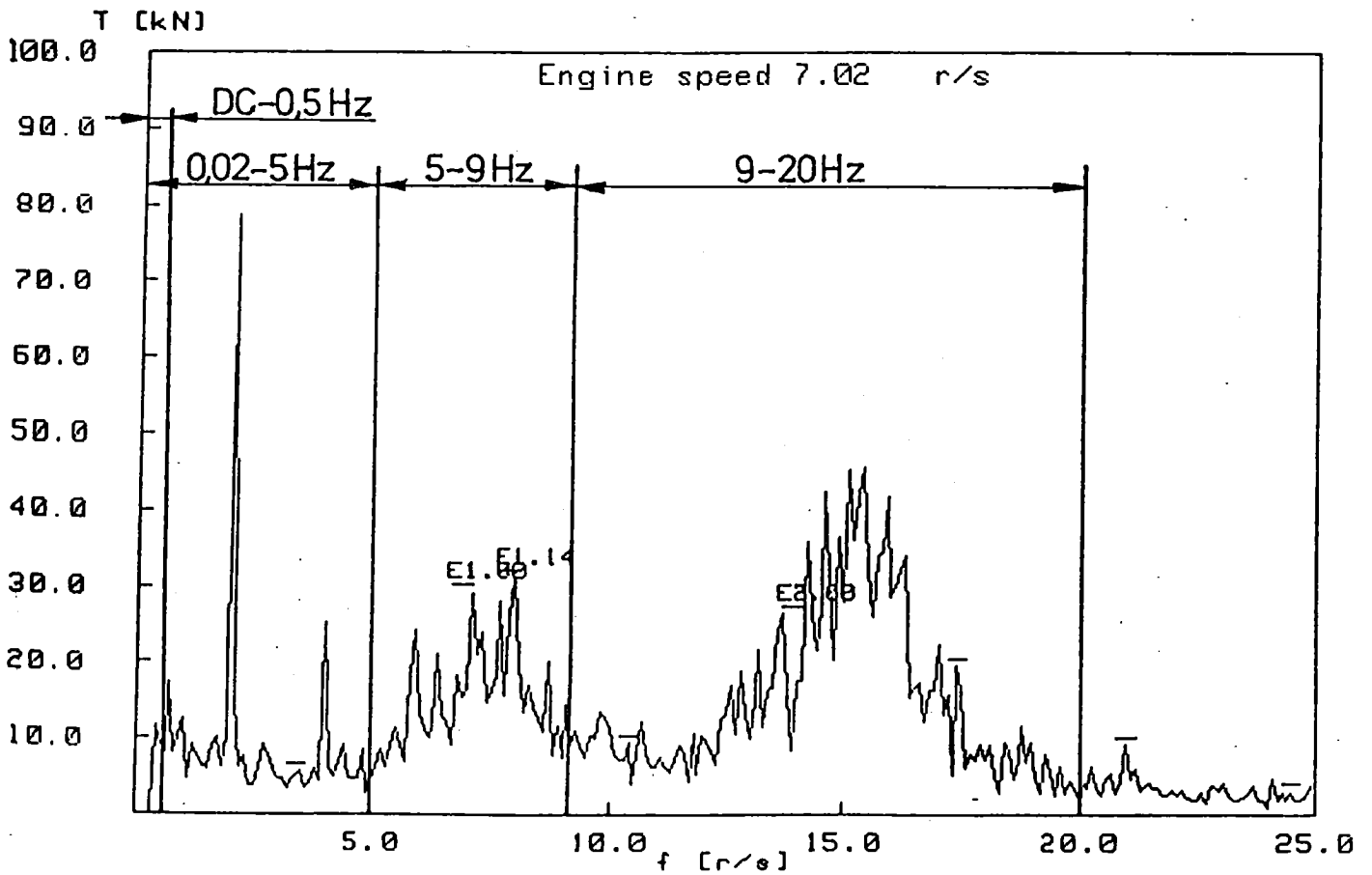


Fig. 8b. The limits of thrust (T) frequency bands.

Propeller pitch was measured with a linear potentiometer from a pitch control device in the engine room. The measured signal was calibrated by comparing it with the meter reading of the control device.

A linear potentiometer was also used for the measuring of rudder angle. Rudder torque was measured with a strain gauge bridge from rudder stock. In long-term measurements rudder torque was given a positive sign when sailing forward and a negative sign when sailing astern.

3.2 Recording devices

In long-term measurements the data was collected with microprocessor controlled recording unit designed and constructed by VTT. The recording unit took 200 samples/s from each measuring channel and converted them into digital form. The digitized samples were distributed according to their magnitude into classes from -31 to +31. The processor formed from the samples for each channel both signal level and amplitude distributions. The formation principles of these distributions are shown in Fig. 9. The distributions were recorded automatically every 24 hours simultaneously on a data tape cassette and on printer paper.

During short-term measurements the measured analog signals were recorded in an analog form on a 21 channel tape recorder. Part of them were simultaneously recorded with a Visicorder Oscillograph.

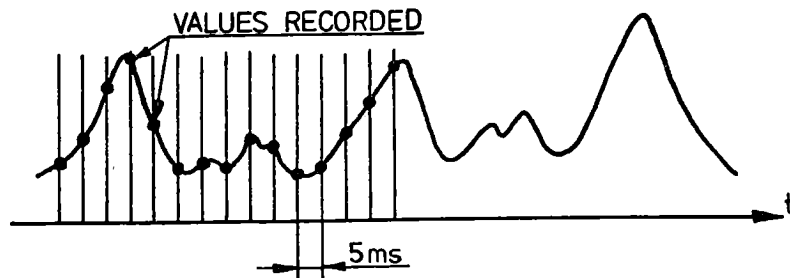


Fig. 9a. The principle of composing of the level distribution recordings.

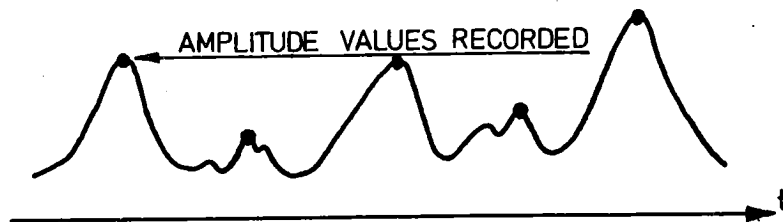


Fig. 9b. The principle of composing of the amplitude distribution recordings.

4 MEASUREMENTS

4.1 Long-term measurements

The long-term measurements were carried out during winters 1983 and 1984. In the first winter the measurements were done in the period of 22.1 - 24.3.1983, during which the data gathering system operated in total 49 days. In the second winter the measuring period was 4.2 - 20.4.1984, during which the data gathering system operated in total 46 days. Approximately one third of the measured data was left unrecorded due to a defect in power supply system, which occasionally disconnected the recording unit. Furthermore some recorded distributions had to be rejected due to disturbances.

Table 3 gives the channels connected to the microprocessor during the long-term measurements. The schedules of Sotka during the measuring periods are shown in Tables 5 and 6 on pages 52 ... 55. The noting east/west in the remarks-column indicates whether the ship has used the inner coastal route (east) or sailed via Ahvenanmeri (west) when passing the Ahvenanmaa-archipelago.

The development of ice conditions in the ship's normal operating area can be seen from the ice charts in Appendix 2. Winter 1983 was as a whole milder than an average one, but winter 1984 was close to the average.

Table 3. Channels used in long-term measurements.

Sampling channel	Winter 1983		Winter 1984	
	Signal	Signal description	Signal	Signal description
00	Q(0-20)	torque in range 0-20 Hz	Q(0-20)	torque in range 0-20 Hz
01	Q(0.02-5)	" 0.02-5 Hz	Q(0.02-5)	" 0.02-5 Hz
02	Q(5-12)	" 5-12 Hz	Q(5-12)	" 5-12 Hz
03	Q(12-20)	" 12-20 Hz	Q(12-20)	" 12-20 Hz
04	T(0-20)	thrust in range 0-20 Hz	T(0-20)	thrust in range 0-20 Hz
05	T(0.02-5)	" 0.02-5 Hz	T(0.02-5)	" 0.02-5 Hz
06	T(5-9)	" 5-9 Hz	T(5-9)	" 5-9 Hz
07	T(9-20)	" 9-20 Hz	T(9-20)	" 9-20 Hz
08	RA	rudder angle	RA	rudder angle
09	RQ	rudder stock torque	RQ	rudder stock torque
10	P/D	pitch ratio setting	RPM	number of shaft revolut.
11	Power	shaft power	Power	shaft power
12	-	-	P/D	pitch ratio setting

4.2 Short-term measurements

The short-term measurements were carried out during a ship's normal voyage from Kemi to Porvoo on 17 - 19.3.1983. The purpose of these measurements was to improve the knowledge of the propeller-ice interaction and to find out the characteristics of ice loads and ice-induced shaft vibrations especially for this installation. Also the effects of some parameters, such as ship speed and pitch ratio, were subjects of interest.

The measurements were recorded with a 21 channel tape recorder and partly also with a Visicorder oscillograph. These recordings covered almost 20 hours of measurements in various ice conditions. Table 4 gives the measured channels.

Table 4. The channels used in short-term measurements.

TEAC channel	Visicorder channel	Signal	Signal description
1	9	V	ship speed
2	2	T1	thrust
3	-	Q2 (0.02-9 Hz)	torque in range 0.02-9 Hz
4	8	Q2	torque
5	-	Q2 (5-12 Hz)	torque in range 5-12 Hz
6	7	Q3	torque
7	-	Q2 (12-20 Hz)	torque in range 12-20 Hz
8	6	Q4	torque
9	-	T1-4 (0.02-5 Hz)	thrust in range 0.02-5 Hz
10	-	T1-6 (5-9 Hz)	thrust in range 5-9 Hz
11	-	-	tape servo
12	-	T1-7 (9-20 Hz)	thrust in range 9-20 Hz
13	3	RA	rudder angle
14	1	RQ	rudder stock torque
15	4	P/D	pitch ratio setting
16	5	PWR	shaft power
17	-	RPM	number of shaft revolutions
18	-	Q2-5 (DC-0.5 Hz)	torque in range DC-0.5 Hz
19	-	T1-5 (DC-0.5 Hz)	thrust in range DC-0.5 Hz
20	-	pulse	shaft revolution pulse
21	-	-	memo

The ship's route during the voyage is drawn on the ice chart shown in Fig. 10. During the voyage the ship was in ballast condition and her aft draught was 6.6 m.

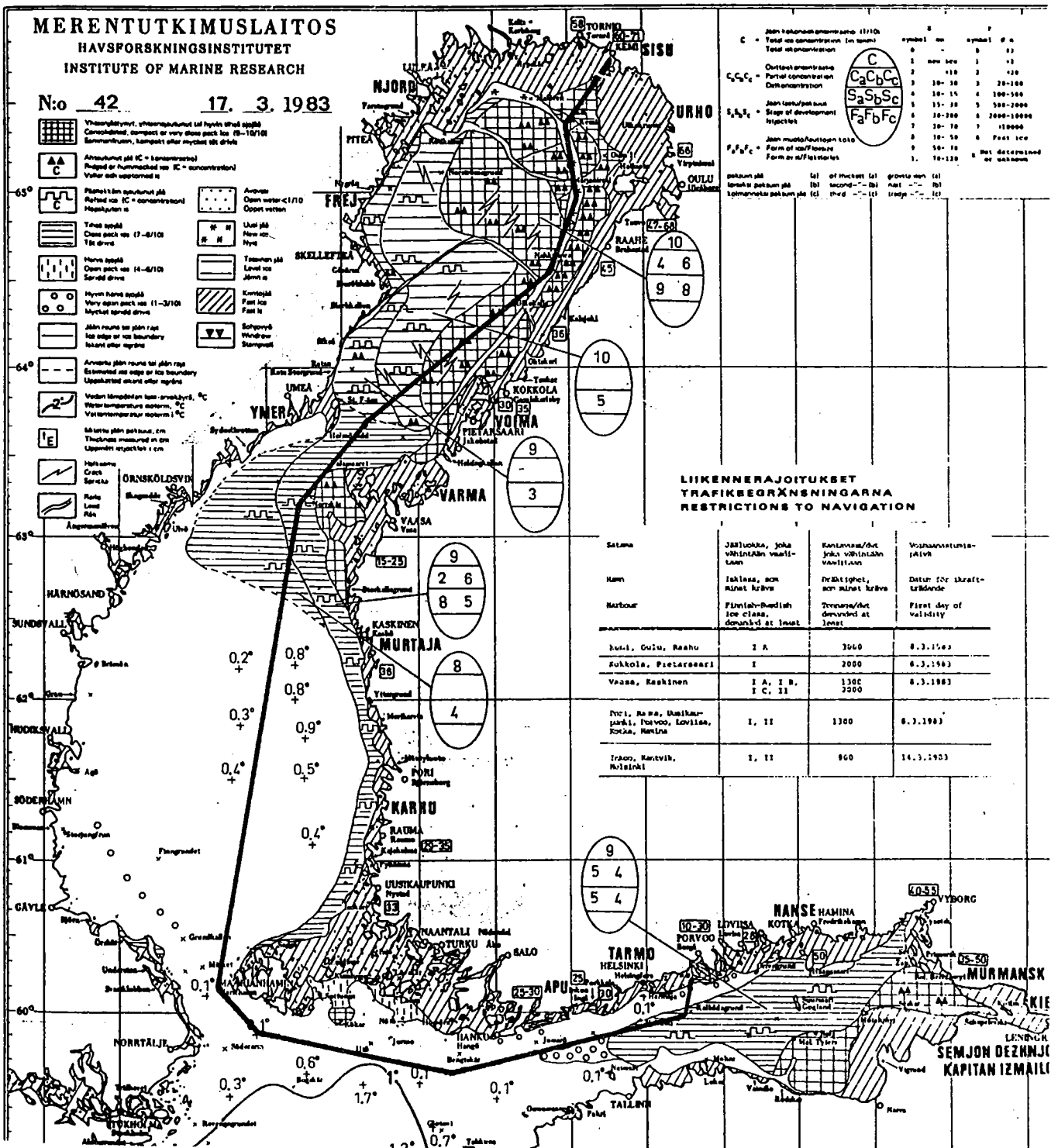


Fig. 10. Ship's route during the short-term measurements.

5 RESULTS OF THE MEASUREMENTS

5.1 Results of the short-term measurements

5.1.1 Analysis of the results

The short-term measurements were examined using visicorder oscillograph and a spectrum analyzer. Some examples of the measured signals in typical open water and ice conditions are shown in Figs. 11a and 12a. The respective frequency spectra of thrust and torque signals are shown in Figs. 11b and 12b. It should be noted that the strong vibration component of 2 Hz in thrust signals is caused by inadequate attachment of the thrust strain gauge. More examples of signals and spectra from different ice conditions are presented in Figs. 13 ... 18. It should be noted about the frequency spectra that their amplitudes are mean values of the sampling periods, and therefore they do not give peak magnitudes of vibration amplitudes in transient ice load situations.

Samples of ice impact series were manually picked up from the recorded signals as shown in Fig. 19. The selected variables were then plotted in order to find out the mutual dependencies between them. Examples of these plots are shown in Figs. 20 ... 25. The regression lines drawn to clarify the tendencies in diagrams were calculated so that the sum of the squared distance values reached minimum.

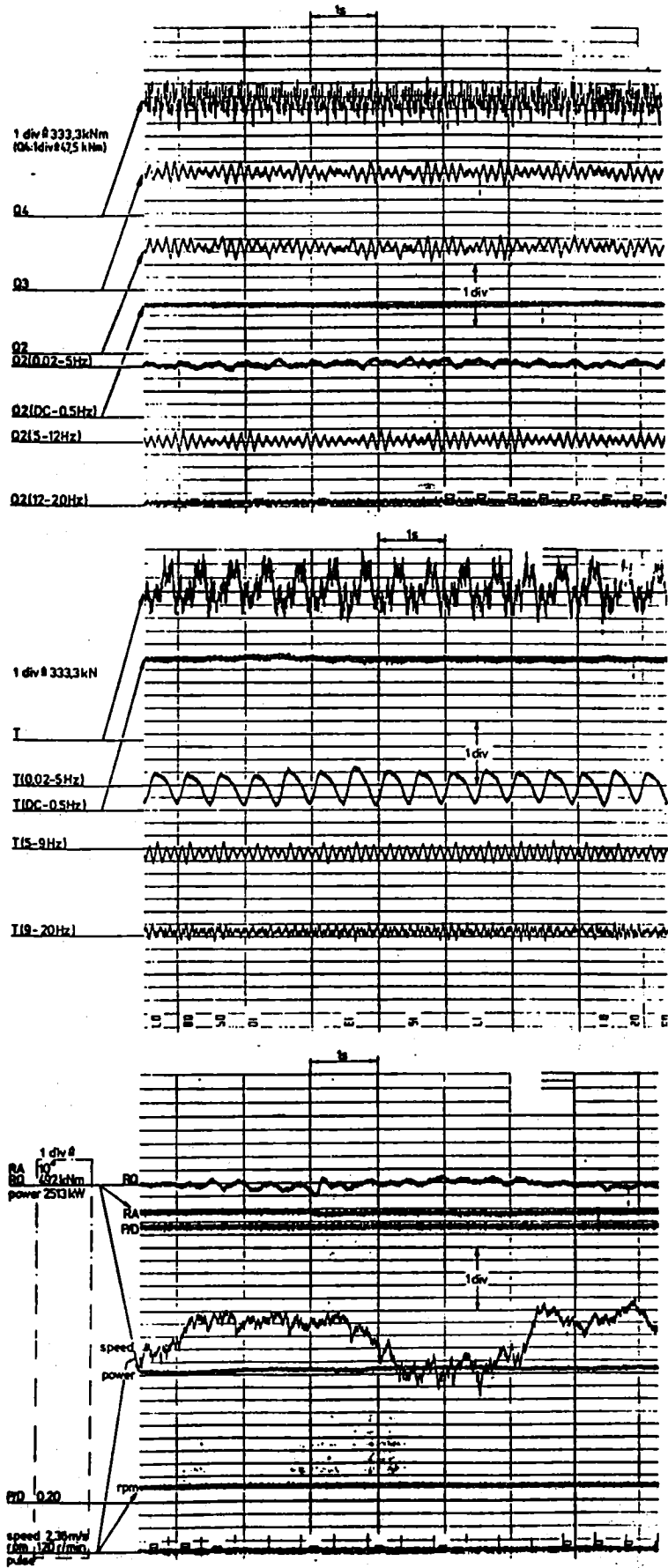


Fig. 11a. Typical measured signals in open water conditions with two engines.

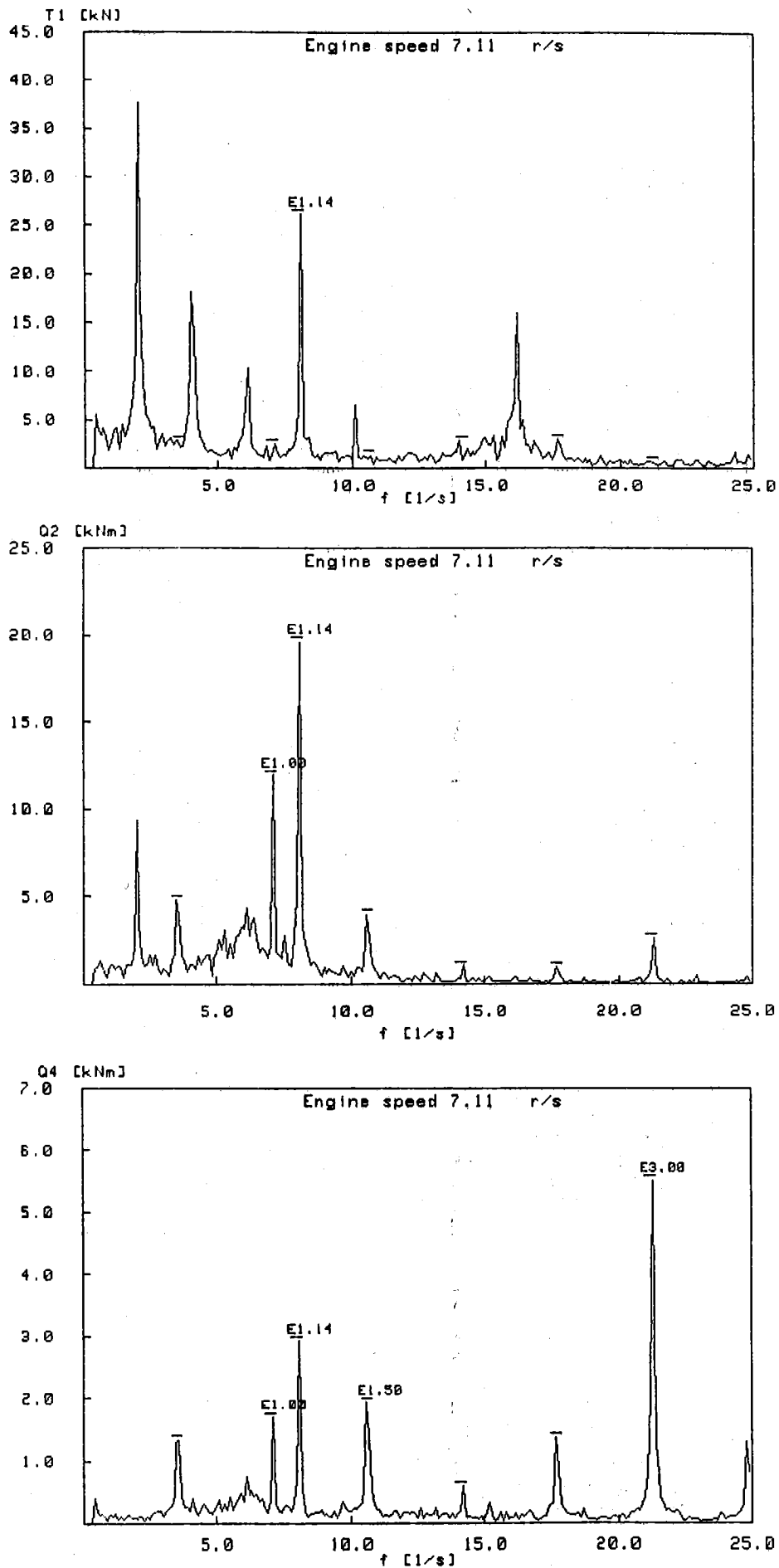


Fig. 11b. The frequency spectra of T1, Q2 and Q4 in open water.

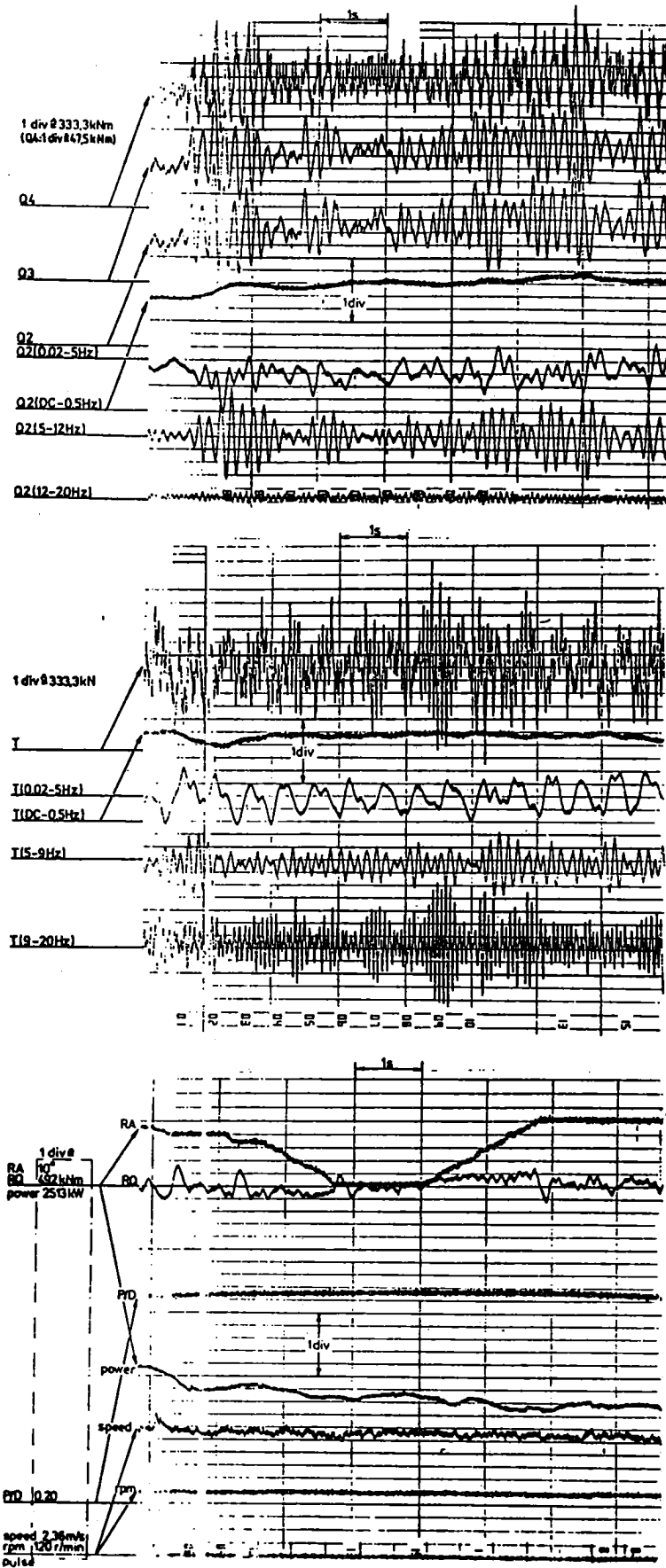


Fig. 12a. Typical measured signals when going ahead with two engines in ice clogged channel.

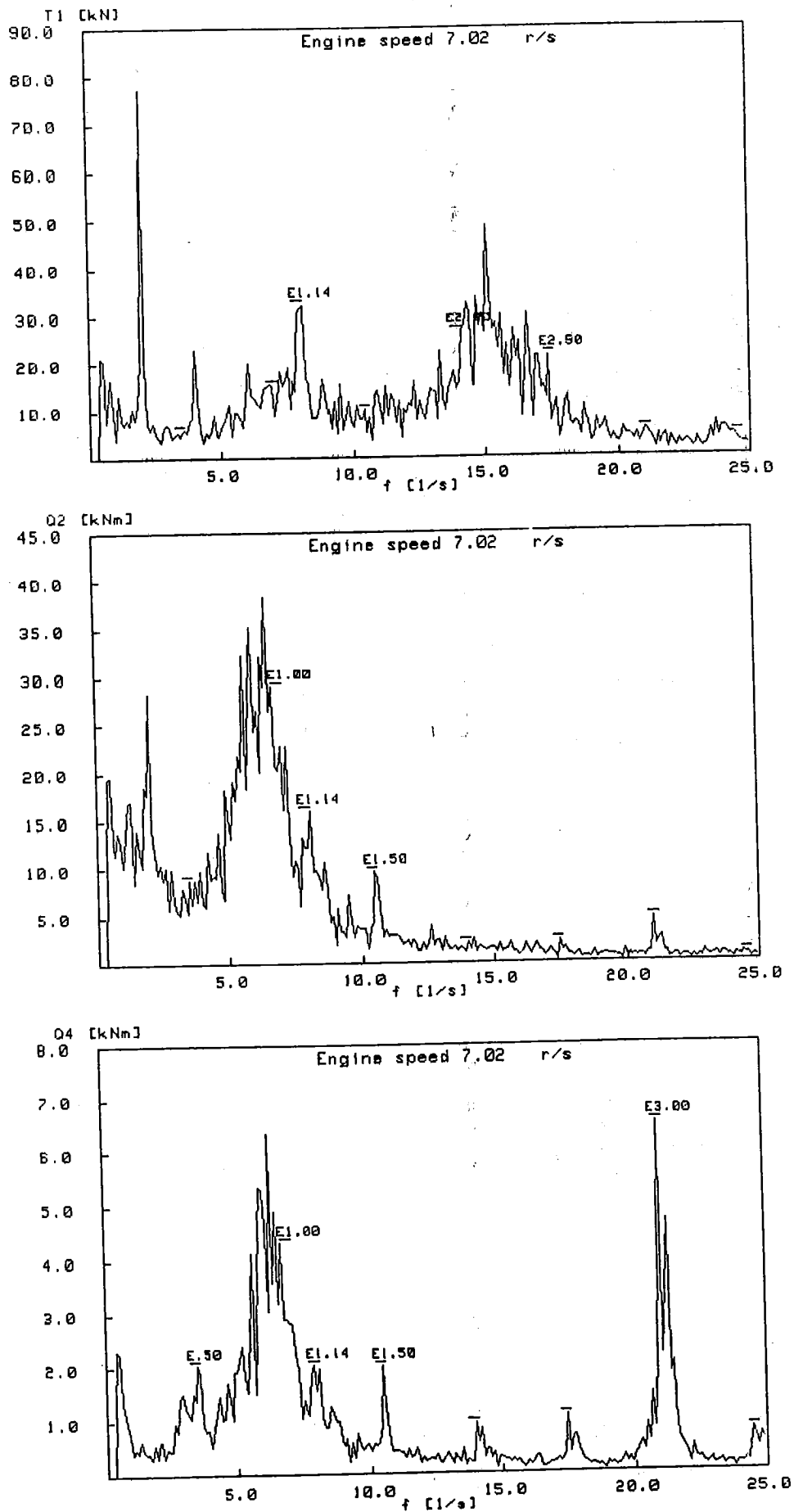


Fig. 12b. Typical frequency spectra of T1, Q2 and Q4 when going ahead with two engines in ice clogged channel.

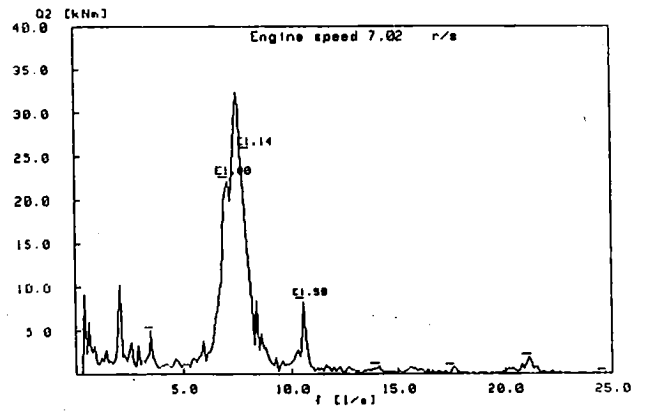
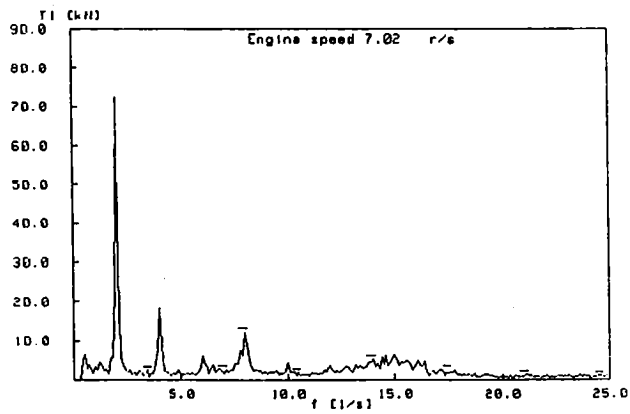
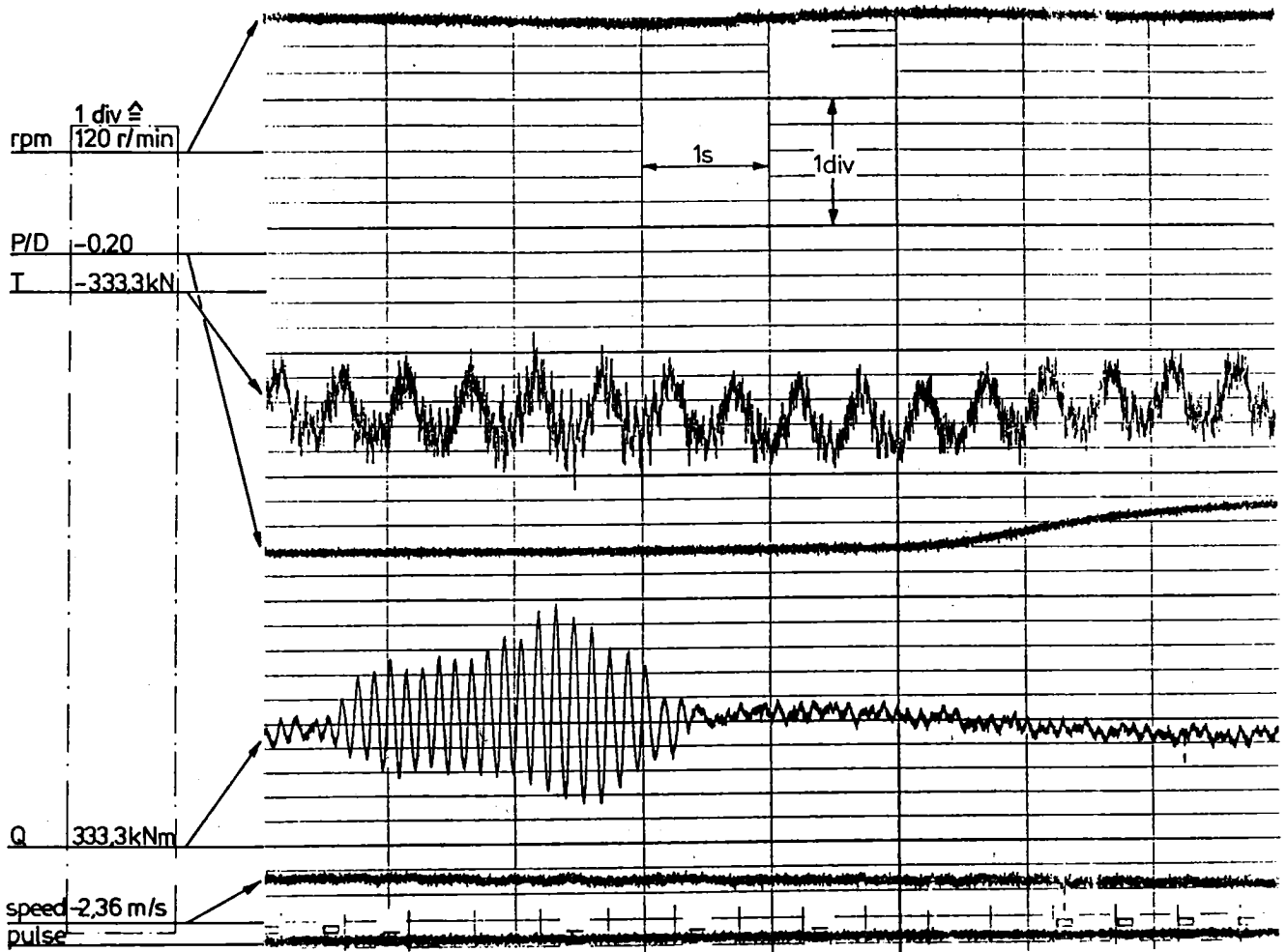


Fig. 13. Measured time histories and frequency spectra of T1 and Q2 when going astern in ice with one engine.

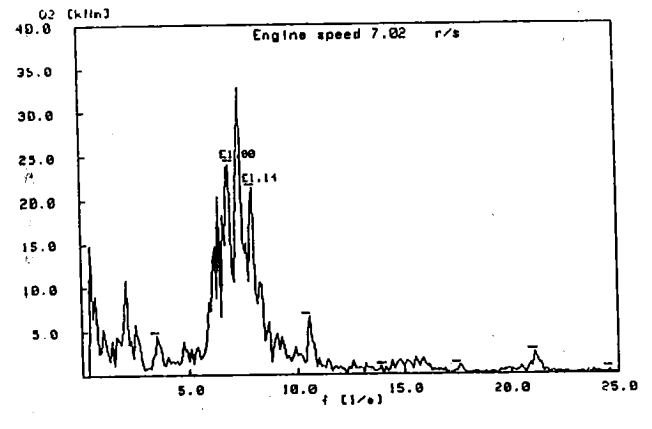
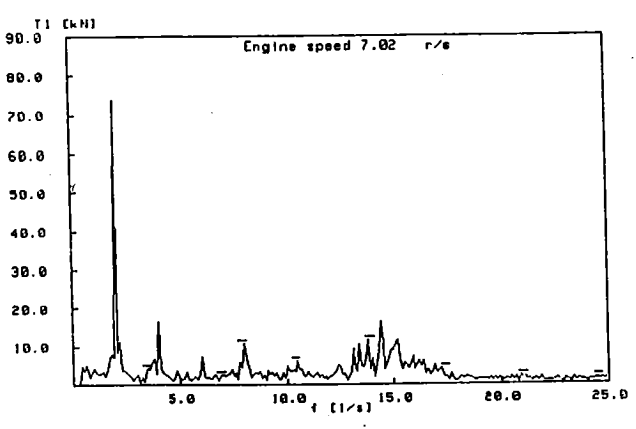
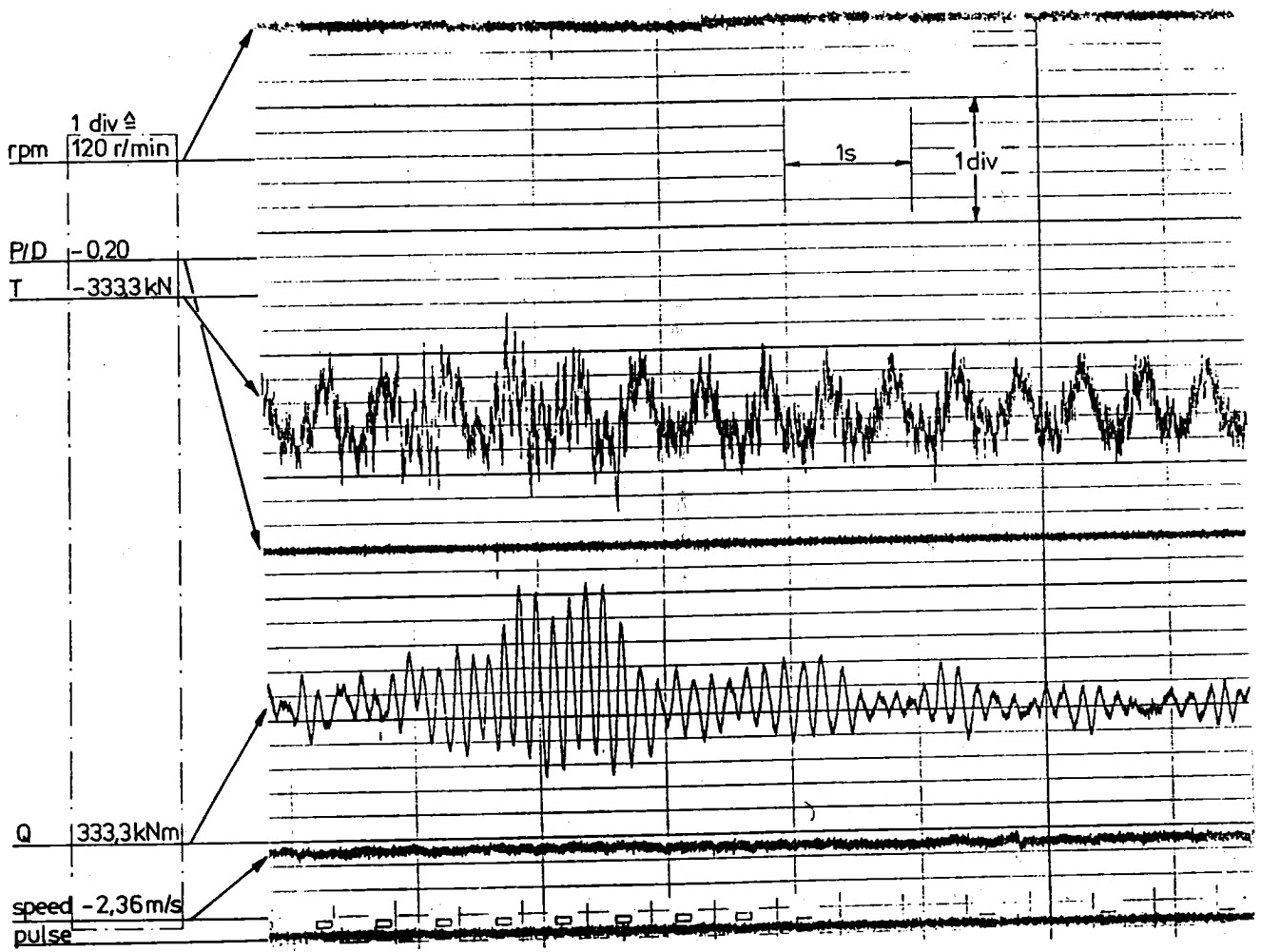


Fig. 14. Measured time histories and frequency spectra of T1 and Q2 when going astern in ice with one engine.

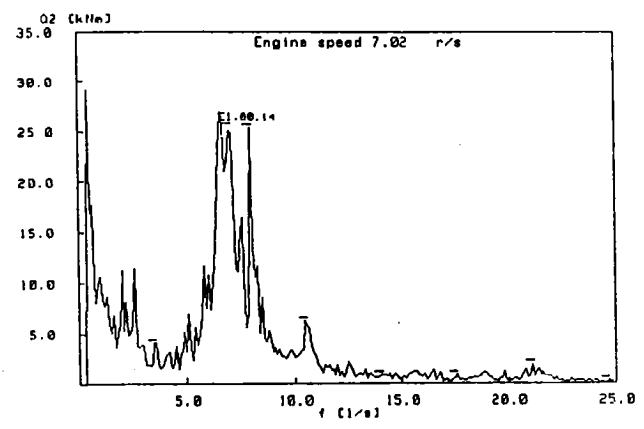
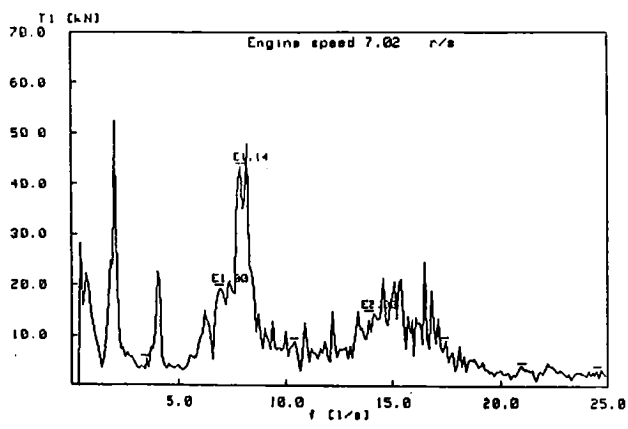
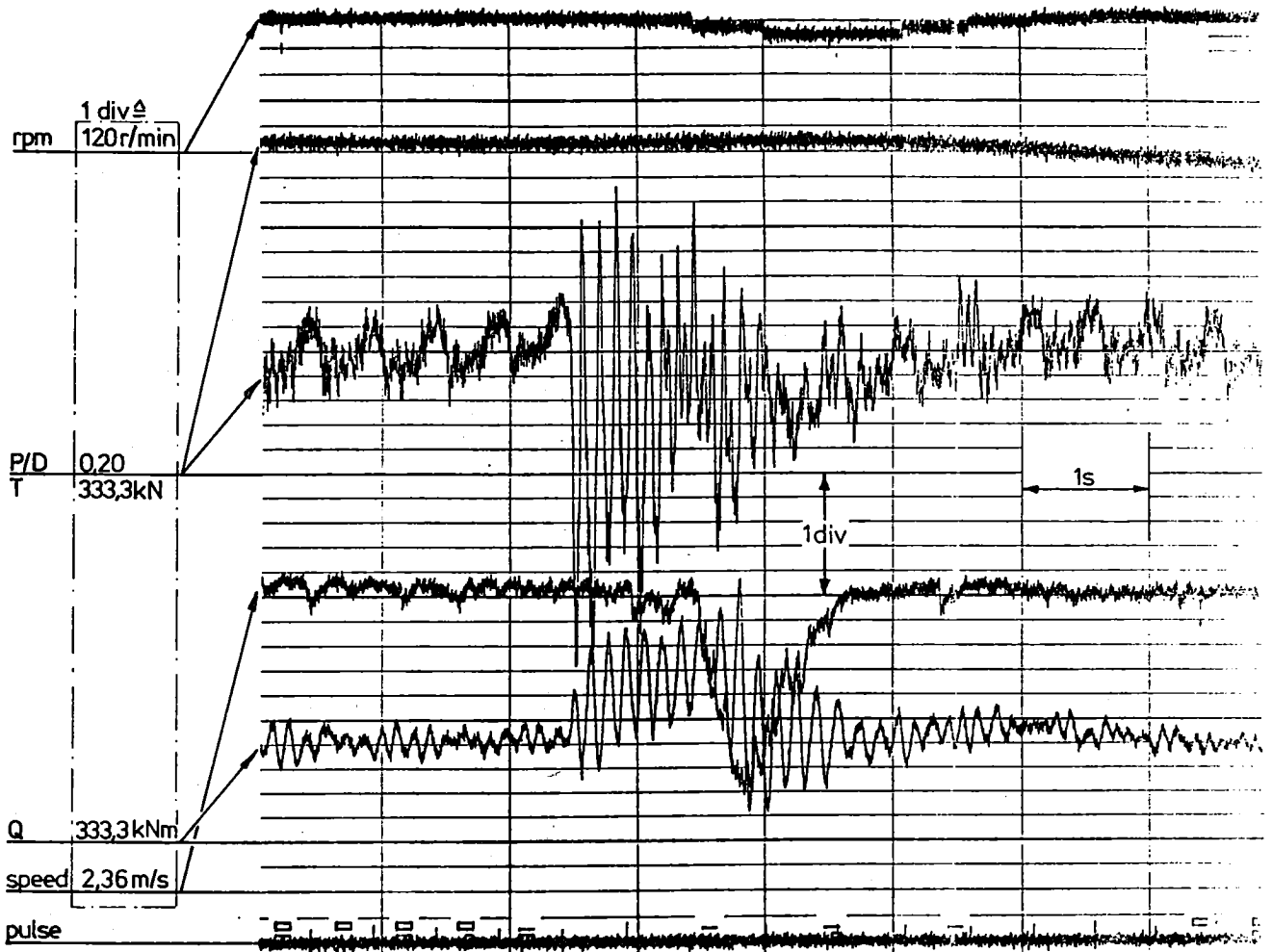


Fig. 15. Measured time histories and frequency spectra of T1 and Q2 when going ahead in pack ice with one engine.

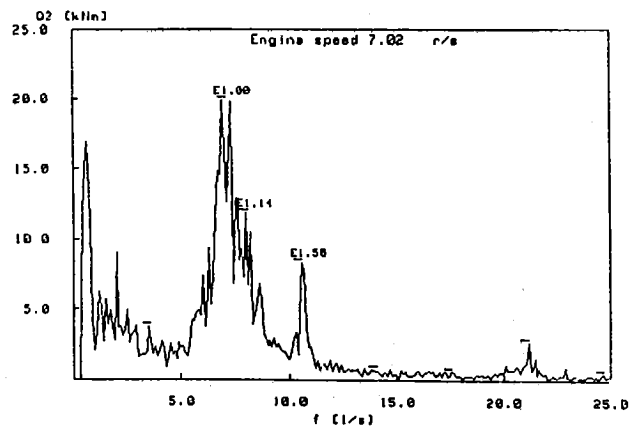
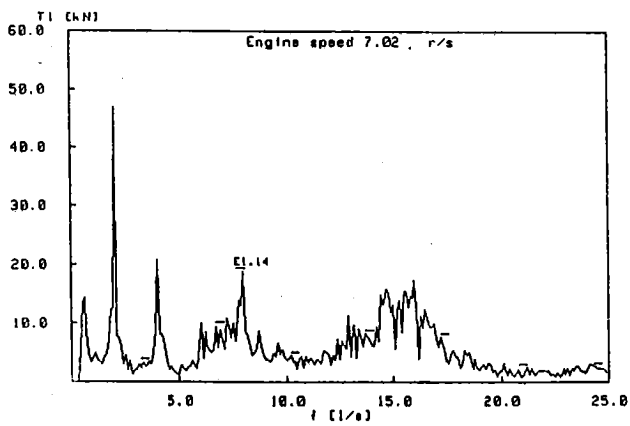
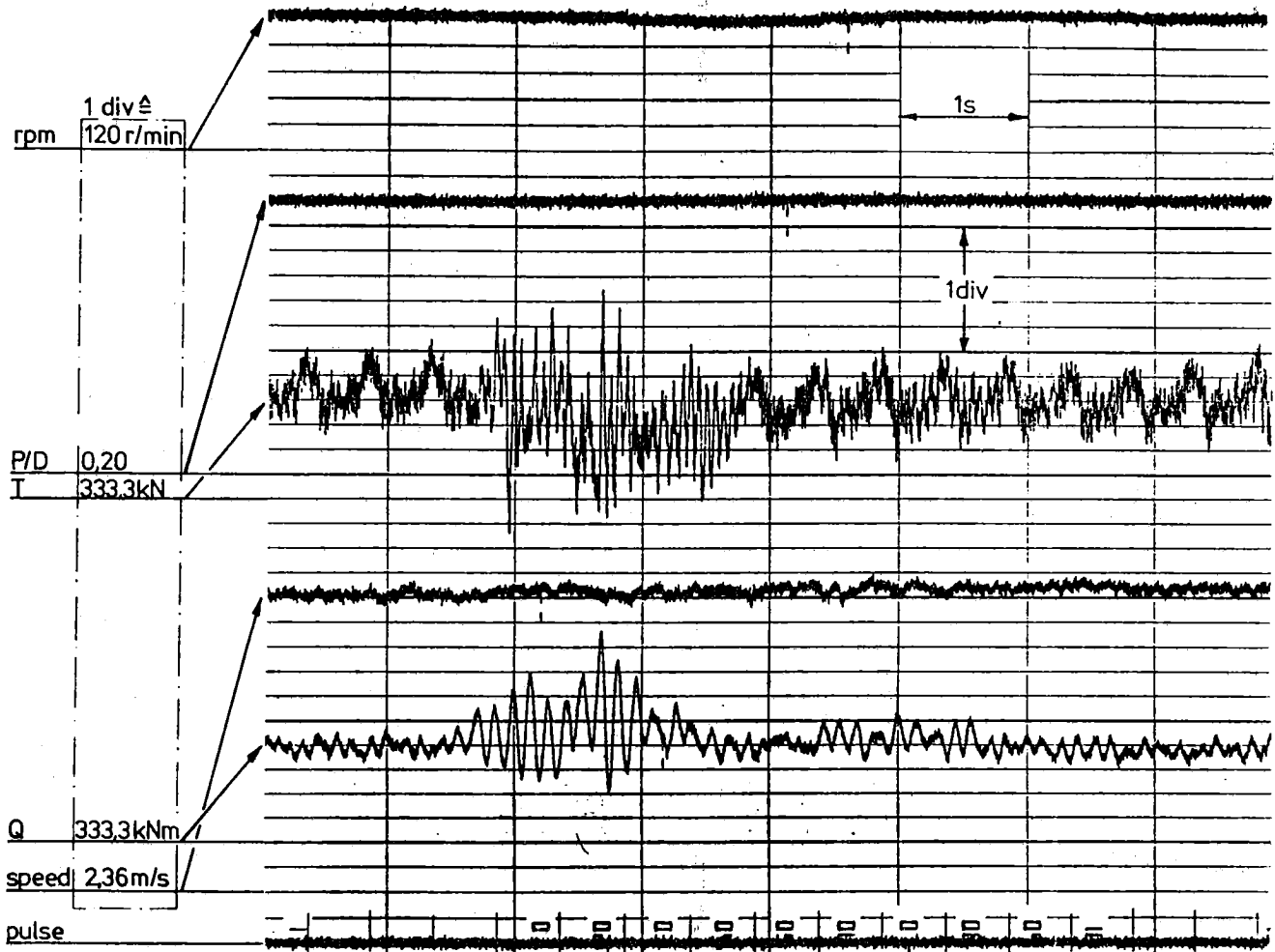


Fig. 16. Measured time histories and frequency spectra of $T1$ and $Q2$ when going ahead in pack ice with one engine.

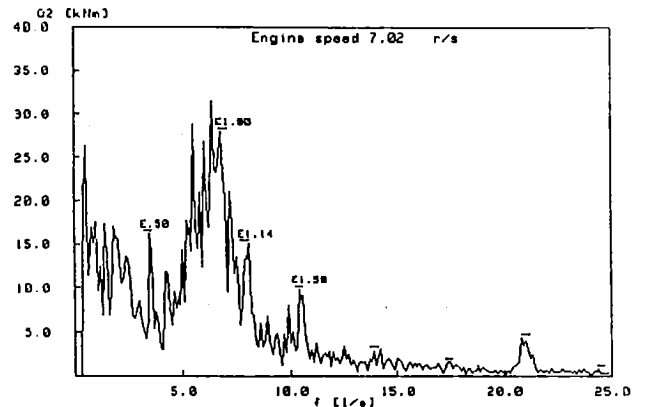
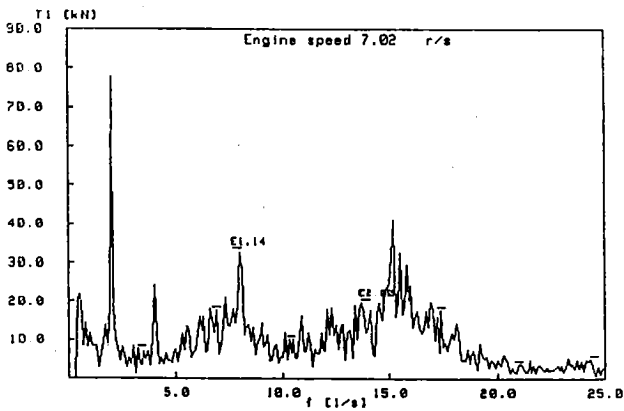
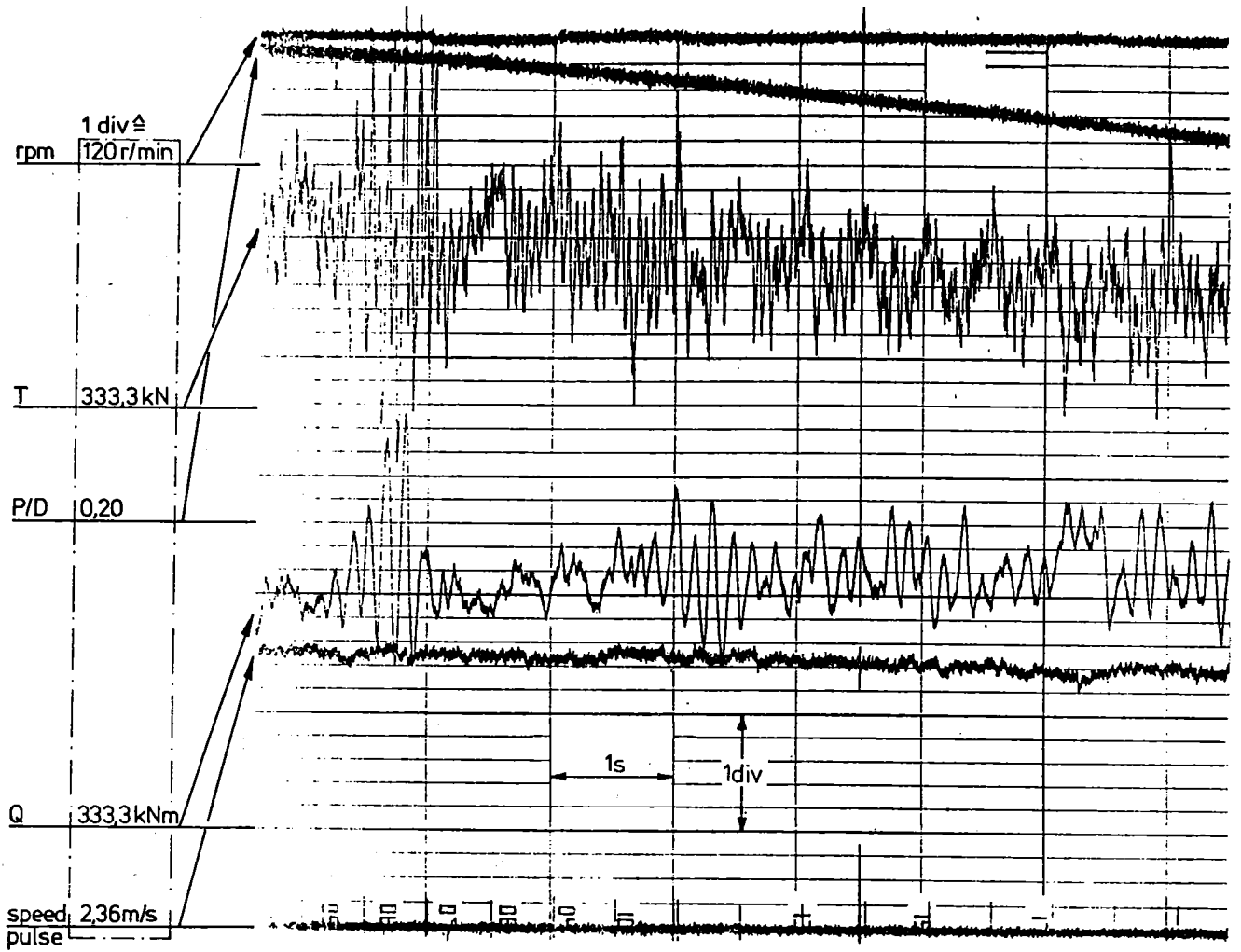


Fig. 17. Measured time histories when going ahead in ice clogged channel with two engines.

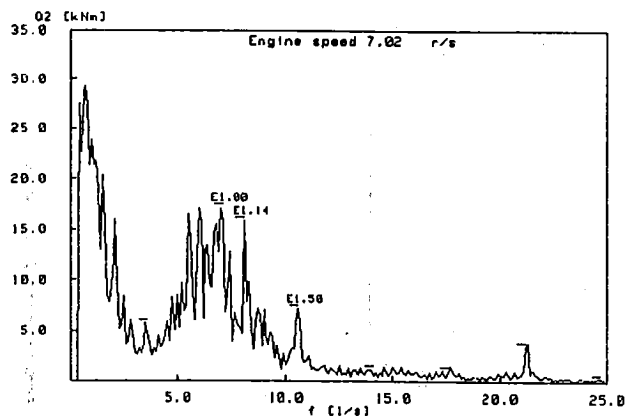
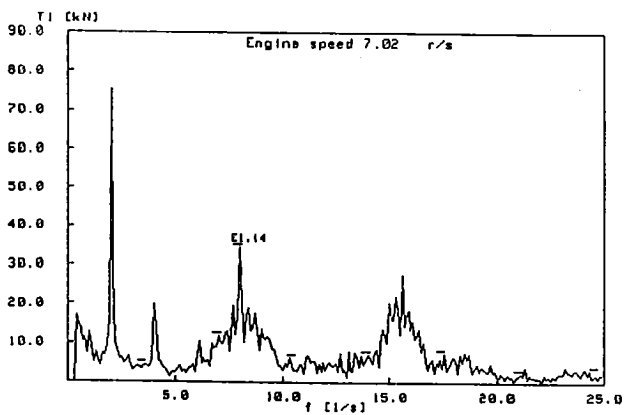
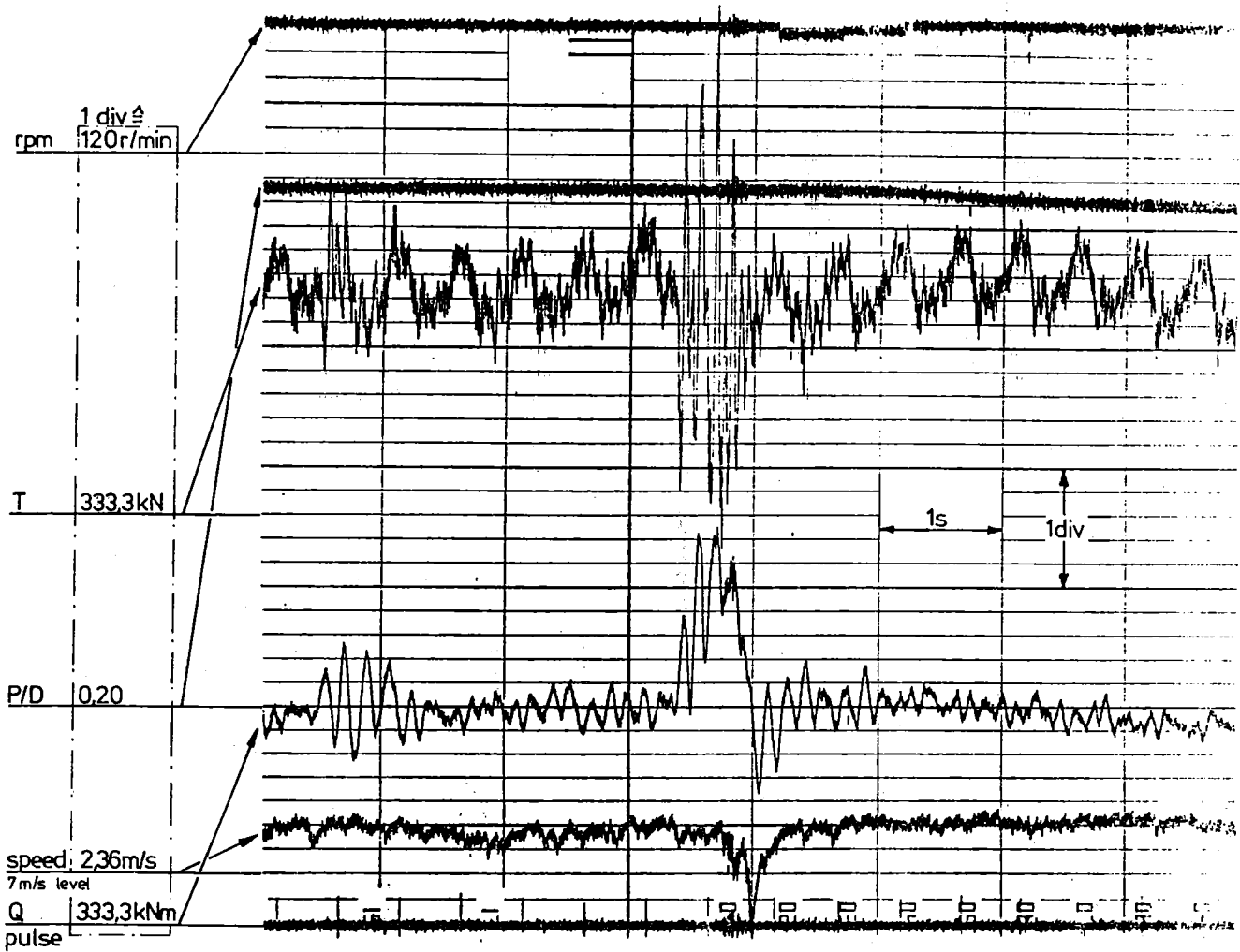


Fig. 18. Measured time histories when going ahead in ice clogged channel with two engines.

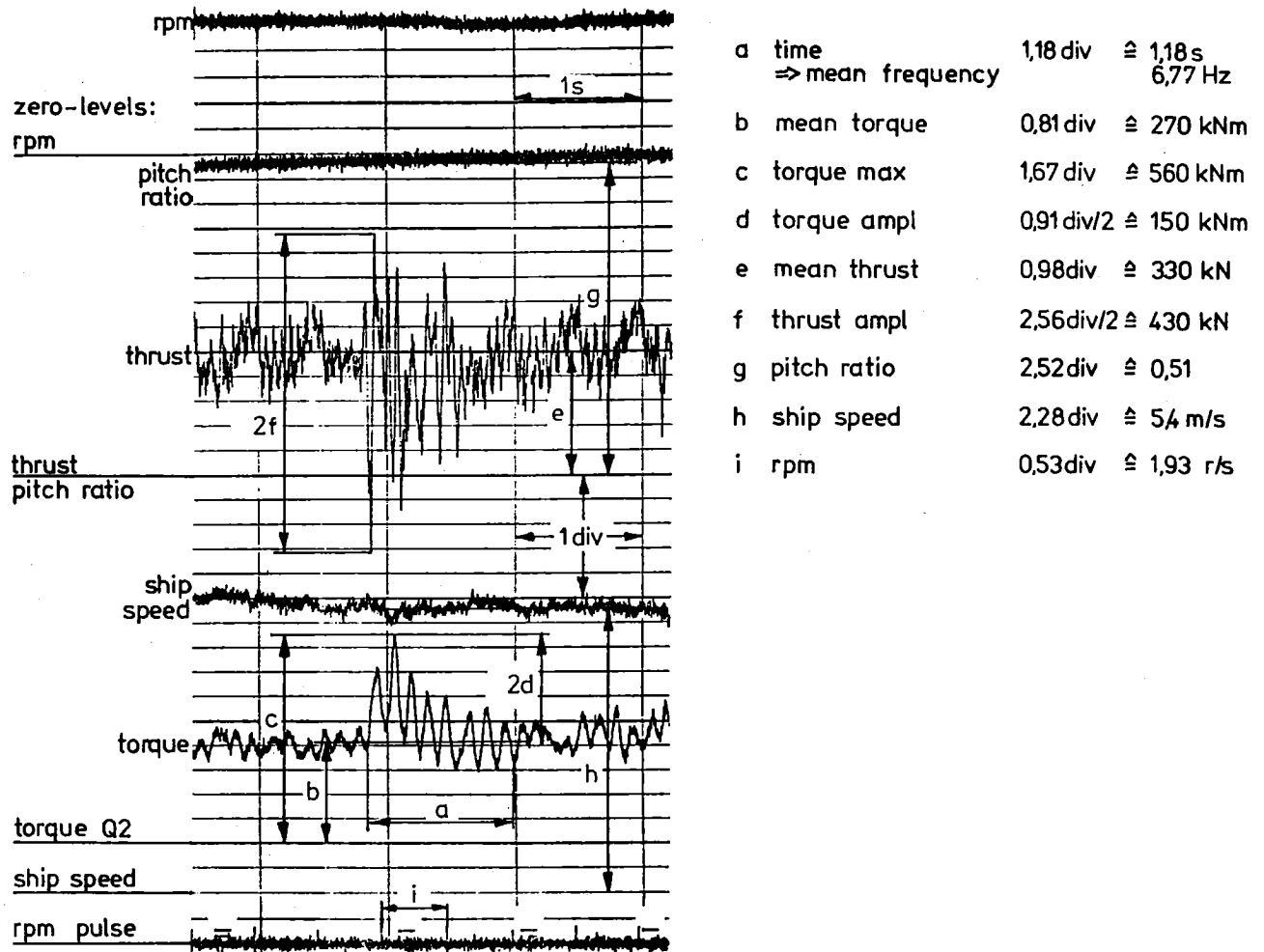


Fig. 19. An example of the samples picked up from plotter paper.

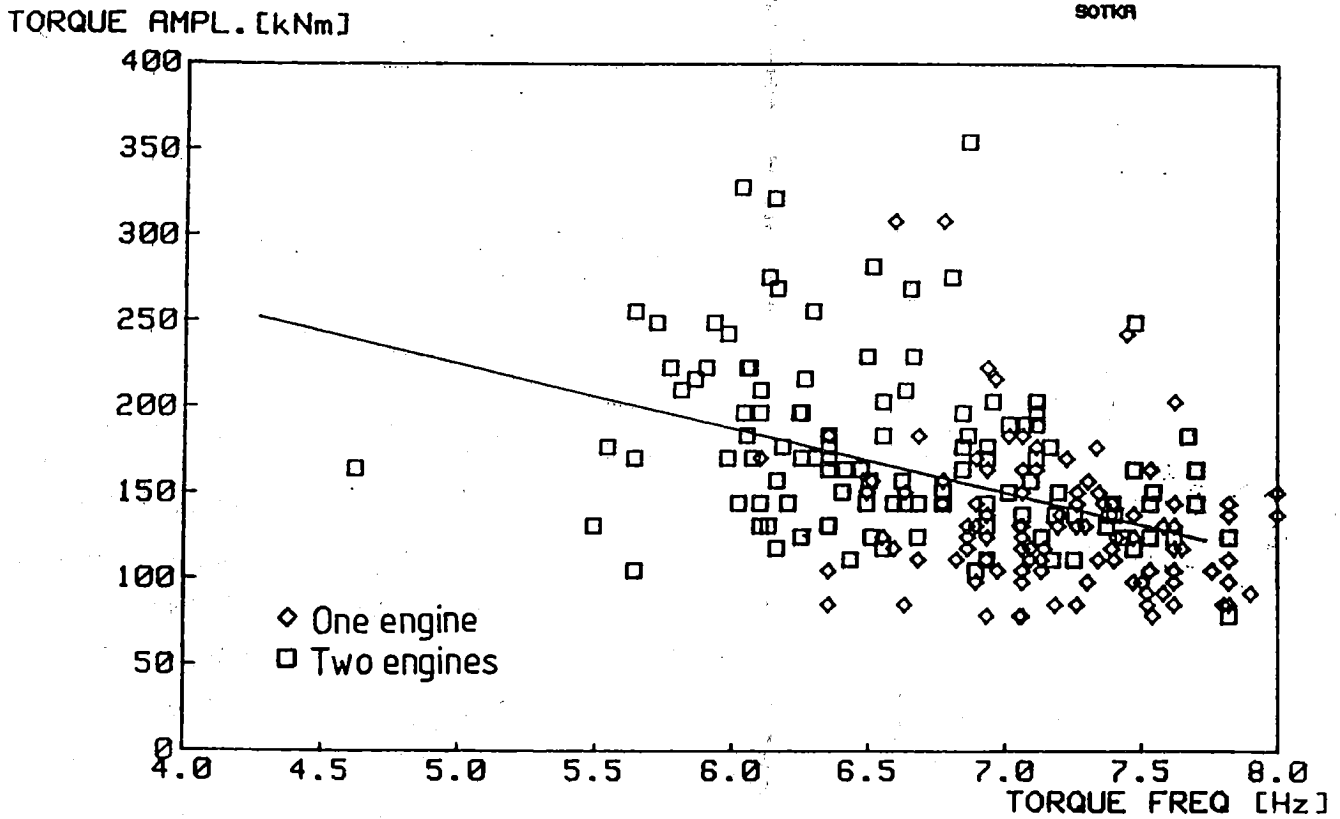


Fig. 20a. The measured frequencies of transient torque signals versus TORQUE MAX [kNm] the torque amplitudes.

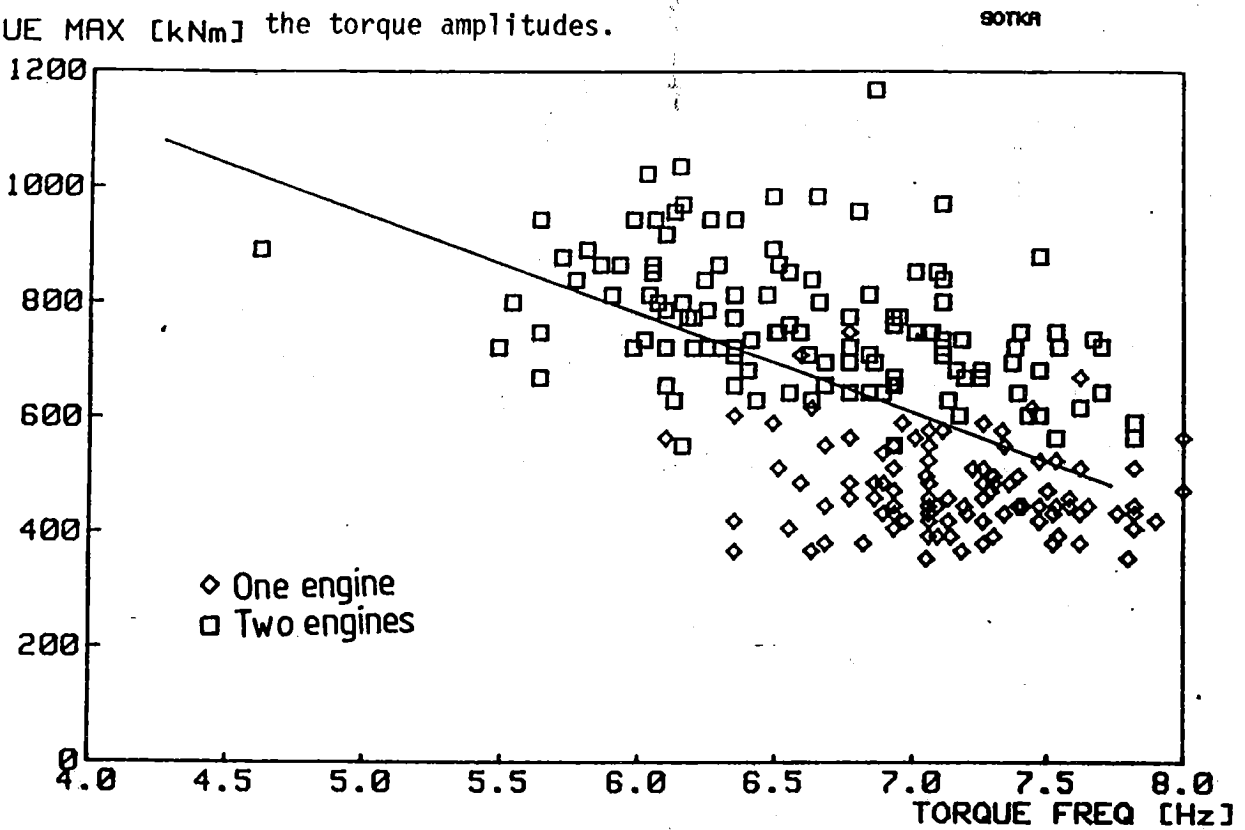


Fig. 20b. The measured frequencies of transient torque signals versus the maximum torque values.

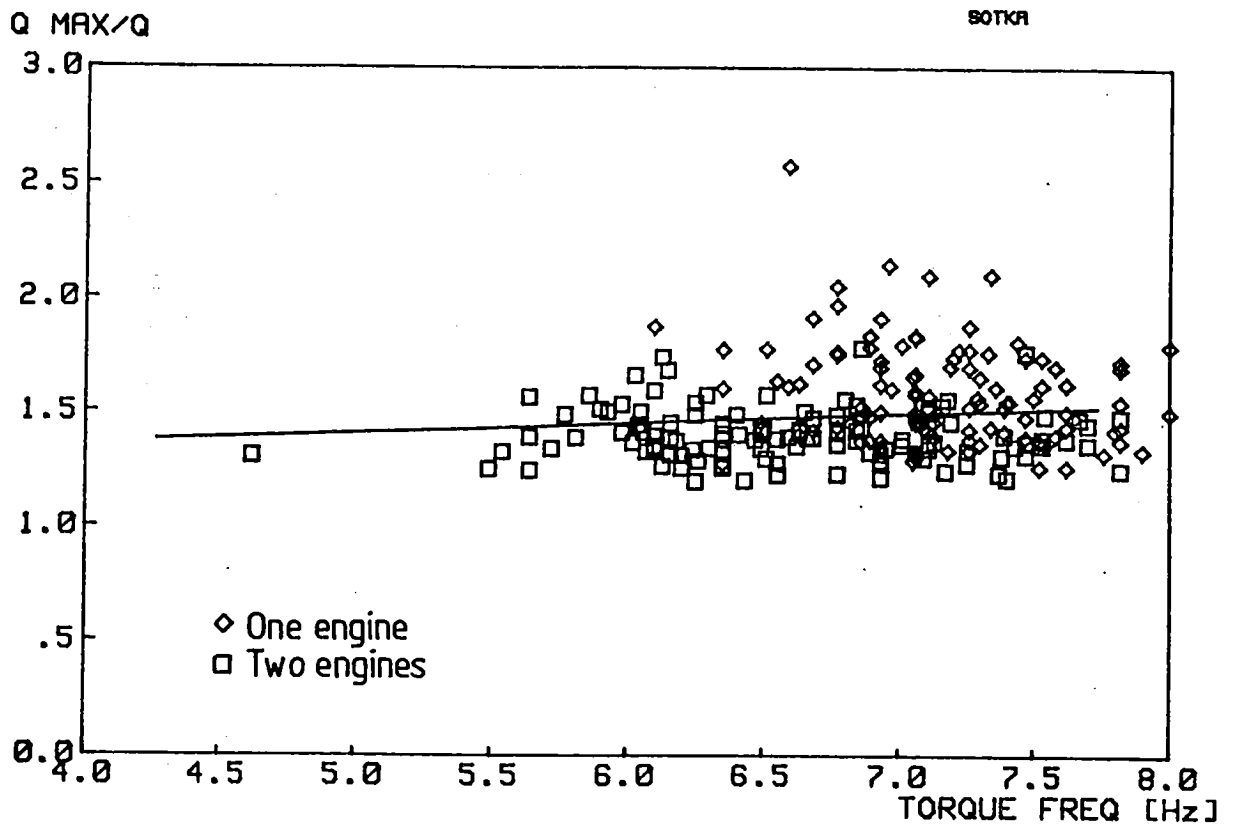


Fig. 20c. The measured frequencies of the transient torque signals versus maximum torque values divided by mean torques.

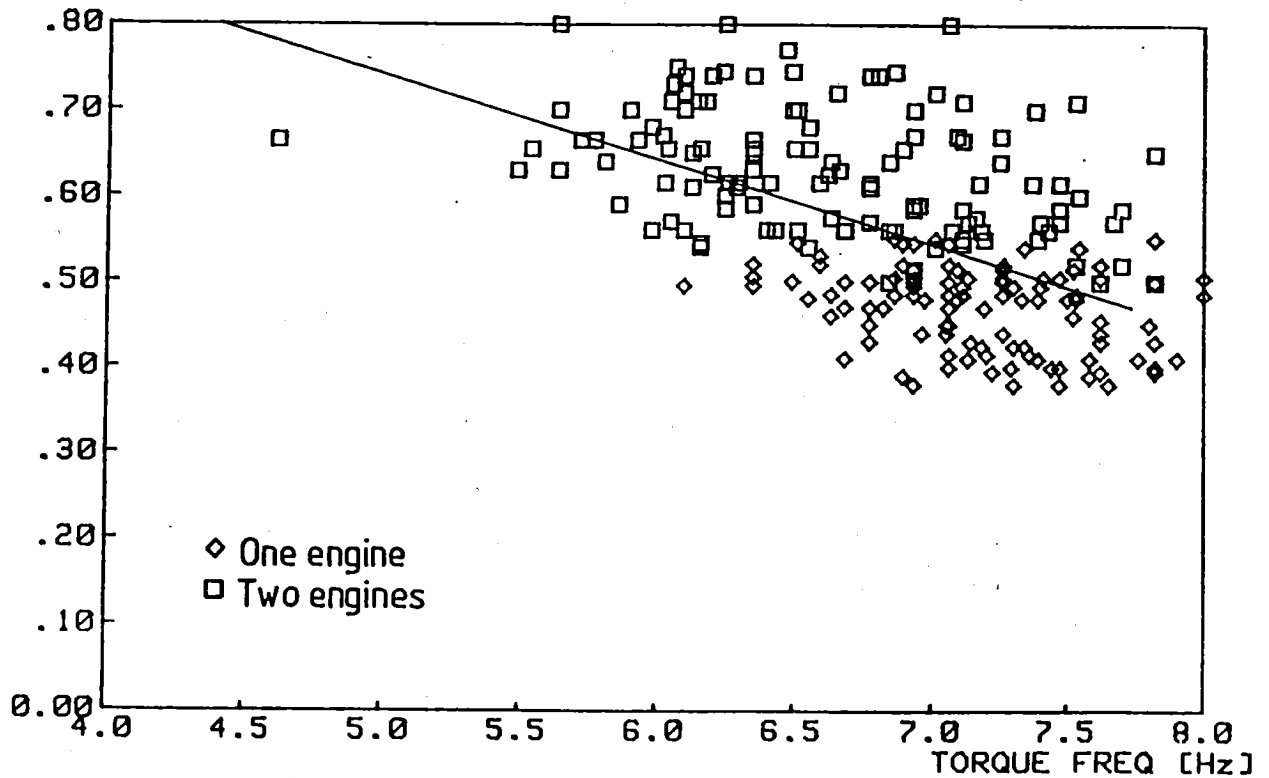


Fig. 20d. The measured frequencies of transient torque signals versus propeller pitch.

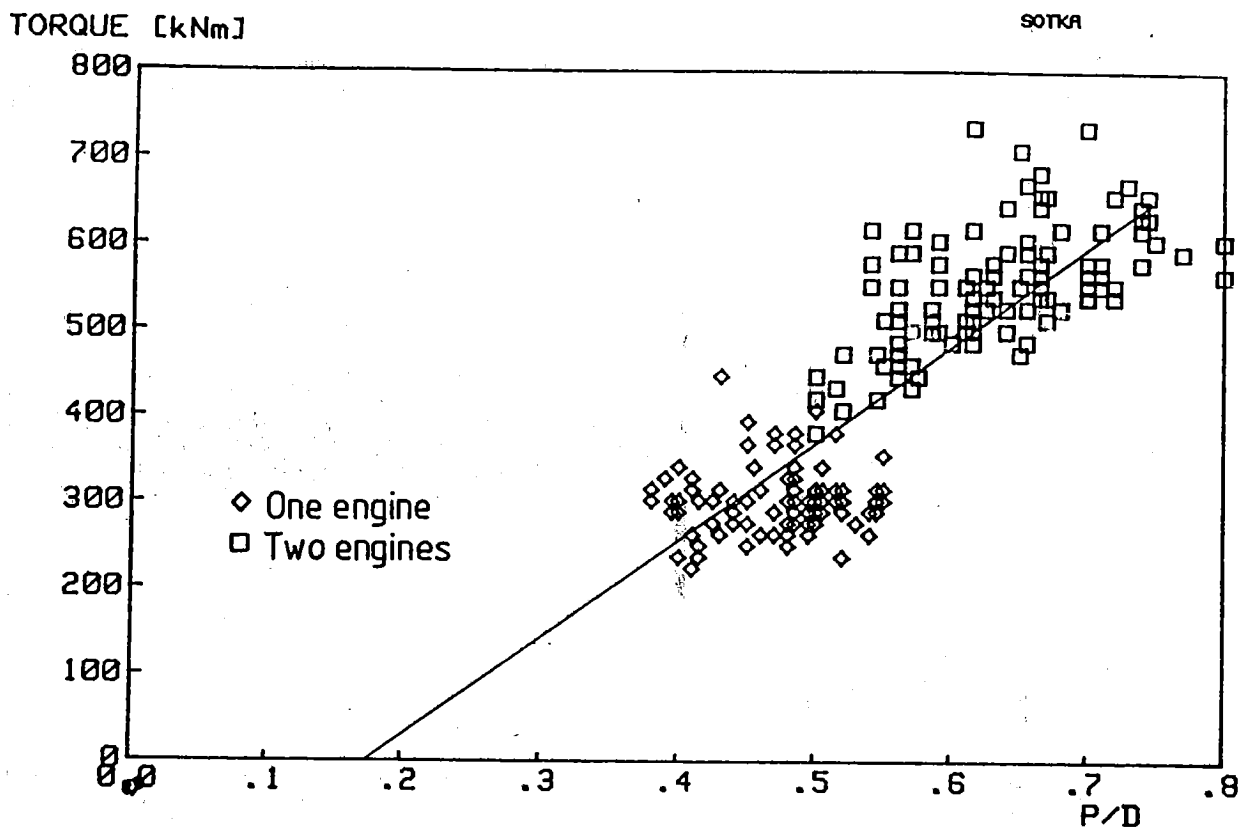


Fig. 21a. The measured propeller pitch versus mean torque.

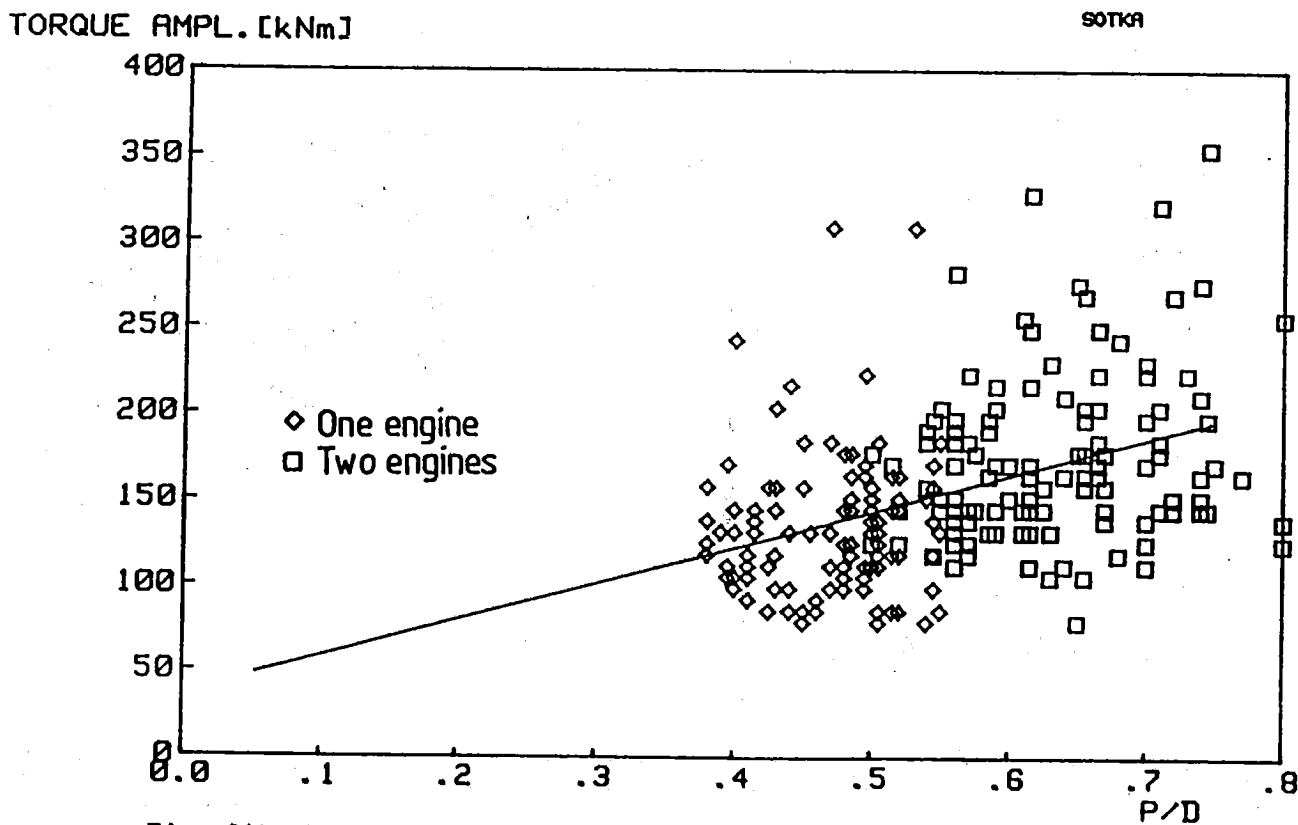


Fig. 21b. The measured propeller pitch versus torque amplitudes.

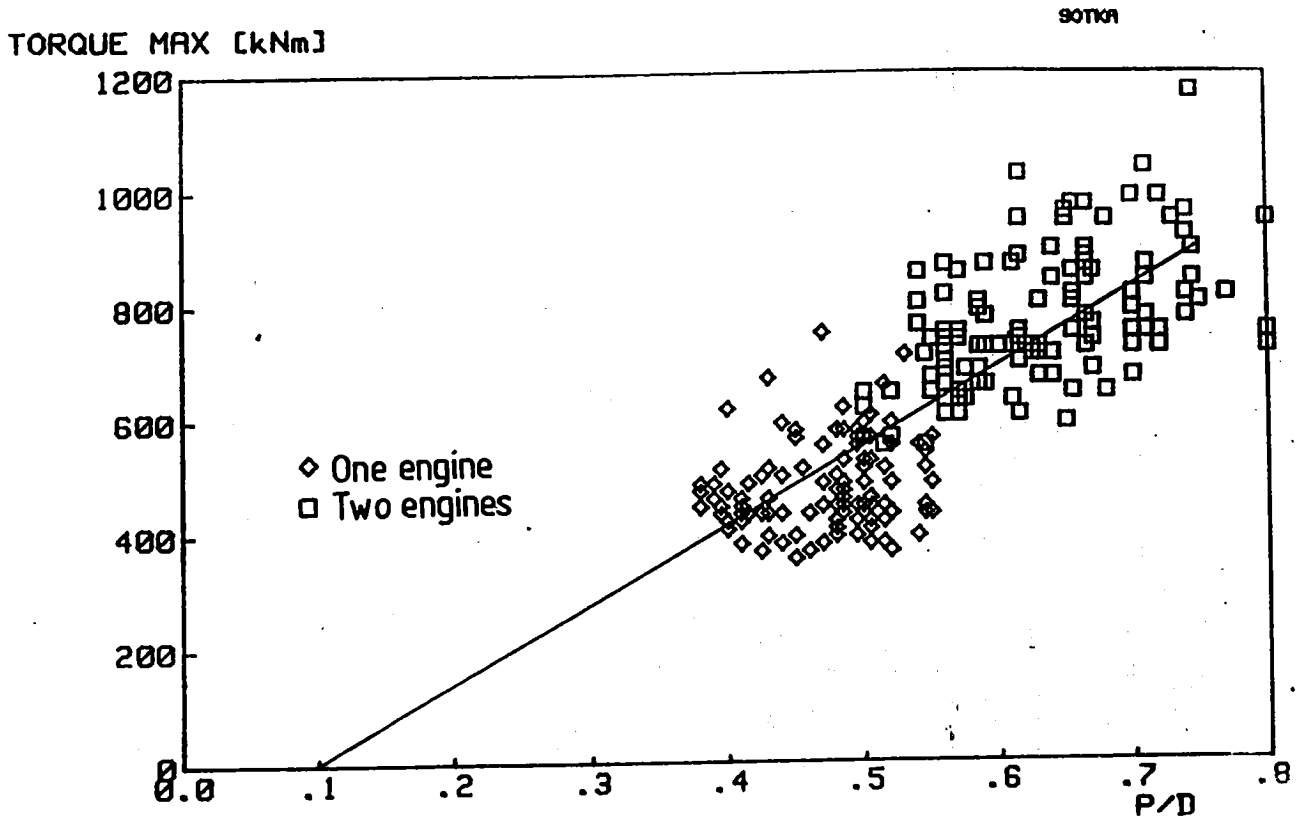


Fig. 21c. The measured propeller pitch versus maximum torque values.

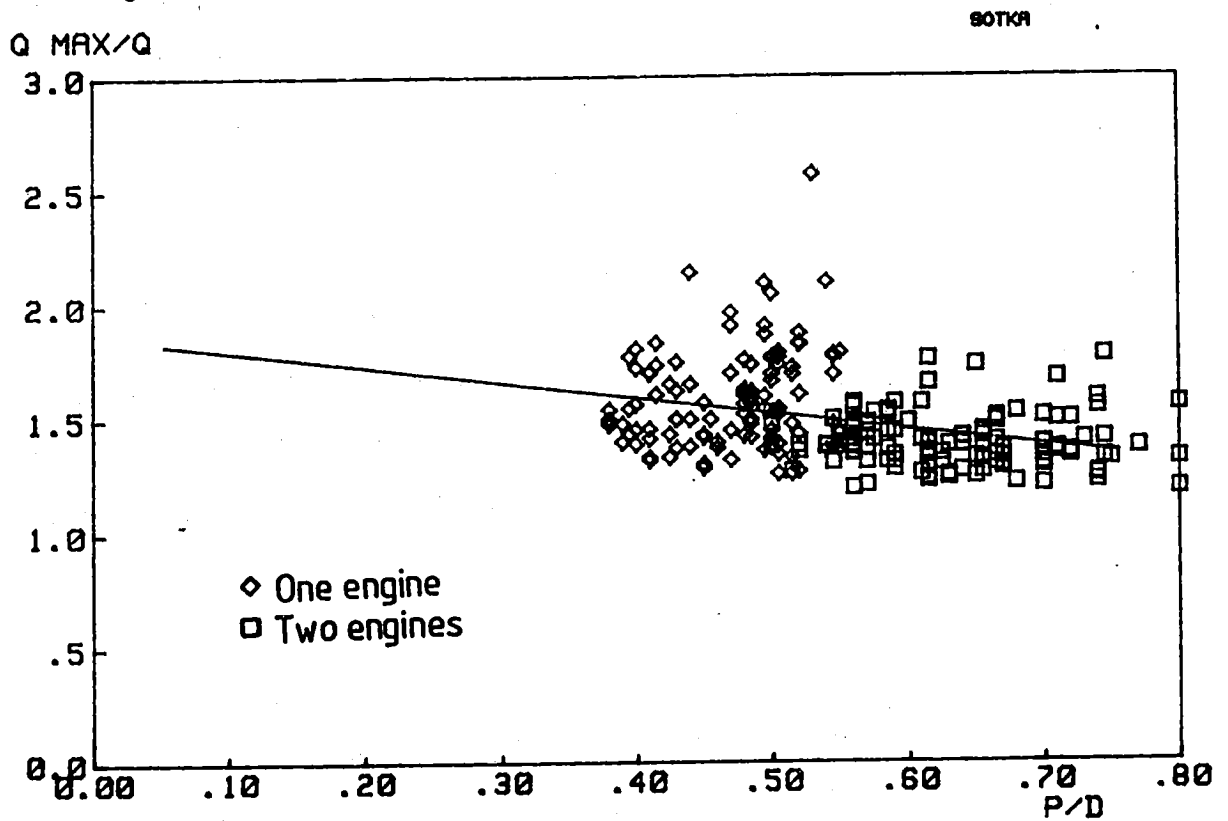


Fig. 21d. The measured propeller pitch versus maximum torque values divided by mean torques.

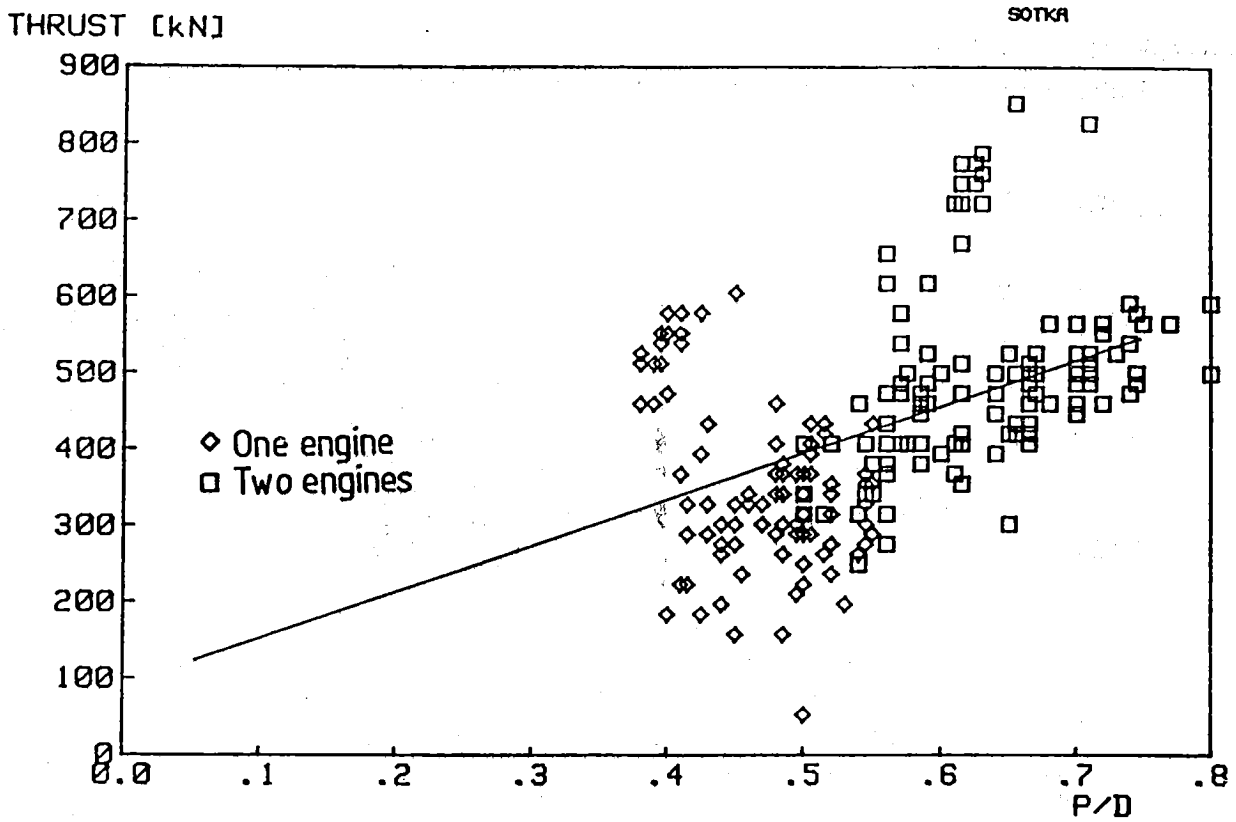


Fig. 21e. The measured propeller pitch versus mean thrust.

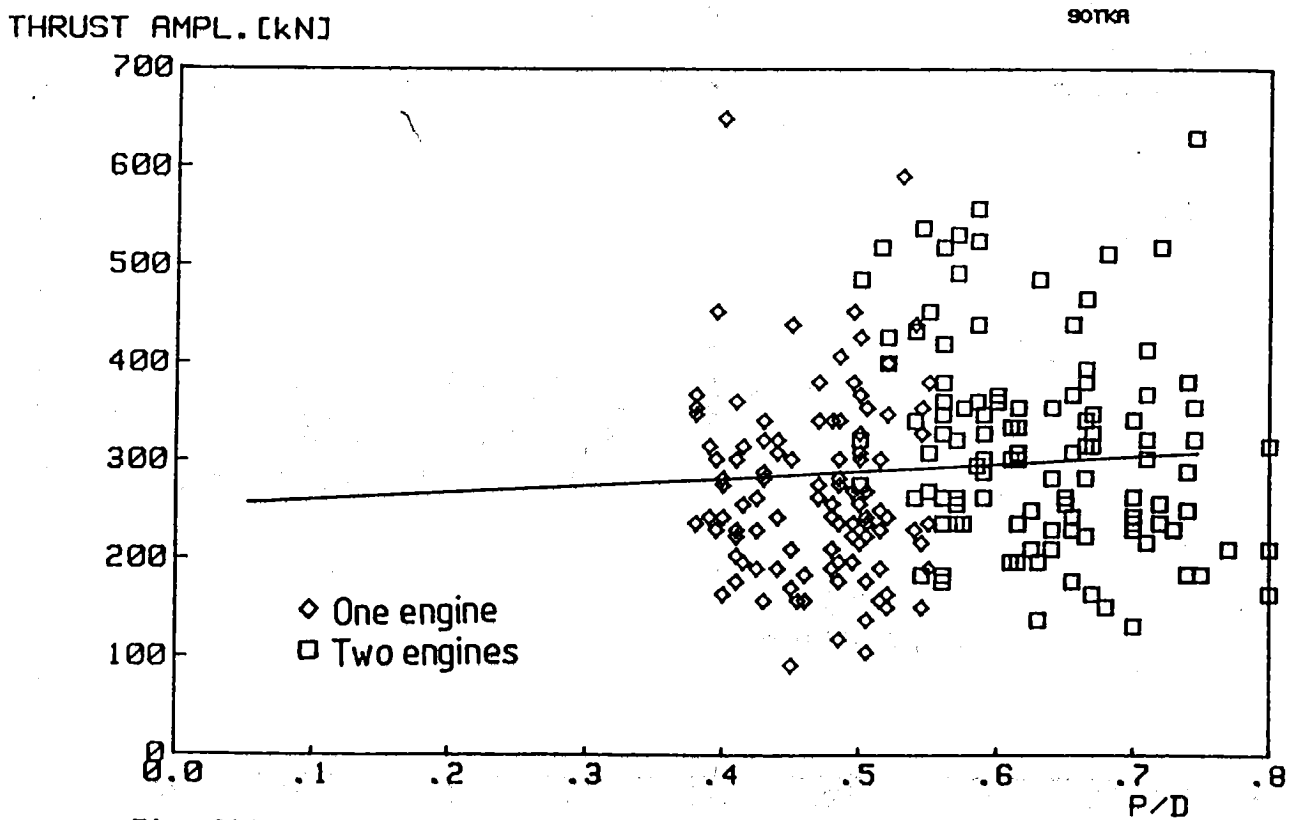


Fig. 21f. The measured propeller pitch versus thrust amplitudes.

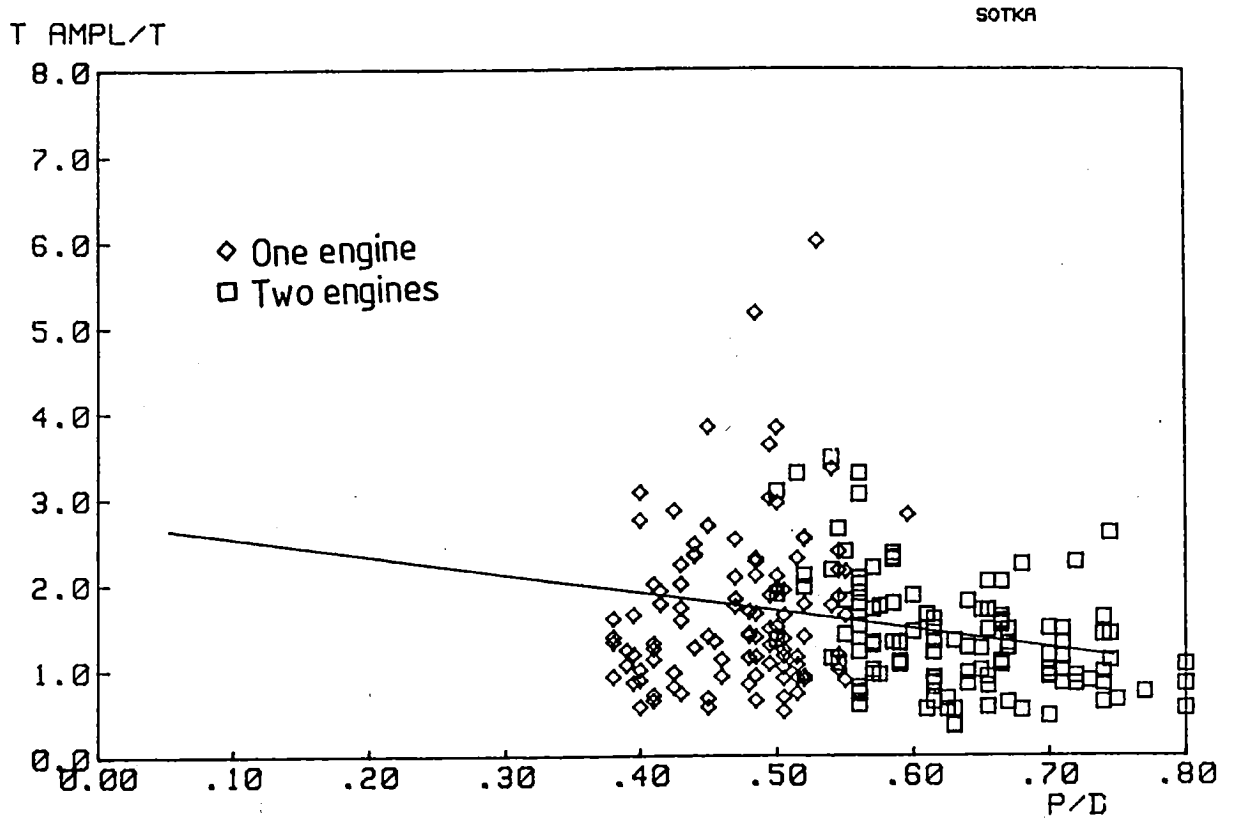


Fig. 21g. The measured propeller pitch versus thrust amplitudes divided by mean thrust.

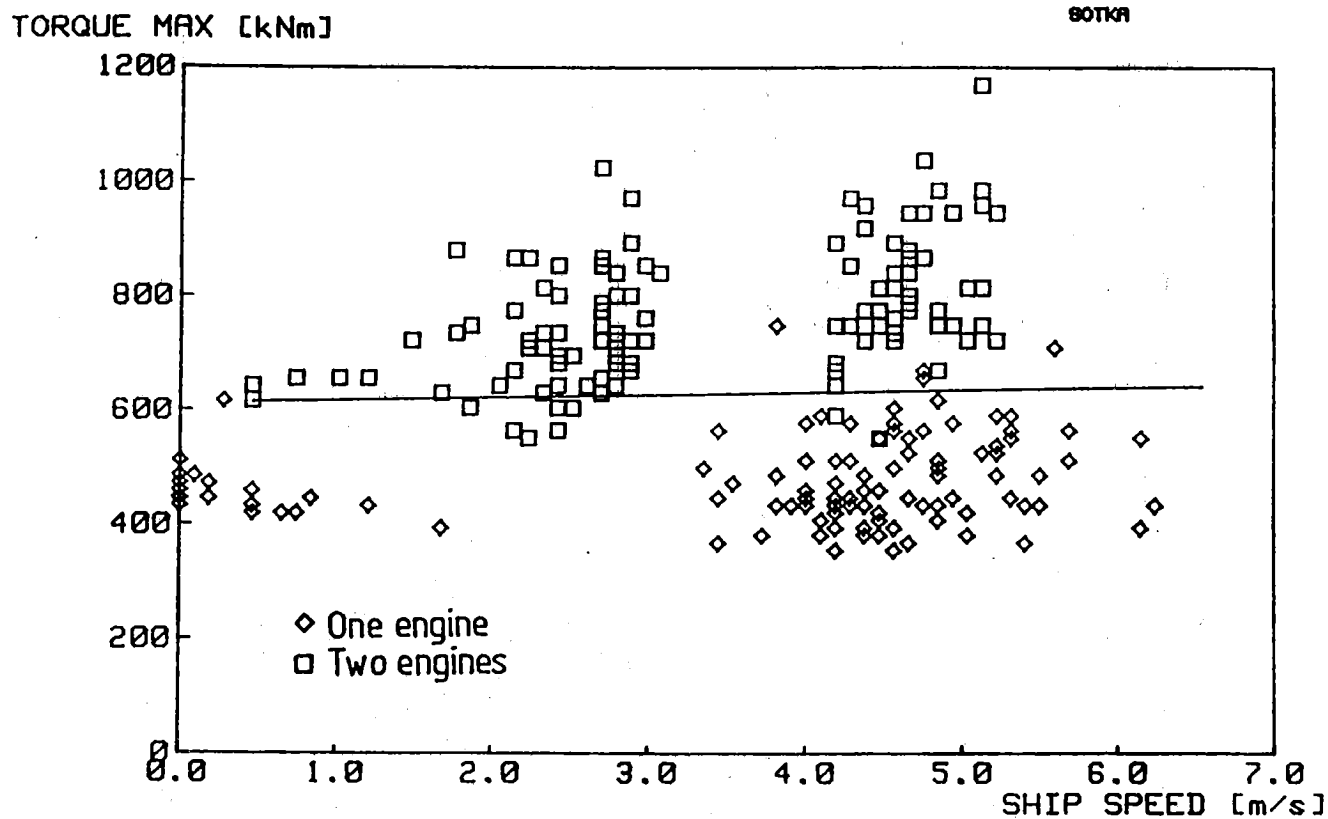


Fig. 22a. The measured ship's speed versus maximum torque values.

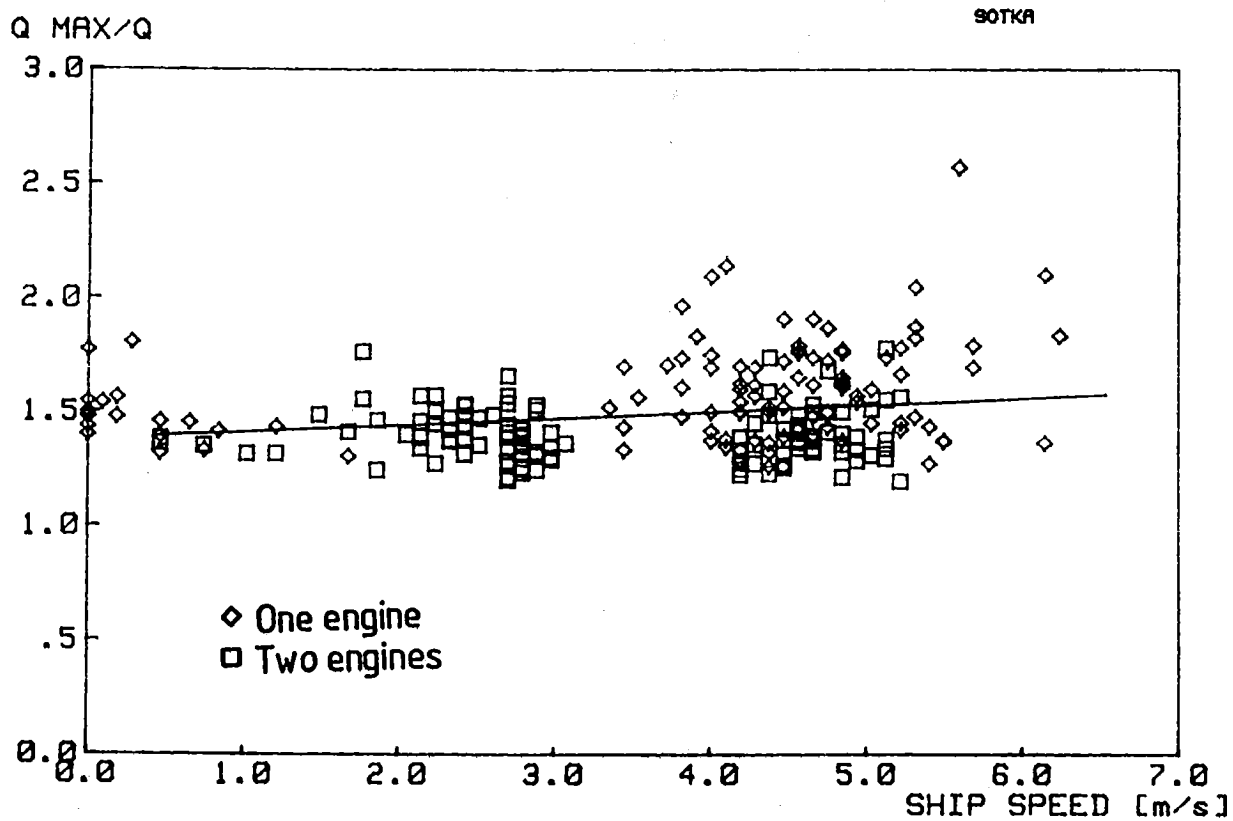


Fig. 22b. The measured ship's speed versus maximum torque values divided by mean torques.

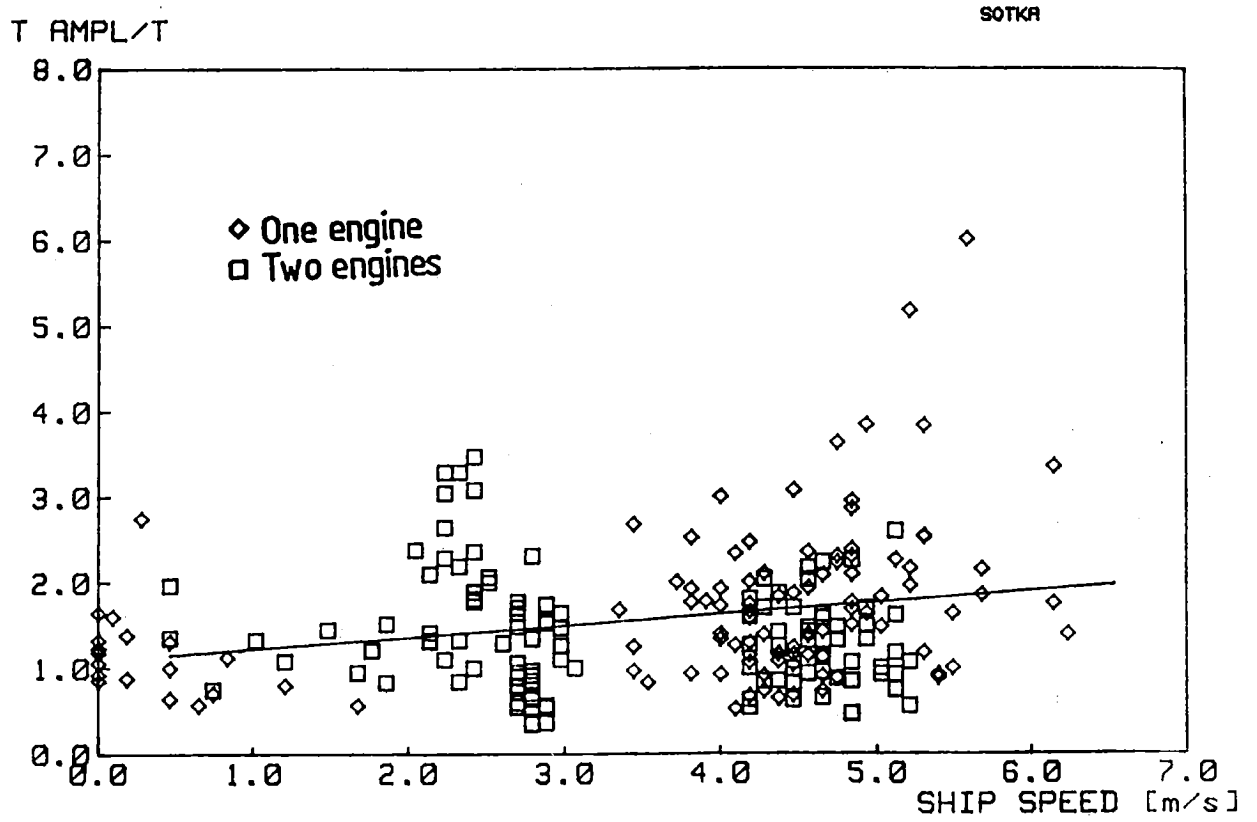


Fig. 22c. The measured ship's speed versus thrust amplitudes divided by mean thrust.

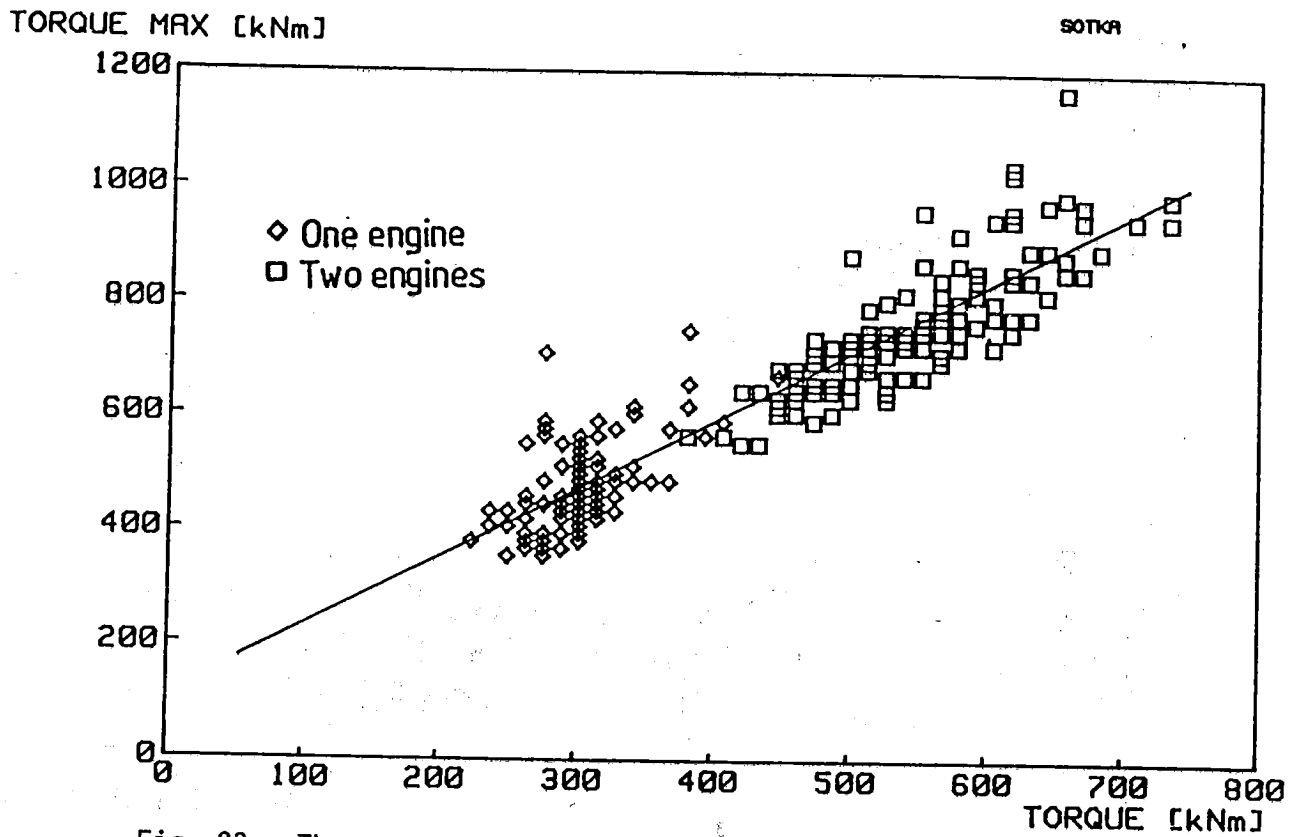


Fig. 23a. The measured mean torques versus maximum torque values.

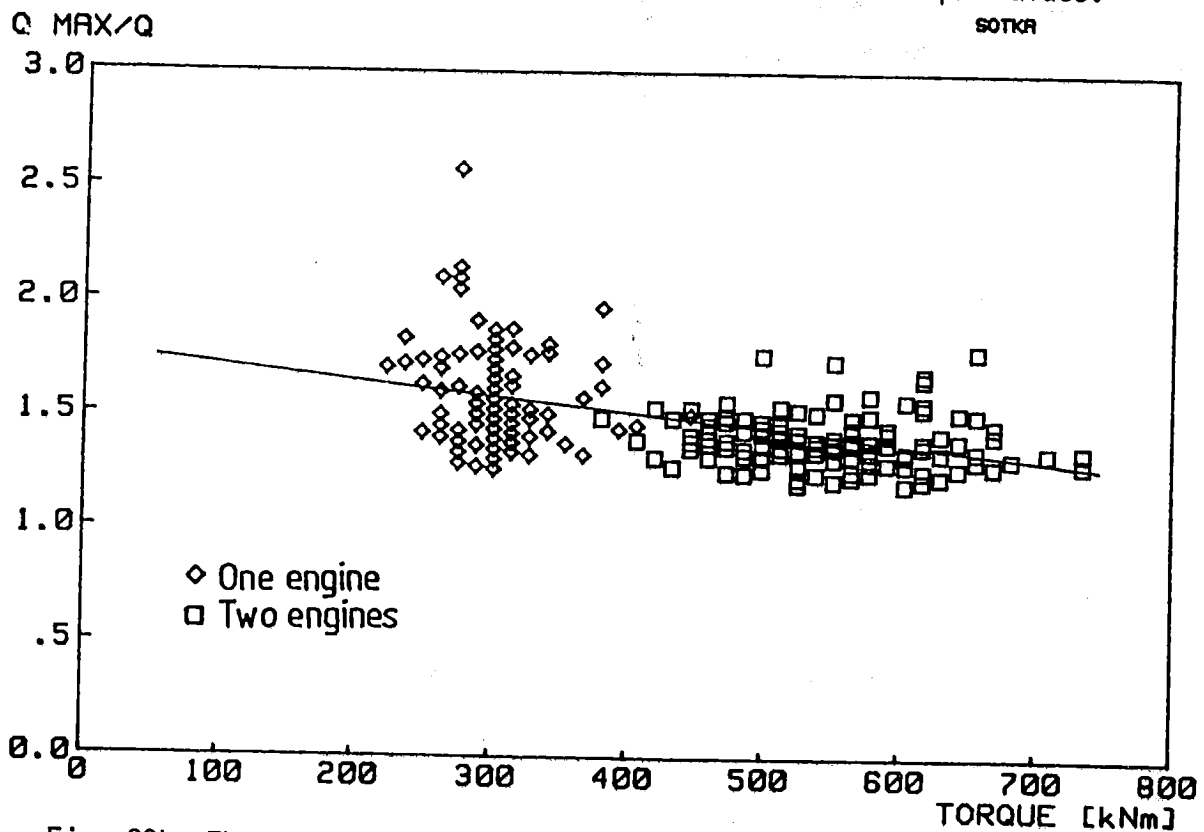


Fig. 23b. The measured nominal torque versus maximum torque values divided by mean torques.

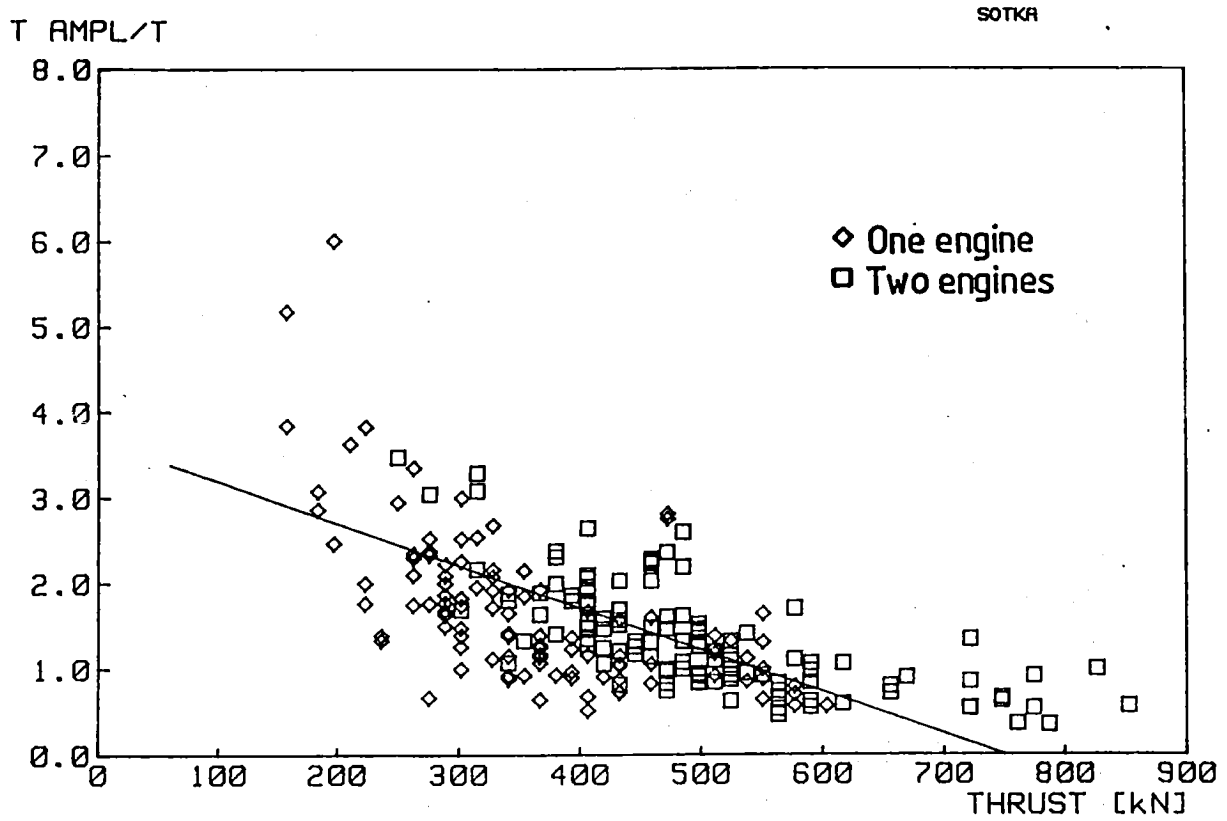


Fig. 24. The measured mean thrust versus thrust amplitudes divided by THRUST AMPL. [kN] mean thrust.

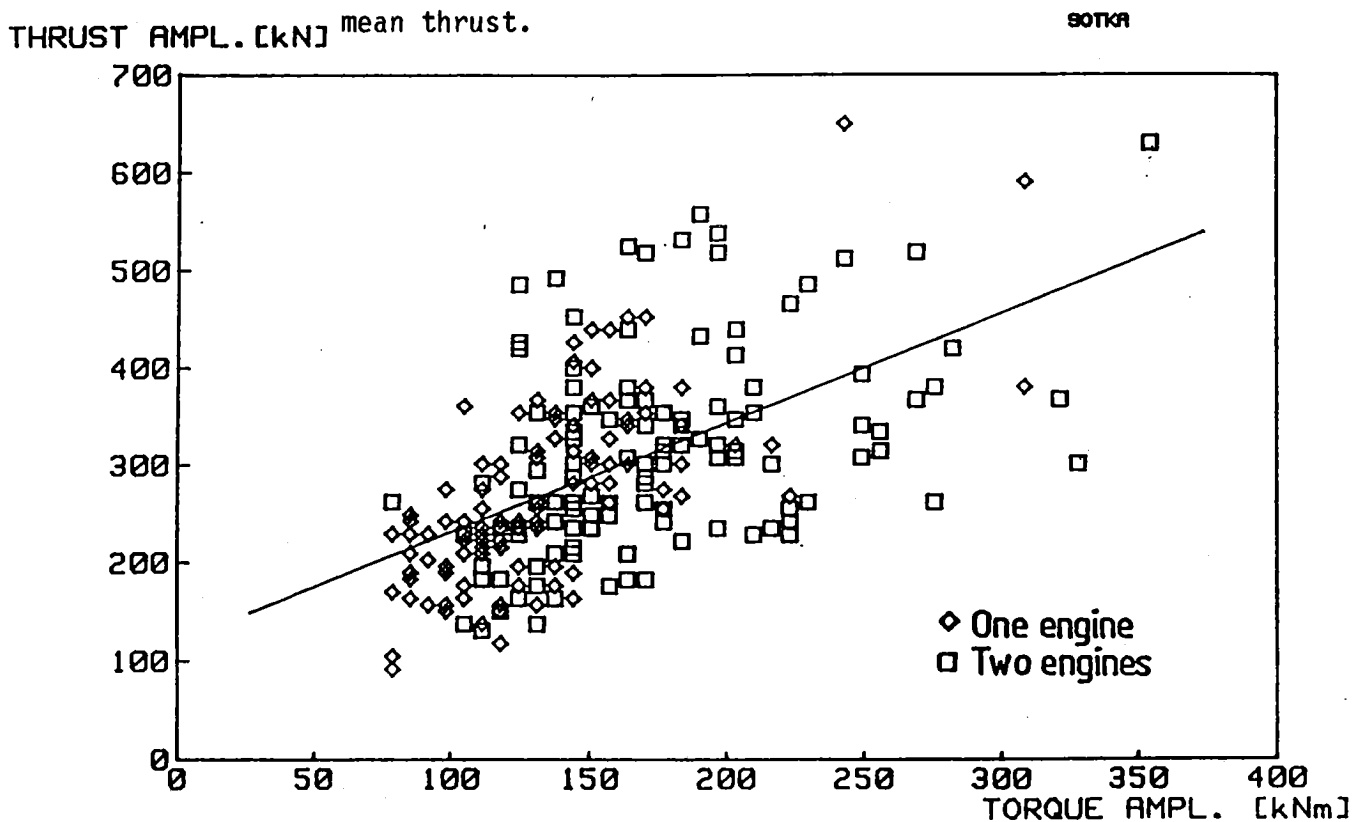


Fig. 25. The measured torque amplitudes versus thrust amplitudes.

When studying the diagrams one should keep in mind the following aspects, which may have twisted the tendencies appearing in the diagrams. Firstly some of the measured factors do not distribute uniformly to their whole range, but are concentrated in several groups according to changes in ice conditions and ship operations (e.g. Fig. 22a: ship in heavy and light ice conditions with one or two engines). Secondly all samples are picked up from such ice load situations, where there is one dominating vibration component in torque signals. Situations, in which no clear vibration frequency could be set apart, were not included. Thirdly the mean values of thrust can sometimes be a bit inaccurate due to the drift of zero-point. Sometimes also low frequency vibrations make it difficult to find the exact mean values of thrust and torque.

5.1.2 Discussion of the results

The time histories of the measured signals reveal the influence of ice conditions on the occurrence intensity of propeller ice loads. In heavy ice clogged channel and in ridged or rafted ice there are continuously ice impacts on propeller blades. In level ice or in pack ice propeller ice loads occur more occasionally and there are often long periods without any significant ice impacts.

Propeller ice loads seem to be mostly caused by loose ice blocks causing short series (normally 3-12) of successive response oscillation. The frequencies of ice induced torque peaks are mostly in the range 6.0 - 7.5 Hz, while the blade frequency is about 8 Hz. It has to be noted that one of the natural frequencies of the shafting system is inside that range. This means that short impact loads will excite the corresponding natural mode and its effect will be seen from the measured signals. Another explanation for lower response frequency may be the possibility that the smaller ice floes will entrain the propeller. The tendency of decreasing response frequency with increasing pitch may be in connection with changes of added mass

of the propeller and stronger rotation of ice pieces as a function of the pitch. In the short-term measurements the only milling situations clearly in blade frequency were measured, when the ship was going astern.

The torque strain gauges Q3 and Q4 placed on opposite sides of the reduction gear showed, that vibrations in frequency band 5-15 Hz, e.g. vibrations induced by ice loads, propeller blades and engine speed, passes the gear and clutch coupling nearly undamped. On the other hand vibrations in frequencies over and under that band, e.g. vibrations induced by engine torque and propeller shaft speed, were absorbed quite efficiently. Comparison between torque signals Q2 and Q3 showed no significant differences in torque in different parts of the propeller shaft. This is in good accordance with the fact that there are no major mass concentrations between these two measuring points.

In thrust the strongest ice-induced vibrations appeared in the range 14-16 Hz and sometimes also in frequencies about 8 Hz. Vibrations in the area 14-16 Hz are apparently caused by one or more natural frequencies in the area. The natural frequencies of longitudinal vibrations have not, however, been calculated. When the ship was backing thrust vibrations were relatively weak. This resulted most likely from small longitudinal component of ice impacts due to convenient angle of attack between propeller blades and ice blocks.

Rotational speed of the propulsion machinery maintained its nominal value quite well in ice conditions. During short-term measurements the maximum decrease of the nominal rpm was with one engine about 15 % and with two engines about 8 %. The load control system operated quite efficiently and deviations were in all cases corrected in less than five seconds. After greater deviations the rotational speed often temporarily exceeded the nominal value. The exceedings were 5 % in maximum.

A big scatter exists in the measured torque and thrust peaks as shown in Figs. 20 ... 25. Some general tendencies can, however, be seen in the plotted relationships. The increase of the torque amplitudes as a function of the pitch ratio is more pronounced than the increase of thrust amplitudes (see Fig. 21b and 21f). The ratio of maximum torque per mean torque is slightly decreasing with increasing mean torque (see Fig. 23b). This effect is much stronger for the thrust amplitudes as can be seen in Fig. 24. Fig. 25 illustrates the clear correlation in the measured thrust and torque amplitudes.

5.2 Results of the long-term measurements

5.2.1 Analysis of the results

The results of the long-term measurements are presented in form of distribution histograms. Torque $Q(0-20 \text{ Hz})$ and propeller shaft power are presented in level distributions. Thrust and torque frequency band channels and rudder torque are presented in amplitude distributions. The histograms covering the measurements of both winters are shown in Fig. 26. (The distribution histogram of thrust frequency band $T(0.02-5 \text{ Hz})$ includes only the measurements of winter 1984). The histograms for both winters separately and some examples of daily histograms are shown in Appendix 3. In rudder torque histograms the marking forward/astern indicates whether the amplitudes were measured when the ship was going forward or when she was backing.

In thrust histograms the positive sign means increase of thrust and negative sign decrease of thrust.

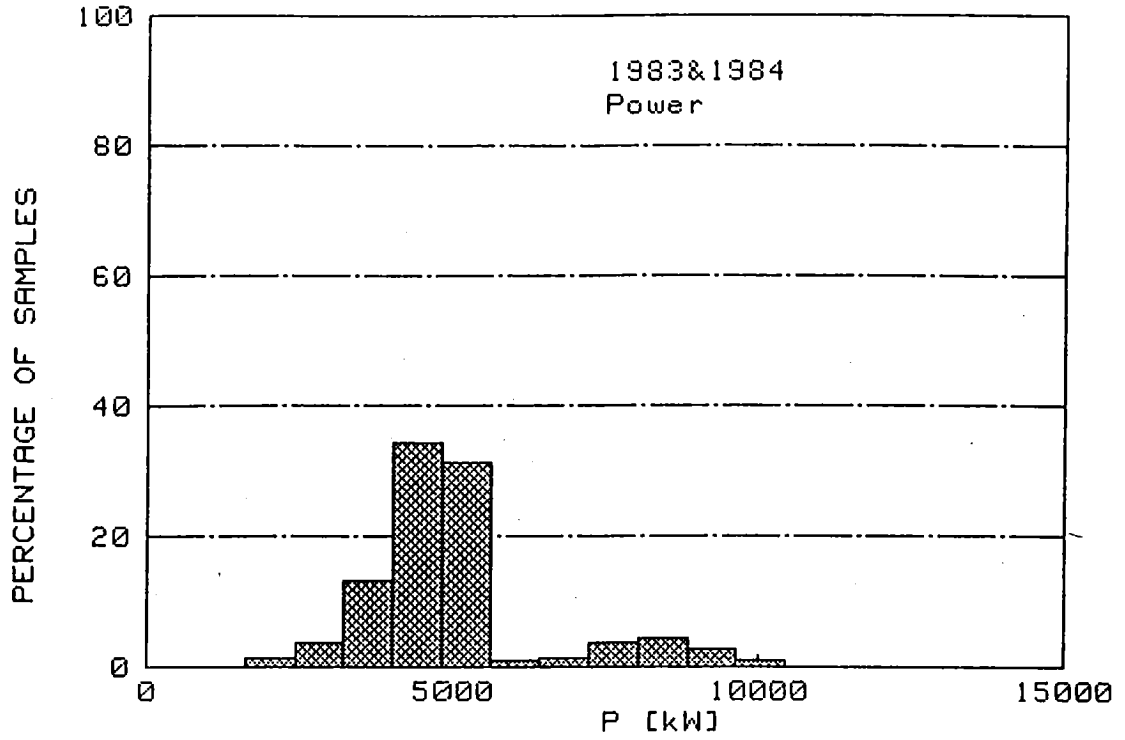


Fig. 26a. Power (84 days, 1191.5 h at sea)

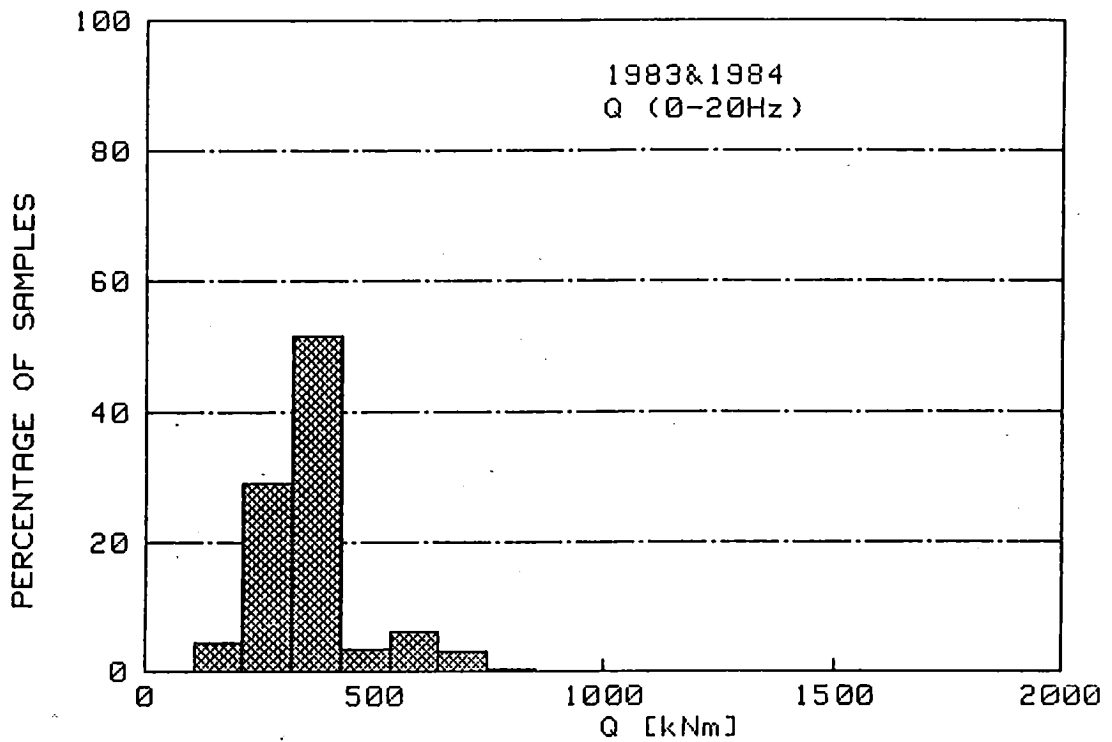


Fig. 26b. Torque Q(0-20 Hz) (95 days, 1389.5 h at sea).

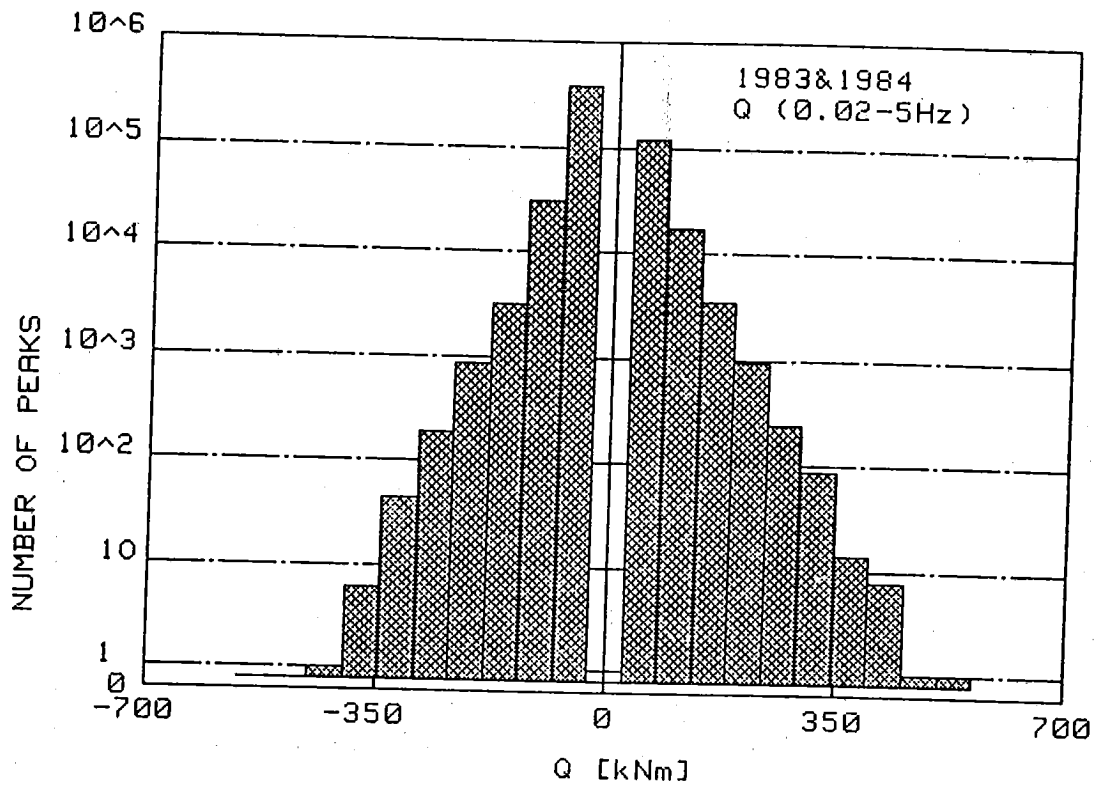


Fig. 26c. Torque $Q(0.02-5 \text{ Hz})$ (91 days, 1321 h at sea).

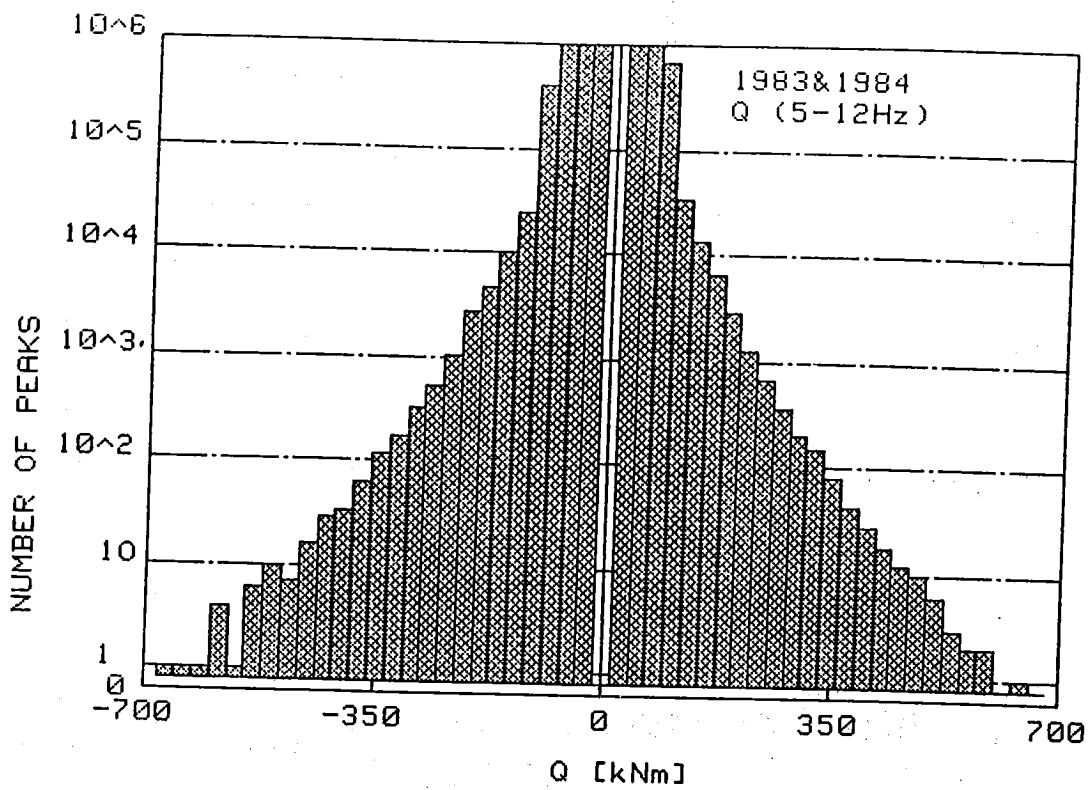


Fig. 26d. Torque $Q(5-12 \text{ Hz})$ (90 days, 1297 h at sea).

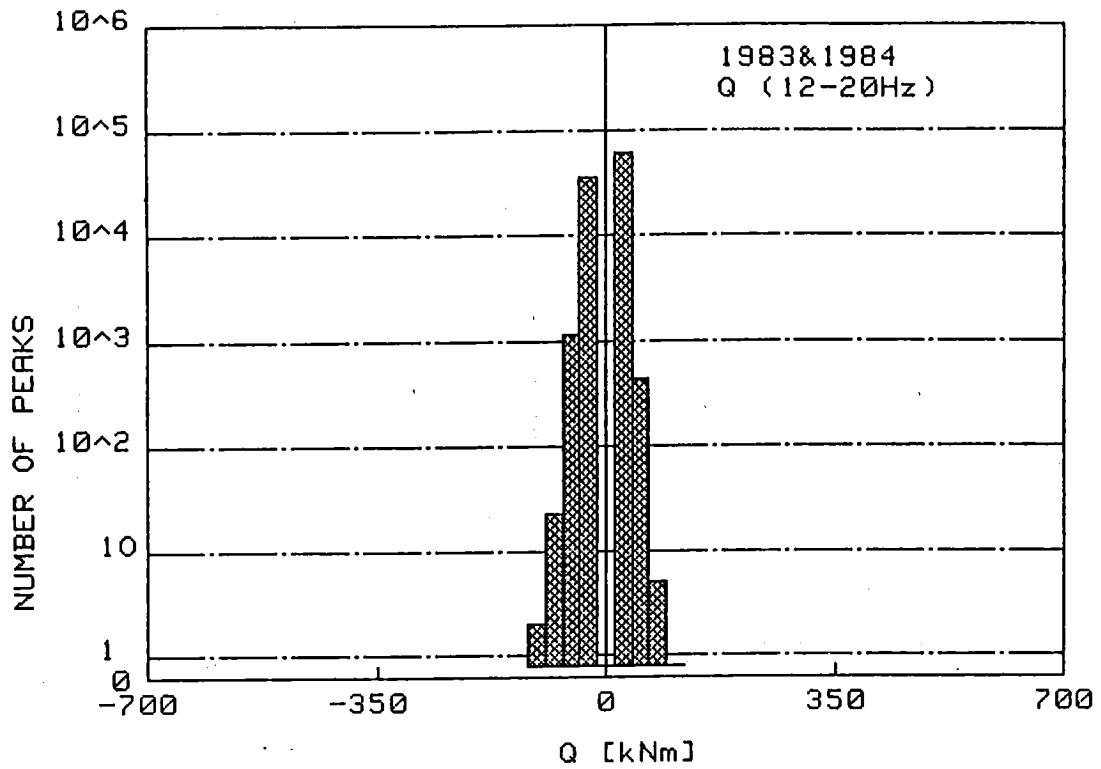


Fig. 26e. Torque Q(12-20 Hz) (89 days, 1284 h at sea).

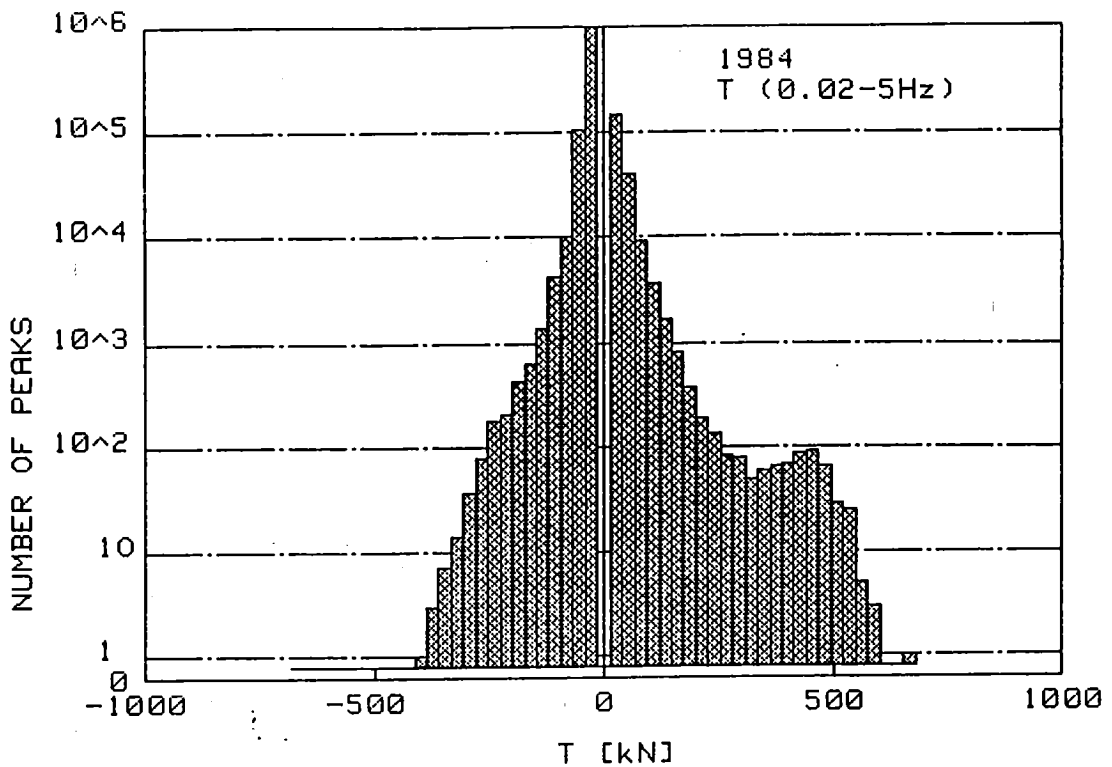


Fig. 26f. Thrust T(0.02-5 Hz) (44 days, 660 h at sea).

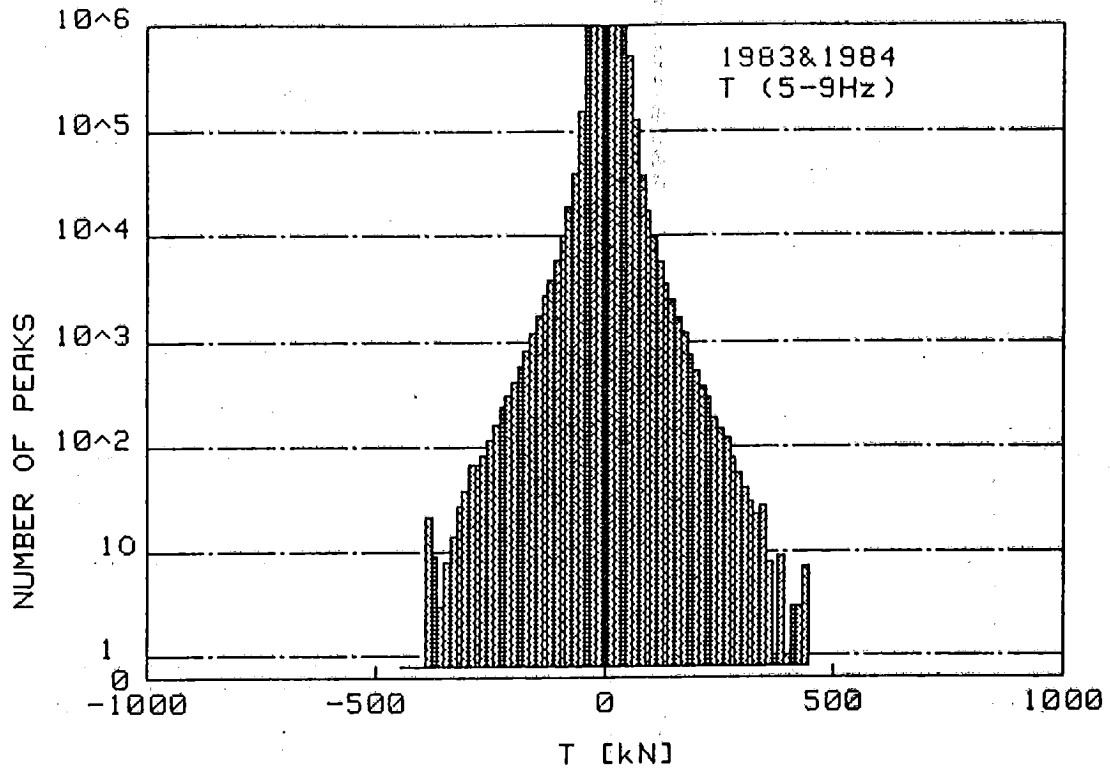


Fig. 26g. Thrust T(5-9 Hz) (88 days, 1287 h at sea).

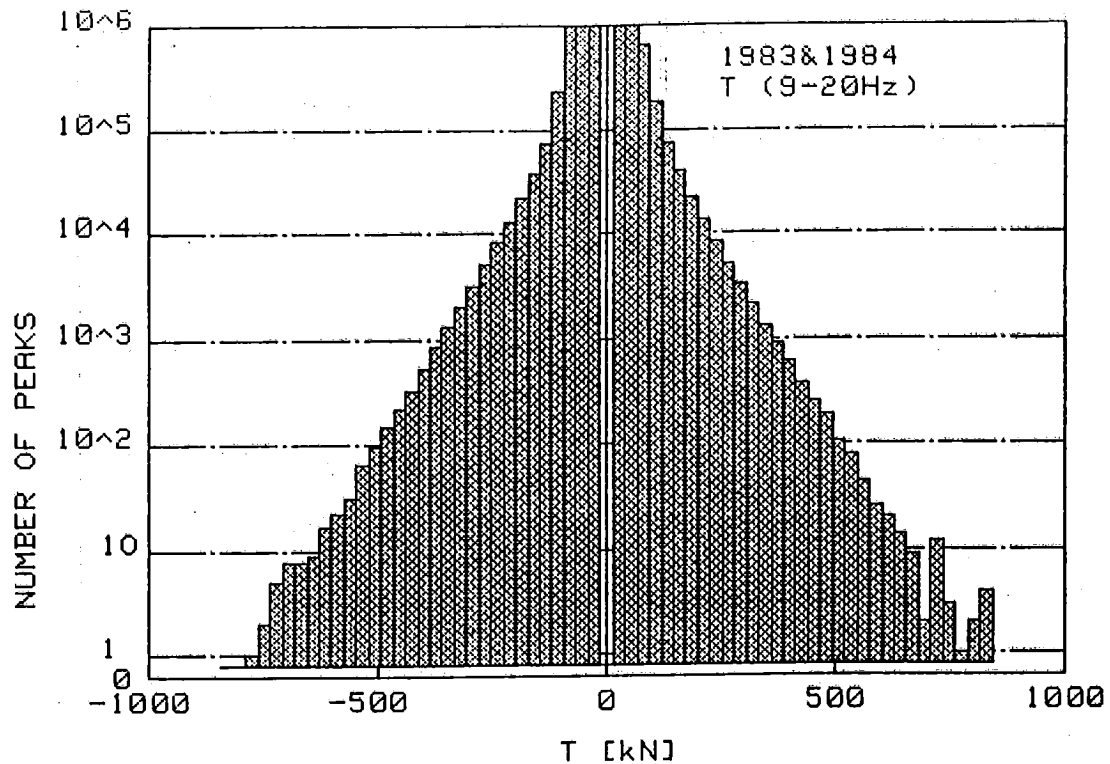


Fig. 26h. Thrust T(9-20 Hz) (88 days, 1287 h at sea).

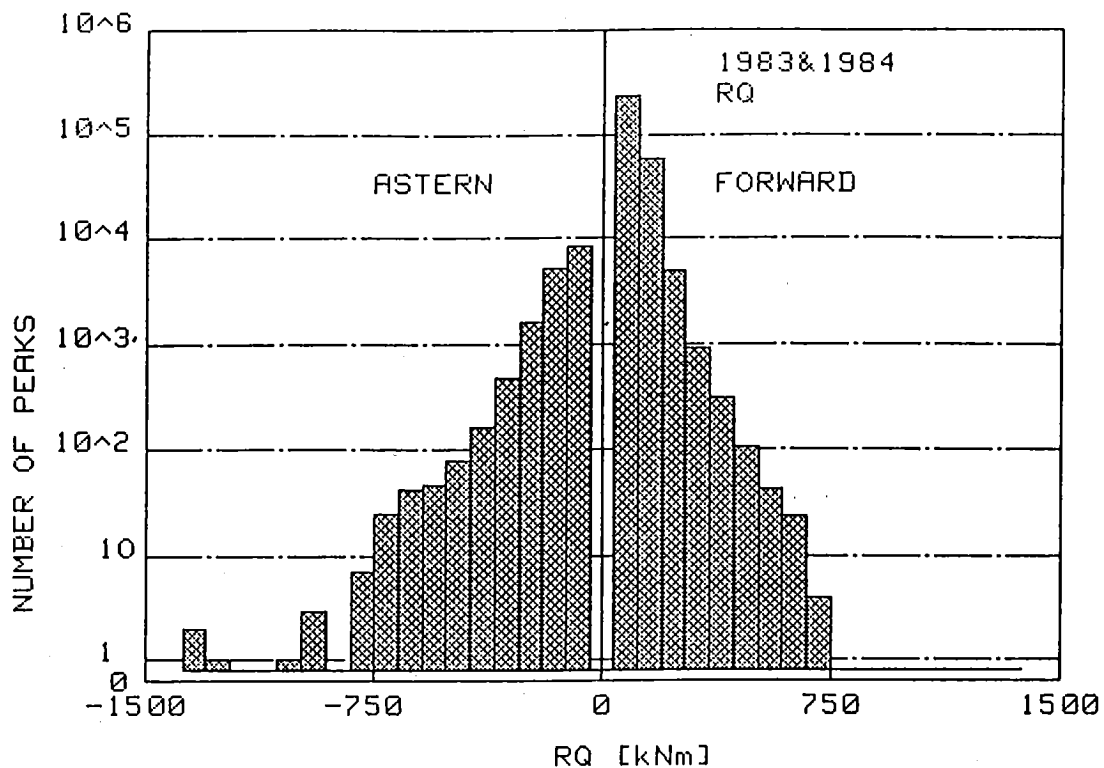


Fig. 27. Rudder torque RQ (87 days, 1258.5 h at sea).

The daily maximum values together with the schedule of Sotka are presented in Tables 5 and 6. The maximum measured values of both winters have been encircled. The noting east/west in the remarks column indicates from which side Sotka has passed the Ahvenanmaa-archipelago.

5.2.2 Discussion of the results

The maximum measured torque values were about twice the maximum mean torque (about 850 kNm). The maxima of the dynamic part of torque, which were registered in the middle frequency band Q(5-12 Hz), were about 80 % of the maximum mean torque. Considerable vibrations appeared in two lower frequency bands, whereas the vibrations in the highest band were quite insignificant.

Table 6. Cont.

Date	Time	Harbour	Draught Remarks aft [m]	Q (0-20 Hz) [kNm]	Q (0.02-5 Hz) [kNm]	Q (5-12 Hz) [kNm]	Q (12-20 Hz) [kNm]	T (0.02-5 Hz) [kN]	T (5-9 Hz) [kN]	T (9-20 Hz) [kN]	RQ form. [kNm]	RQ ast. at sea [kNm]	RQ Measurement at sea [h,min]
14.3	17.25	Dep. Oulu	6.40	1227	427	400	53	507	413	667	709	1339	6.35
15.3				1227	320	347	53	560	387	613	709	709	24.00
16.3	19.00	Arr. Porvoo		907	160	187	27	560	173	400	394	236	19.00
17.3	06.10	Dep. Porvoo	9.70	800	160	187	27	533	240	293	472	236	17.50
18.3	00.15	Arr. Naantali		267	53	27	0	53	40	133	157	0	0.15
19.3	01.20	Dep. Naantali	9.55	587	107	133	27	533	133	320	315	236	12.55
14.15		Arr. Pori											
20.3	11.30	Dep. Pori	6.65	800	160	213	27	427	133	213	236	236	12.30
21.3	19.00	Arr. Porvoo		800	160	187	27	533	227	427	236	787	19.00
22.3	08.30	Dep. Porvoo	9.70	800	160	213	27	480	133	373	315	236	15.30
23.3				907	160	240	27	320	293	400	551	157	24.00
24.3	16.05	Arr. Oulu		1227	427	240	53	507	360	507	630	315	16.05
25.3	05.15	Dep. Oulu	6.70	1333	373	347	53	507	387	747	472	787	18.45
26.3				480	107	160	27	107	173	213	236	0	24.00
27.3	08.30	Arr. Porvoo		1120	320	240	53	533	333	560	472	157	7.30
19.10		Dep. Porvoo	8.90										
23.20		Arr. Helsinki											
28.3													
29.3	06.25	Dep. Helsinki	6.70										
11.10		Arr. Porvoo											
19.10		Dep. Porvoo	9.15										
30.3													
31.3	16.35	Arr. Kokkola											
1.4	11.50	Dep. Kokkola											
13.05		Arr. Kokkola											
2.4	06.00	Dep. Kokkola	6.60										
3.4	08.35	Arr. Naantali											
4.4	00.35	Dep. Naantali	9.45	693	213	187	27	453	227	720	394	236	9.30
5.4	17.25	Arr. Kemi											
6.4	08.20	Dep. Kemi	6.70										
7.4													
8.4	07.10	Arr. Porvoo		480	107	133	27				315	79	6.10
17.50		Dep. Porvoo	9.70										
9.4	10.35	Arr. Naantali											
20.40		Dep. Naantali	6.40										
10.4	12.50	Arr. Porvoo											
11.4	03.00	Dep. Porvoo											
03.30		Arr. Porvoo											
14.10		Dep. Porvoo	9.60										
12.4	07.10	Arr. Naantali											
15.35		Dep. Naantali	6.55										
13.4	07.30	Arr. Porvoo	9.05										
18.20		Dep. Porvoo											
14.4	03.10	Arr. Hamina											
17.15		Dep. Hamina	6.55										
15.4	01.10	Arr. Porvoo		480	160	187	53				394	0	11.05
12.55		Dep. Porvoo	9.70										
16.4				480	53	80	27	80	107	213	472	0	24.00
17.4	18.30	Arr. Oulu											
18.4	08.45	Dep. Oulu	6.50	1333	480	320	80	667	440	827	630	315	14.15
19.4				587	107	160	27	160	173	640	236	0	24.00
20.4	07.35	Arr. Porvoo											

Table 6. cont.

In thrust signal considerable vibrations appeared in all three frequency bands. The maximum values were measured in the highest frequency band where there is an apparent natural frequency somewhere in the area 14-16 Hz. Compared to the bollard pull thrust value 1320 kN (an estimate from the model tests) the dynamic part was about 65 %.

The power measurements show, that the ship operates mainly with one engine also during the winter seasons. Only approximately 15 % of the measured time at sea both engines were used. As could be expected, two engines were used primarily when operating in northern part of the Gulf of Bothnia. The average power level was in general a bit lower in 1983 than in 1984.

The maximum rudder torque values were measured when the ship was going astern. The measured maximum was about 1340 kNm. The maxima measured when the ship was going ahead were about half of the maxima of backing situations.

The influence of draught on ice loads was also one subject of interest. In the results of the long-term measurements there was a slight tendency that in ballast condition (draught about 6.6 m) there were a little more and higher ice loads than in loaded condition (draught about 9.5 m). Due to changing ice conditions the results were, however, a bit inconsistent and therefore no firm conclusions can be drawn.

The distribution of the measured maxima according to the ship's operational area met quite well the expectations. The highest ice load values were measured in the northern part of the Gulf of Bothnia, but also in the Gulf of Finland, above all in the eastern part of it, the measured maxima were nearly as high. Furthermore it should be noted, that some of maximum of the long-term measurements were measured during ice trials, during which the operation of the ship was a bit exceptional.

5.3 Extrapolation of extreme values

Due to changing ice conditions and casual nature of ice loads, measurements do not usually yield the real maximum ice load values. Maximum values can, however, be evaluated even from a relatively short period of measurements by means of extreme value statistics. In this study the extrapolated extreme values were obtained by applying the Gumbel asymptotic method, the cumulative distribution functions of which are as follows:

$$H(y_n) = e^{-e^{-c(y_n - u)}} \quad \text{Type I}$$

$$H(y_n) = e^{-\left(\frac{b - y_n}{b - v}\right)^k} \quad y_n \leq b, v < b \quad \text{Type III}$$

Parameters c , u , b , v and k were calculated from a distribution of the measured daily maximum values.

In the extrapolation was primarily used type III function, which includes a prediction of the absolute maximum (upper limit b). In those cases, where type III function could not be fitted to the measured data due to the great range of variations, type I function was used instead. Return period values were obtained by formula

$$T = \frac{1}{1 - H(y_n)}$$

The daily maxima distributions formed the basic set of samples, to which the cumulative distribution functions were fitted. The maxima distributions included the results from both winters, except the distribution of thrust frequency band (0.02-5 Hz), in which only the 1984 maxima were included. The extreme distributions of rudder torque were calculated separately for forward and astern maxima distributions, and also for a united maxima distribution, to which

the absolute daily maximum values were picked up disregarding whether they were from forward or astern measurements.

The results of the extreme value calculations are shown in Figs. 27 ... 29. In the upper parts are presented the maxima distribution and in the lower parts are drawn the extreme value curves as a function of return period. In Table 7 the extreme values are presented also in a numerical form. When studying the extrapolated results it must be remembered that they are based on the measured results from two quite mild winters.

Table 7. Extrapolated extreme values

Channel		Extrapolated extreme values				Measured maximum values
		Return period [days]				
		10	100	1000	b	
Q (0-20 Hz)	[kNm]	1230	1700	2070	3440	1650
Q (0.02-5 Hz)	[kNm]	340	520	700	2730	530
Q (5-12 Hz)	[kNm]	330	530	710	-	640
Q (12-20 Hz)	[kNm]	50	80	110	-	80
T (0.02-5 Hz)	[kN]	610	650	655	660	590
T (5-9 Hz)	[kN]	320	500	670	4000	440
T (9-20 Hz)	[kN]	580	900	1170	3440	830
RQ	[kNm]	780	1200	1580	-	1340
RQ forward	[kNm]	630	770	840	920	710
RQ astern	[kNm]	760	1250	1730	-	1340

The extrapolated ice load values of the propeller shaft torque can be compared to the maximum torque calculated according to the Finnish-Swedish ice rules. The maximum torque of the rules is obtained by adding the calculated ice torque ($M = m \cdot D^2$, $m = 2.15$, $D = 5.45$ m) to the maximum mean torque (≈ 850 kNm). The ice torque gets the value of 630 kNm and thus the maximum torque is about 1480 kNm. From the extreme value curve of Fig. 27a can be seen that for product tanker Sotka approximately 35 days of navigation in winter time is required to reach that value. Consequently a torque peak having the order of magnitude given by the ice rules occurs some 3 - 4 times during one winter.

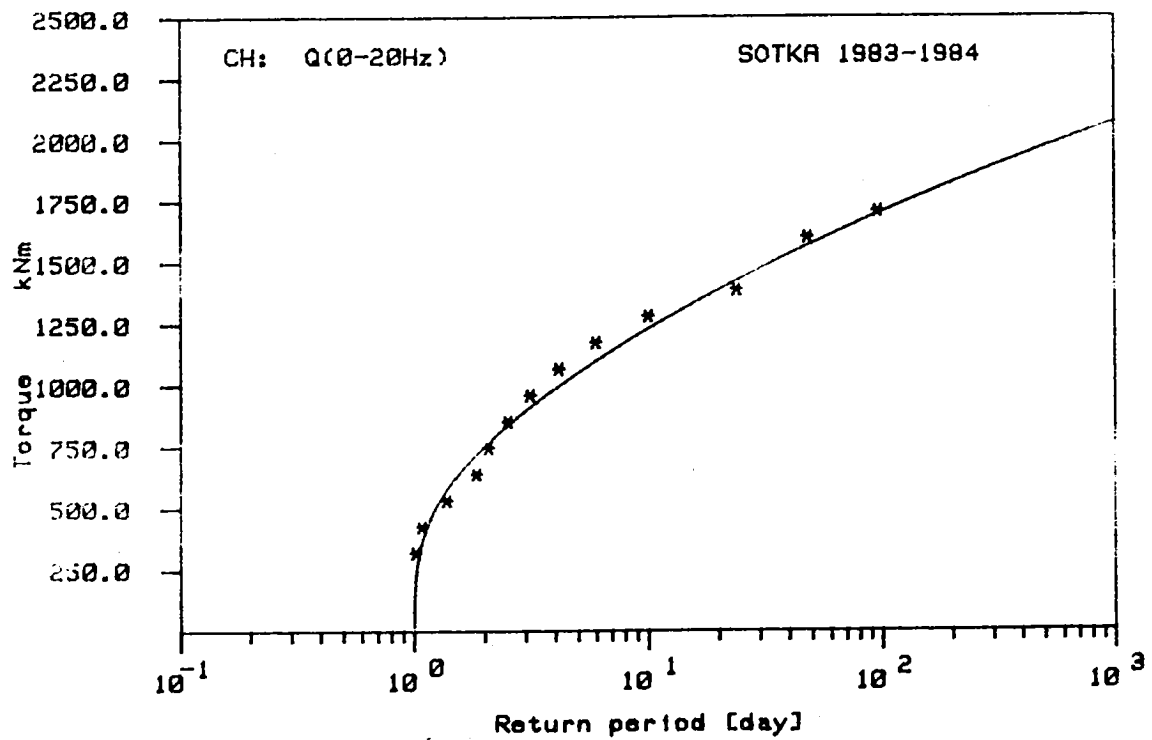
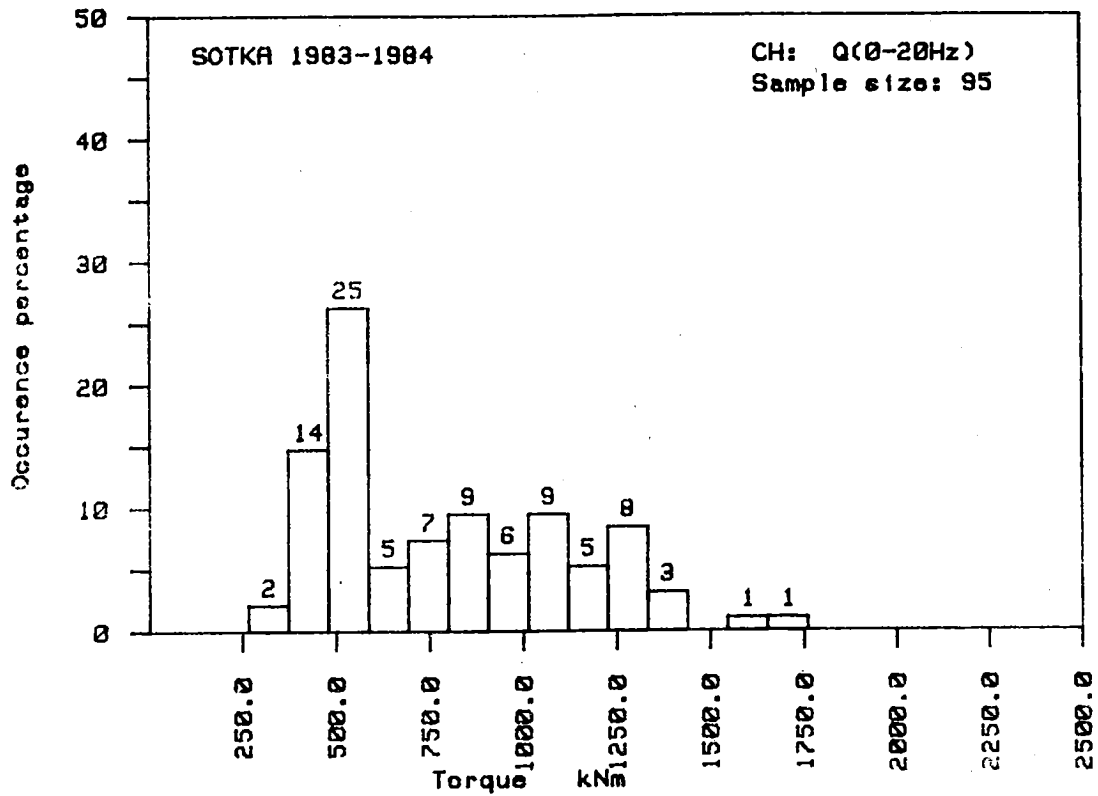


Fig. 27a. Gumbel III distribution fitted on the measured daily maxima of torque Q2 (0-20 Hz).

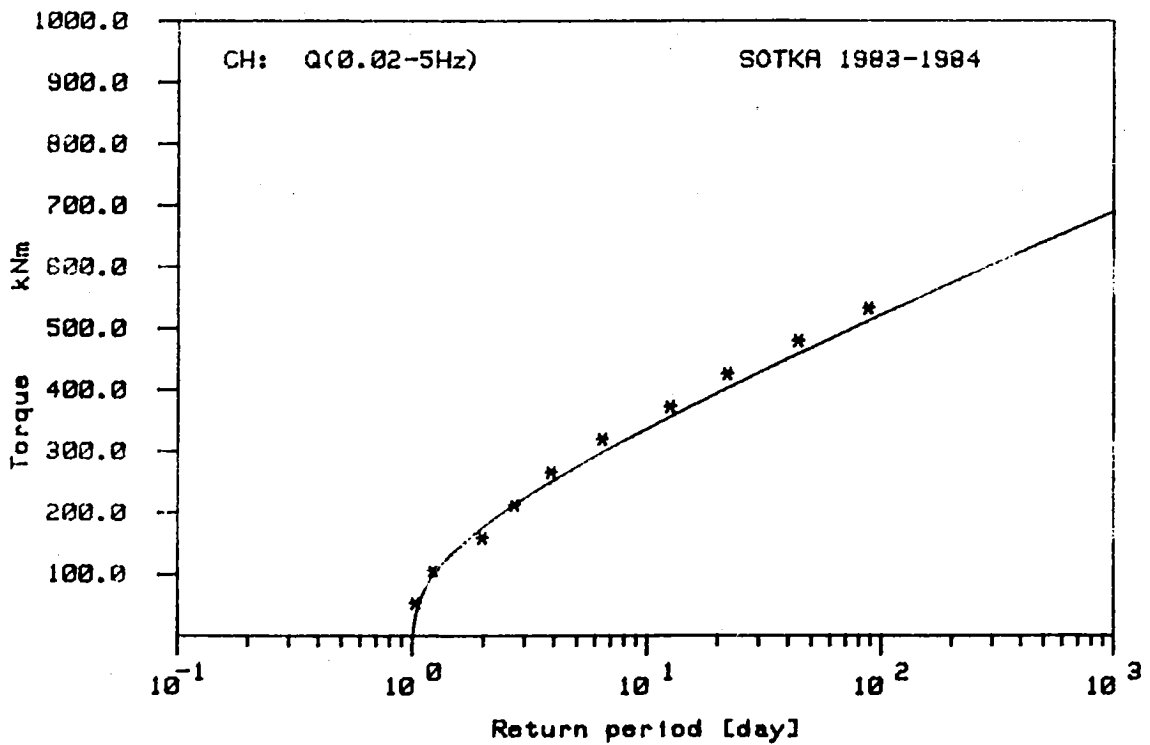
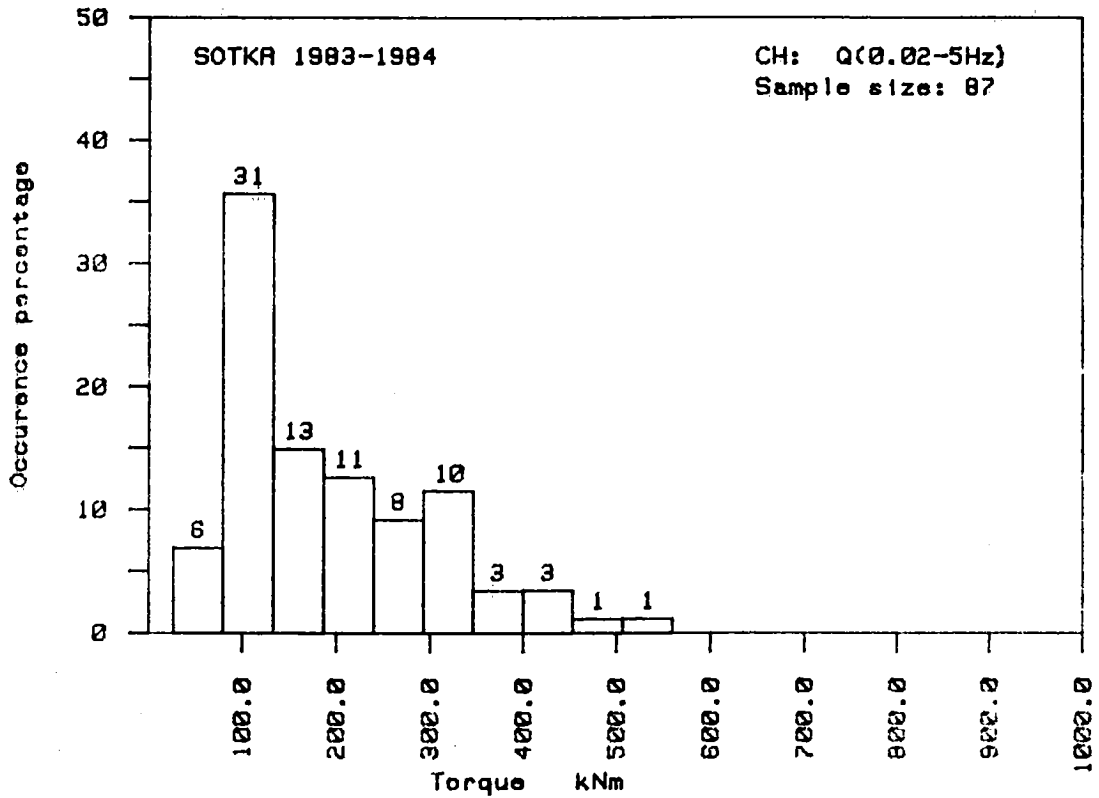


Fig. 27b. Gumbel III distribution fitted on the measured daily maxima of torque Q2 (0.02-5Hz).

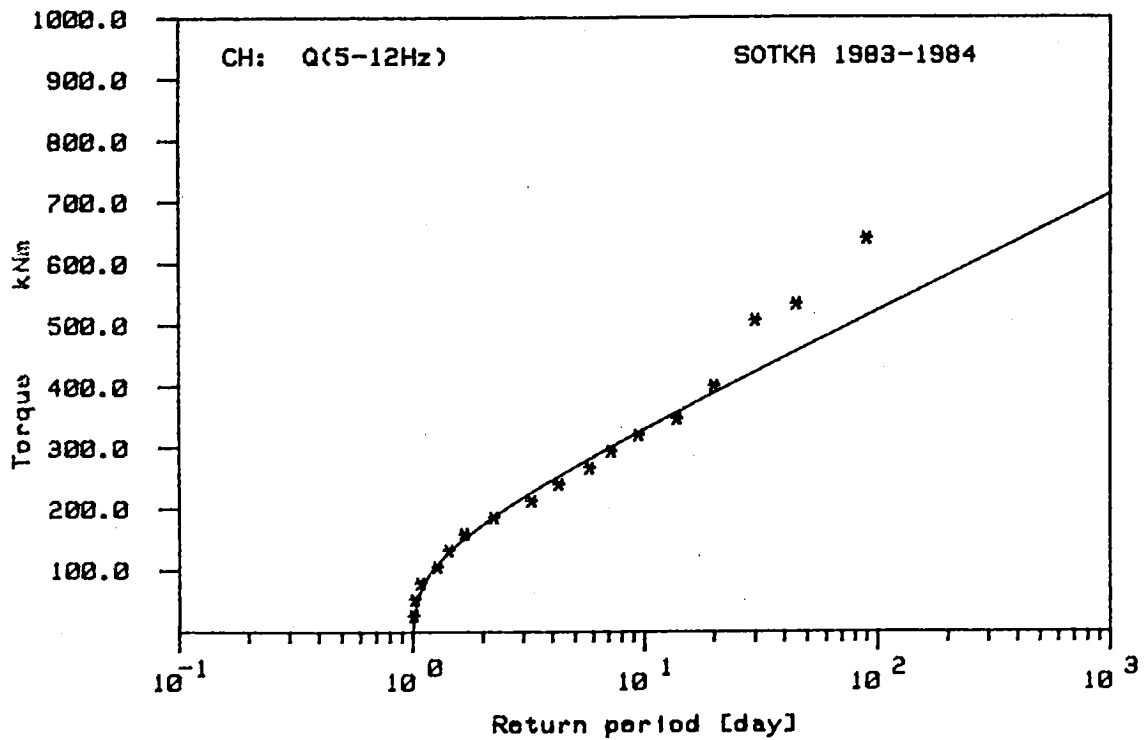
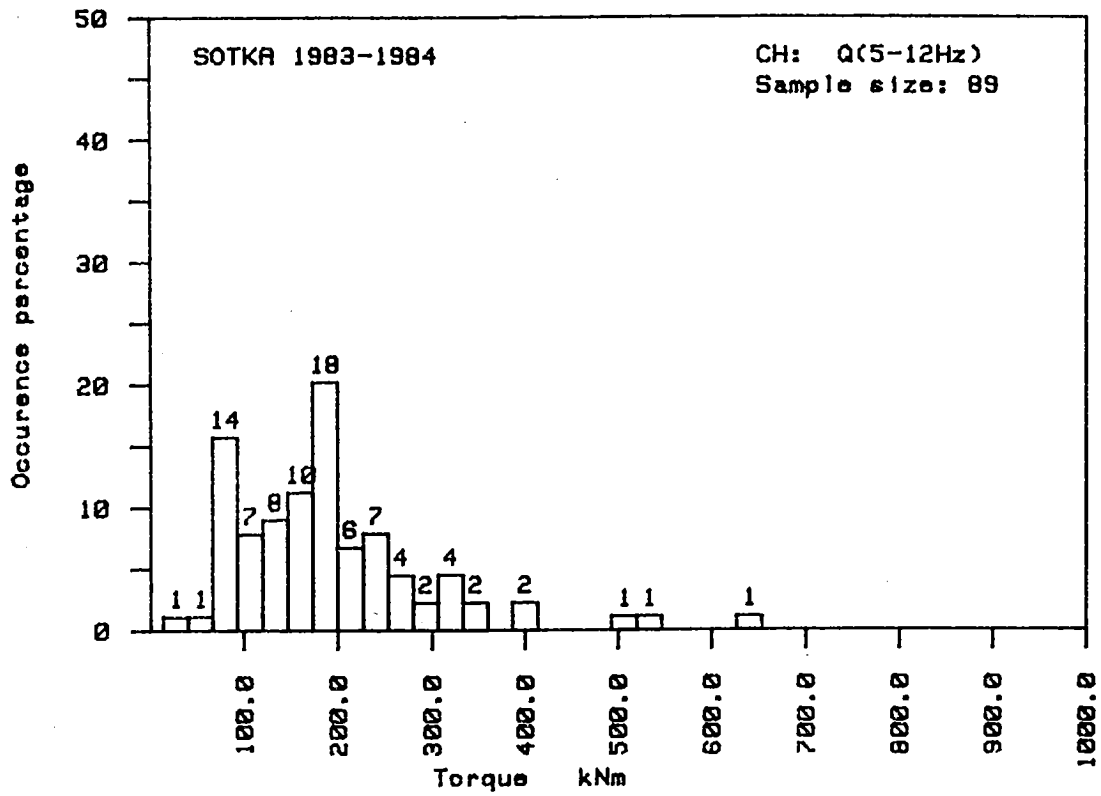


Fig. 27c. Gumbel I distribution fitted on the measured daily maxima of torque Q2 (5-12 Hz).

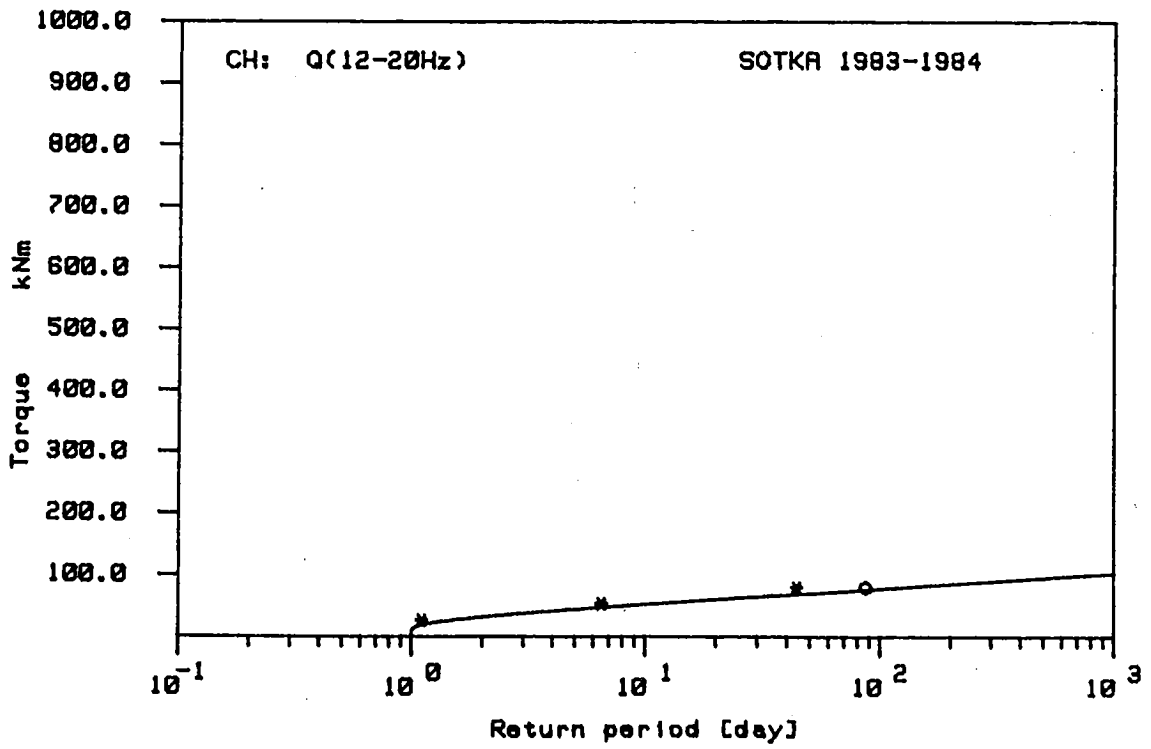
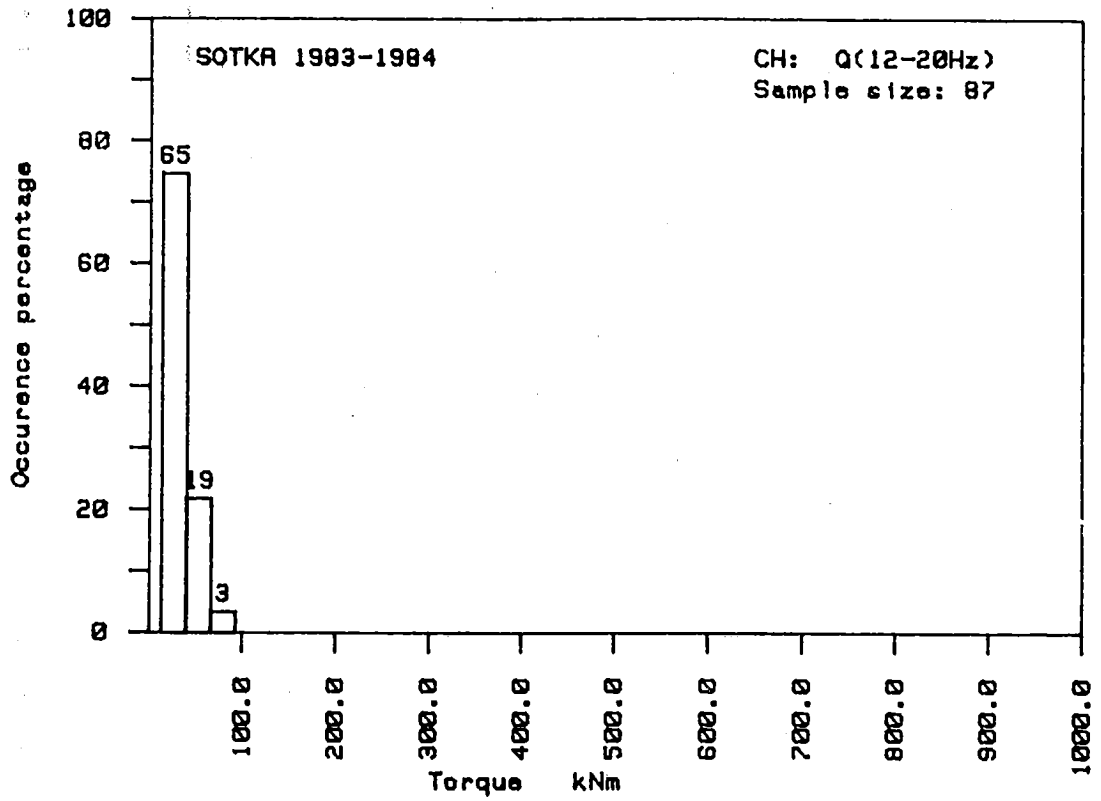


Fig. 27d. Gumbel I distribution fitted on the measured daily maxima of torque Q2 (12-20 Hz).

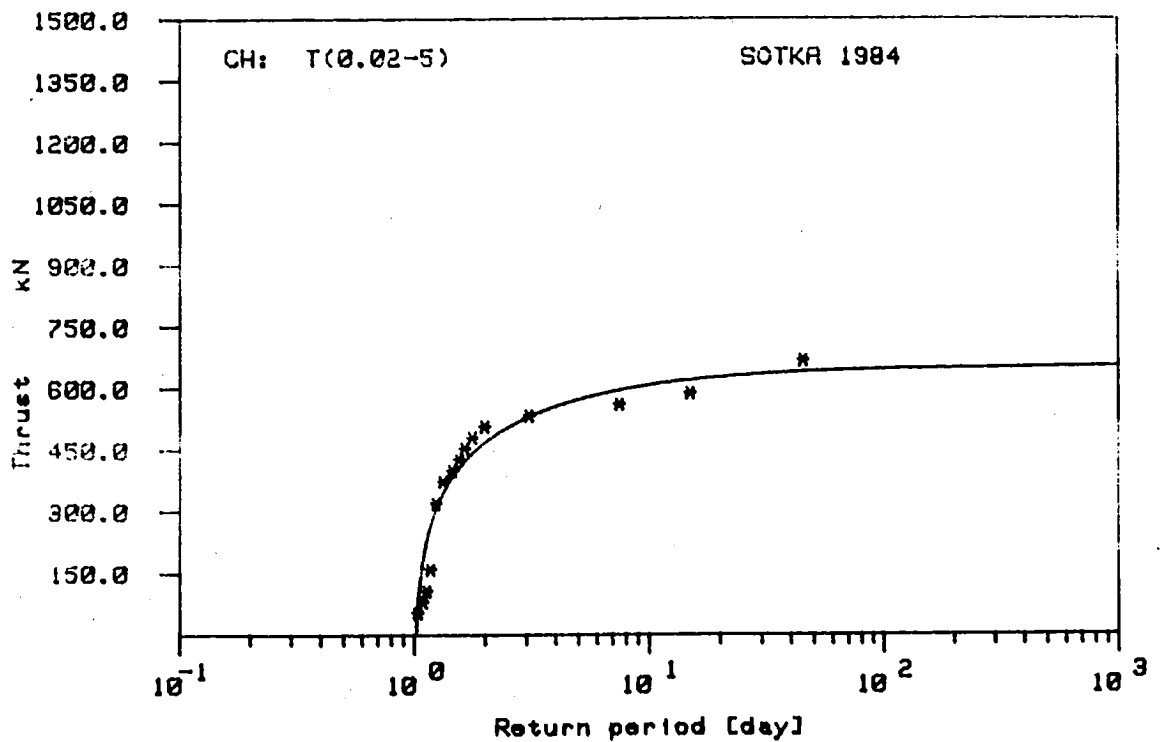
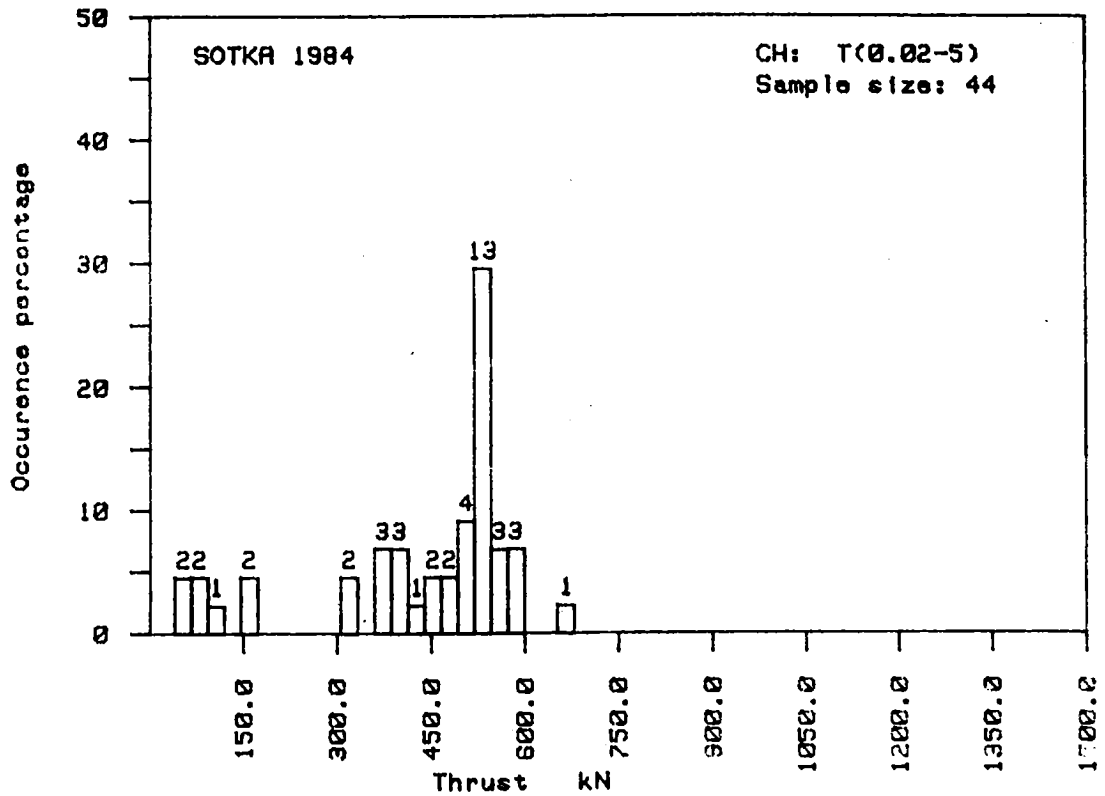


Fig. 28a. Gumbel III distribution fitted on the measured daily maxima of thrust T1 (0.02-5 Hz).

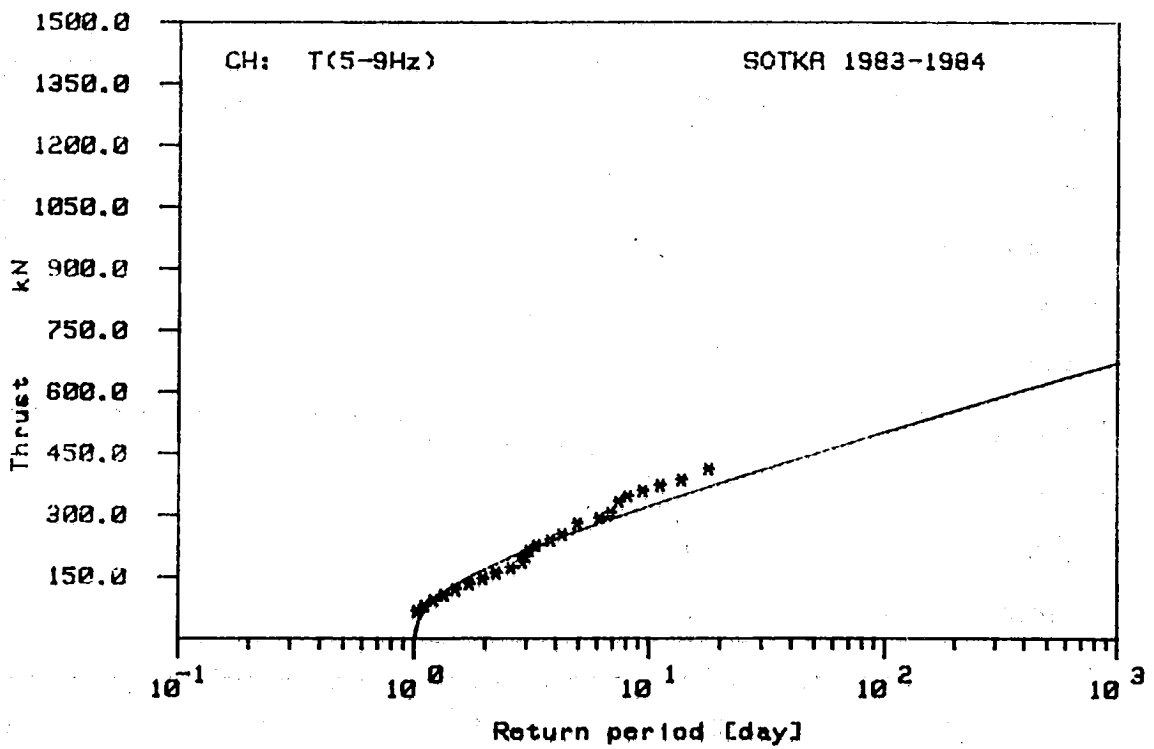
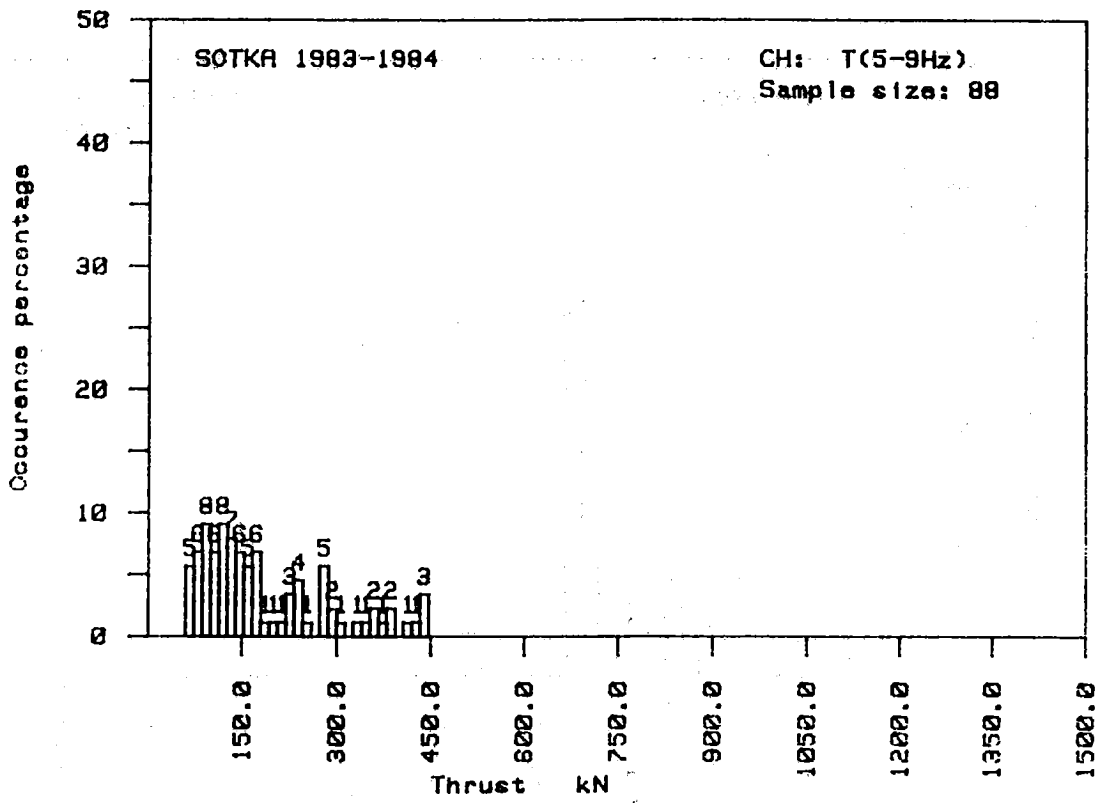


Fig. 28b. Gumbel III distribution fitted on the measured daily maxima of thrust T1 (5-9 Hz).

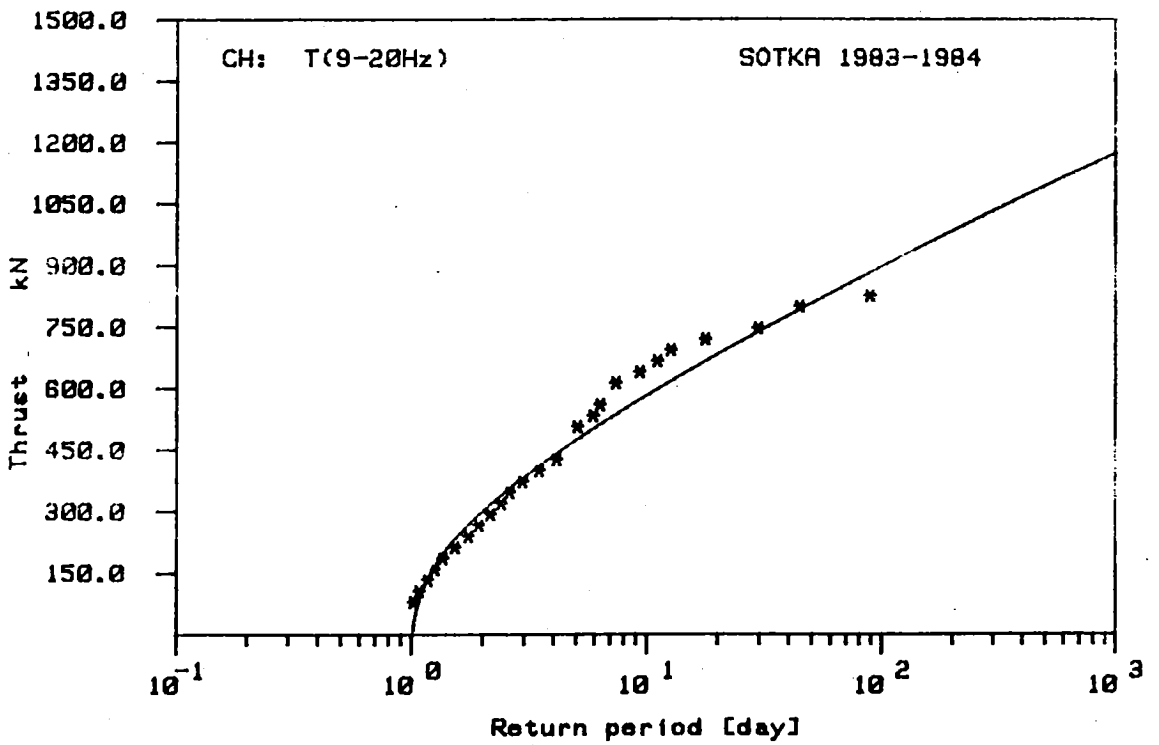
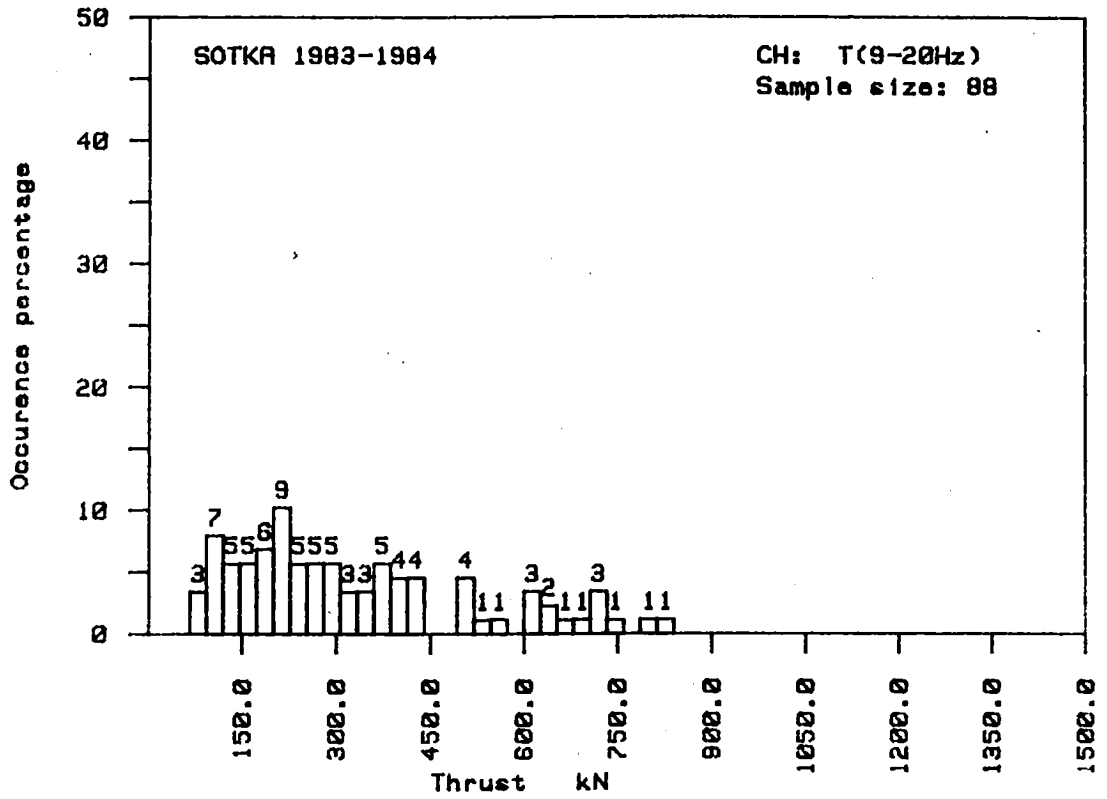


Fig. 28c. Gumbel III distribution fitted on the measured daily maxima of thrust T1 (9-20 Hz).

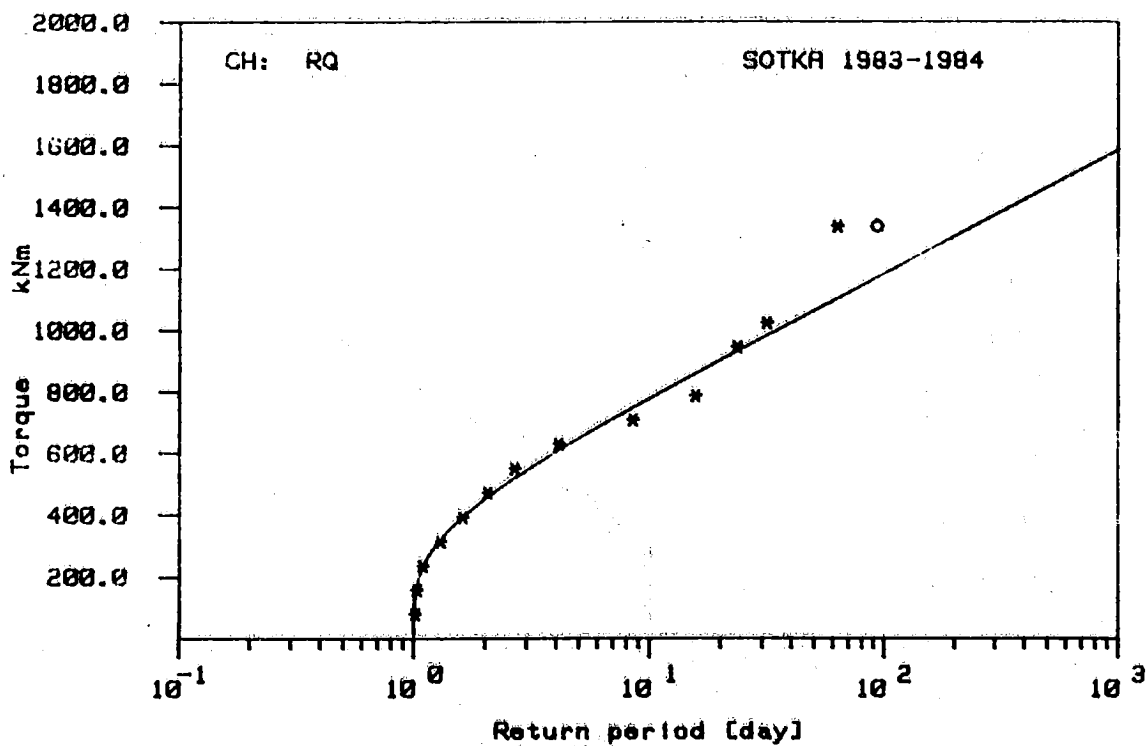
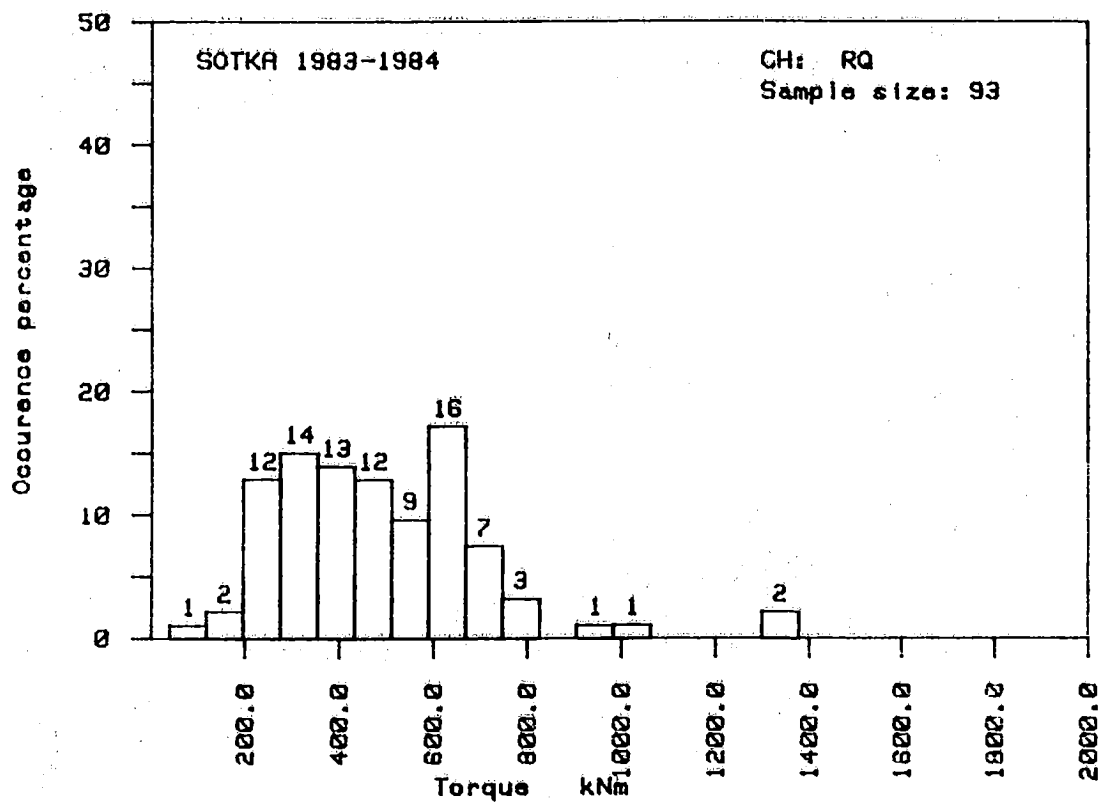


Fig. 29a. Gumbel I distribution fitted on the measured daily maxima of rudder torque RQ.

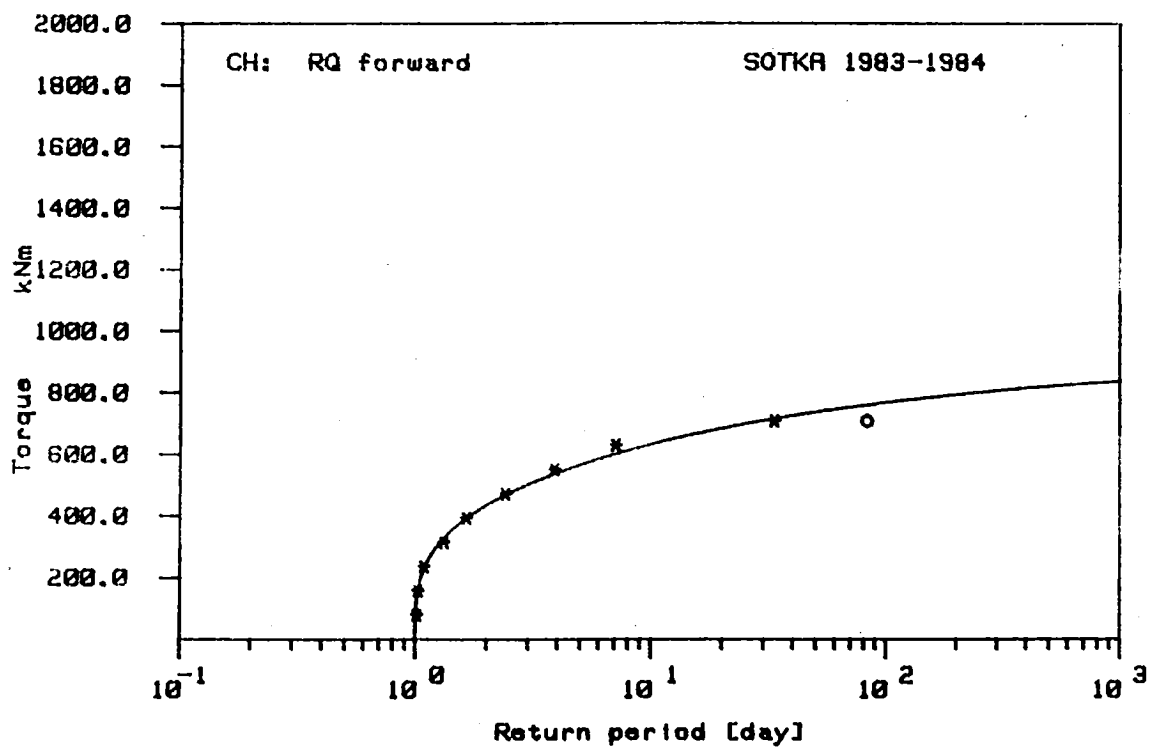
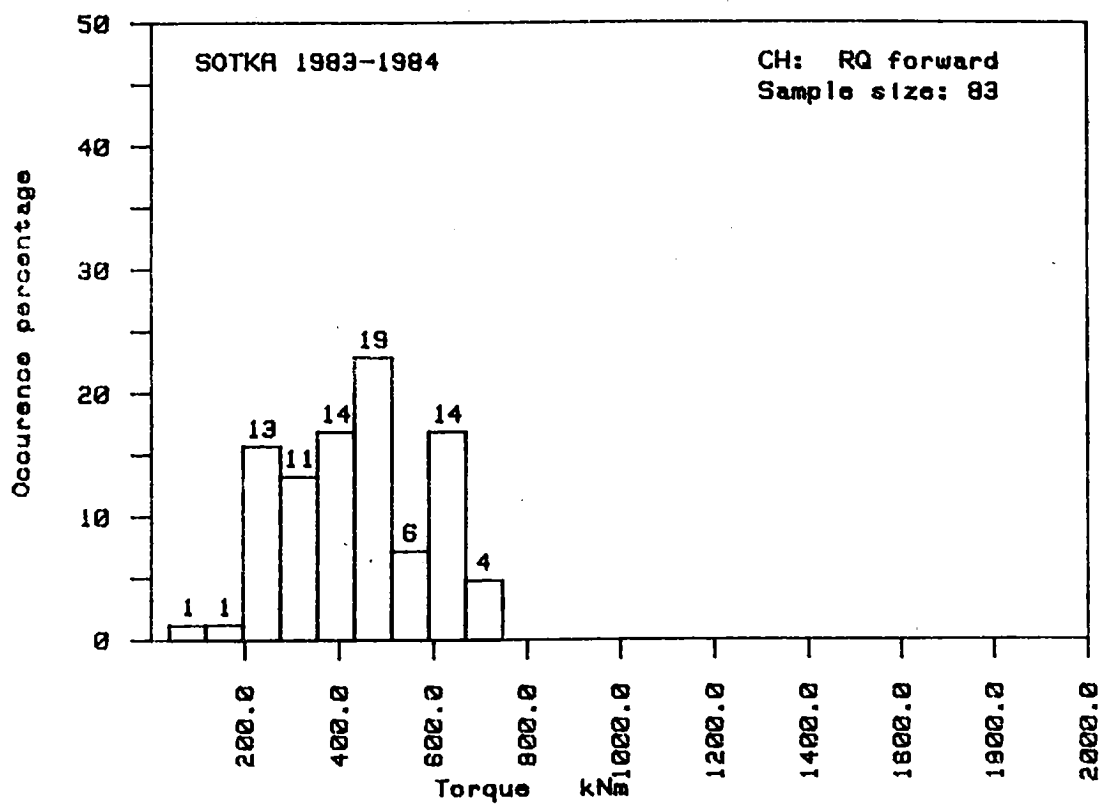
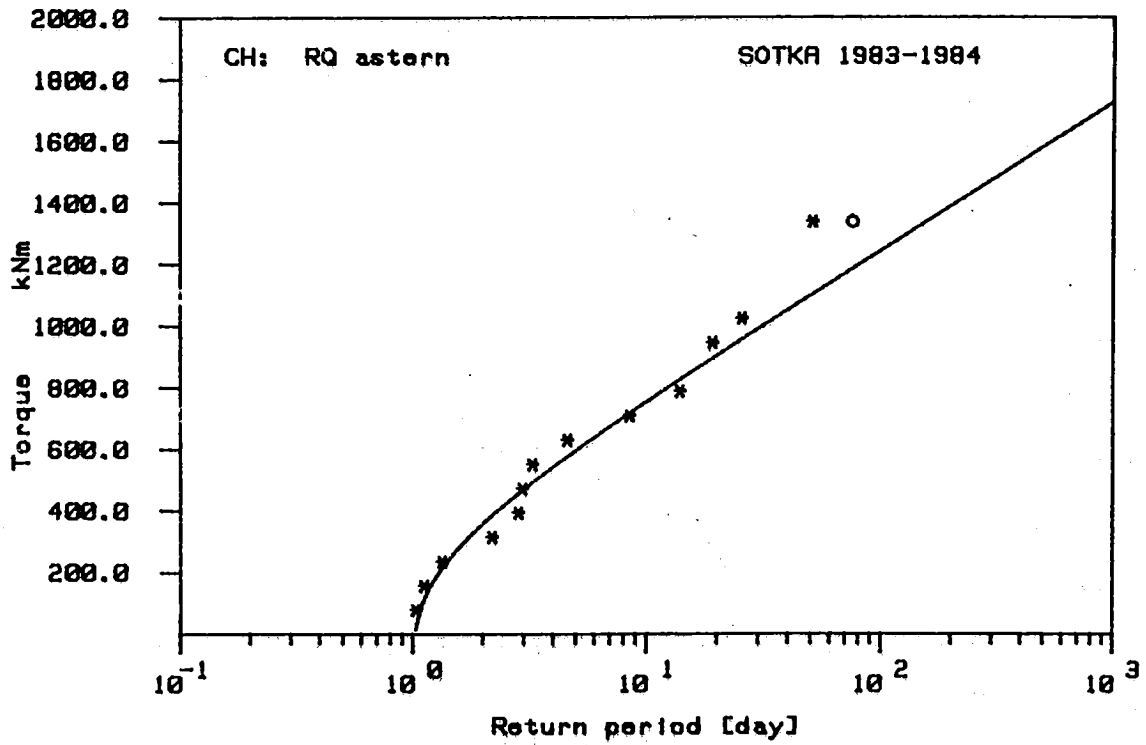
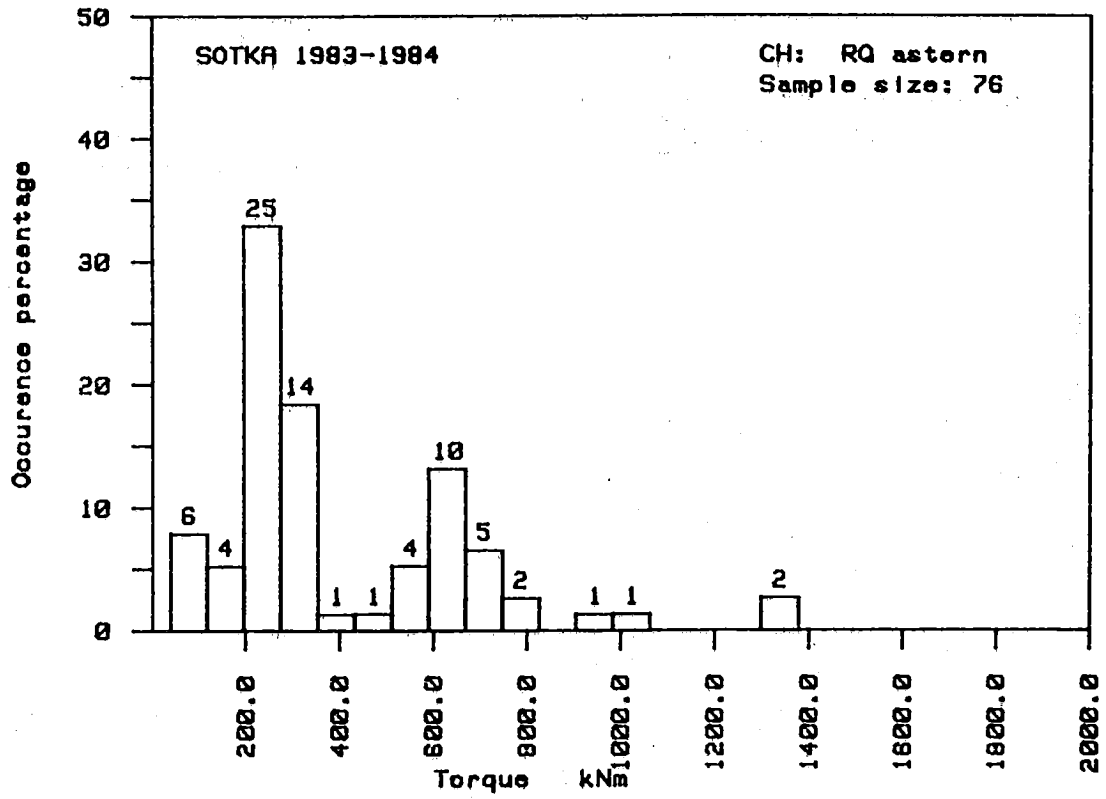


Fig. 29b. Gumbel III distribution fitted on the measured daily maxima of rudder torque when going ahead.



6 CONCLUSIONS

The measurements succeeded in general well despite some difficulties with the power supply of the recording system. Only major drawback was that due to zero-level temperature drift of the thrust strain gauges, reliable mean values of thrust signal could be obtained only during the short-term measurements.

The frequencies of the measured ice induced torque amplitudes were mostly in the range of 6.0 - 7.5 Hz i.e. slightly below the blade frequency 8 Hz. In thrust signal the strongest ice-induced vibrations appeared in the range of 14 - 16 Hz.

The maximum measured torque value was about twice the maximum mean torque having the value of 1650 kNm. The dynamic part of torque signal occurring near the blade frequency was about 80 % of the maximum mean torque. The dynamic part of thrust was at maximum 830 kN which is about 65 % of the estimated bollard pull thrust value. The maxima of rudder torque were measured in situations, where the ship was backing. The maximum was 1340 kNm which was about twice as big as the maximum of ahead condition.

The maximum ice loads that product tanker Sotka is expected to encounter in a longer run, were predicted using Gumbel asymptotic distributions. The Gumbel distributions fit mostly fairly well on the measured daily maxima. The extrapolation indicates that the design ice torque level on the propeller shaft given by Finnish-Swedish ice rules is reached about 3 - 4 times during one winter.

The measured power distribution indicates, that the ship operates mainly with one engine also during winters. Two engines are used primarily when sailing in northern parts of the Gulf of Bothnia. During the measurements two engines were used about 15 % of the total measuring time.

The big scatter on the measured results and the difficulties in evaluation of a reliable mathematical model at the present stage of knowledge to describe the dynamic behaviour of the propulsion machinery complicated the analysis of the phenomena associated with propeller-ice interaction. The results of these full scale measurements are hoped to give, however, valuable data for future work in this field. A proper mathematical modelling of the propeller-ice interaction and of the behaviour of the machinery are required together with field measurements to improve the present state of knowledge.

7 ACKNOWLEDGEMENT

This study was financially supported by The Ministry of Trade and Industry and Finnish Board of Navigation, which is here gratefully acknowledged. The work would not have been possible without close co-operation with Neste Oil Company and the crew of product tanker Sotka. We express our warmest gratitude to the flexible arrangements and helpful atmosphere on board.

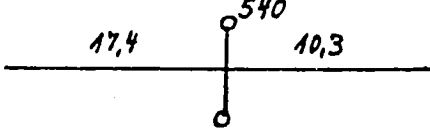
This project at VTT's Ship Laboratory was administrated by Mr. Kaj Riska and the instrumentation was planned in close co-operation with the measuring team of the laboratory. The discussions with Mr. Matti Jussila have also been most valuable. For this encouraging attitude of the VTT personnel we would like to express our special thanks.

REFERENCES

1. First ice-breaking product tanker from Nobiskrug. The Motor Ship, October 1976.
2. Mäkinen, E. & Roos. R., Ice navigation capabilities of Lunni-class icebreaking tankers. SNAME 1977.
3. Gumbel, E.J., Statistics of extremes. Columbia University Press, 1958.

APPENDIX I (4 pages)

THE INERTIA AND STIFFNESS VALUES OF THE PROPULSION MACHINERY

MaK MaK Maschinenbau Kiel GmbH Abteilung 1 Jungfernstieg 10		Reduktion der Massen und Längen		Nr. Nr.: 232026/027/028/029 Motor Nr.: 06034-1343	
				M [kgcms ²]	l red [cm]
Vom freien wellenende angetriebene Aggregate: Wellengenerator nach Zeichnung Nr. SK 42094 der AEG Schwungmoment des Polrades und Erregers $GD^2 = 1323,6 \text{ kpm}^2$				18543	
d	l	l/l	lred		
270	48,0x0,8	0,2309	8,87		
280	31,8	0,1997	6,35		
260	3,5x0,8	0,2686	0,75		
15,97 : u 2					
Schwungmoment des Lüfters $GD^2 = 49,0 \text{ kpm}^2$				686	
260	3,5x0,8	0,2686	0,75		
260	13,0	0,2686	3,49		
230	8,6	0,4385	3,77		
220	6,0	0,5239	3,14		
190	19,2	0,9417	18,08		
220	5,4	0,5239	2,83		
180	30,0x0,4	1,169	14,03		
46,09 : u 2					8,4
Lohmann & Stolterfoht Spiroflexkupplung KJR 220 M, Ausführung 1002 Schwungmoment Innenteile $GD^2 = 67,06 \text{ kpcm} / \text{rad}$ Dyn.Drehfedersteife $C_{dyn} = 2,1 \times 10^6 \text{ kpcm/rad}$ Schwungmoment Außenteile $GD^2 = 164,6 \text{ kpcm/rad}$ Lohmann & Stolterfoht Übersetzungsgetriebe Type GAA 560, $u=1:2,544$ Drehschwingungsschema nach L.u.St.Zchnng.Nr. 3/3016/5014/2				939 2306	867
<div style="display: flex; align-items: center;"> <div style="margin-right: 20px;"> <p>Motorseite</p> <p>Antrieb</p> </div>  </div>					
Airflex-Schnalkupplung 38VC 1200 Außenteile der Airflex-Kupplung $GD^2 = 611 \text{ kpm}^2$ Dyn.Drehfedersteife der Airflex-Kupplung $C_{dyn} = 871 \times 10^6 \text{ kpcm/rad}$ Innenteile der Airflex-Kupplung und Außenteil der biege-elastischen Gelenkkupplung GFL 50 K 8 $GD^2 = 440,7 \text{ kpm}^2$ Dyn.Drehfedersteife der Gelenkkupplung $C_{dyn} = 600 \times 10^6 \text{ kpcm/rad}$ Innenteile der Gelenkkupplung $GD^2 = 6,99 \text{ kpm}^2$ Zwischenwelle $C = 749,8 \times 10^6 \text{ kpcm/rad}$ Geislinger-Kupplung Typ BE 72/15/13 Innenteil der Geislinger-Kupplung $GD^2 = 3,5 \text{ kpm}^2$ Statische Drehfedersteife $C_{st} = 12,5 \times 10^6 \text{ kpcm/rad}$ Außenteile der Geislinger-Kupplung $GD^2 = 191,9 \text{ kpm}^2$				1558 1124 17,8 18,9 8,9 489	11,5 16,7 13,3 800

Erläuterung: Die Drehsteifigkeiten von Wellen sind auf $G \cdot l_{po} = 10^{10} \text{ kgcm}^2$ bezogen. Dieses entspricht einer Reduktion auf eine Stahlwelle von 187,3 mm \varnothing mit einem Schubmodul von $G = 830000 \text{ kg/cm}^2$.

Es ist also: $l_{red} = \frac{(G \cdot l_{po})_{red}}{G \cdot l_{po}} \cdot l = \frac{10^{10}}{G \cdot l_{po}} \cdot l = \frac{10^{10}}{C} \text{ [cm]}$ wobei $C = \frac{G \cdot l_{po}}{l} \text{ [kgcm/Rad]}$ Drehsteifigkeit

Die Massen sind nicht auf einen bestimmten Radius bezogen (Kurbelradius), sondern es wird mit Massenträgheitsmomenten [kgcms²] gerechnet. $M \text{ [kgcms}^2] = m \cdot r^2 = 255 \cdot GD^2 \text{ [kgm}^2]$

Bei einem zwischengeschalteten Untersetzungsgetriebe sind die Massenträgheitsmomente und elastischen Längen aller Anlagenteile, die nicht mit Motordrehzahl umlaufen, auf Motordrehzahl reduziert.

MaK MaK Maschinenbau Kiel GmbH Abteilung für Schwingungsberechnung	Reduktion der Massen und Längen	Ktr. Nr.: 232026/027/028/029
		Motor Nr.: 60 034-041
		θ [kgcm ²]
		l_{red} [cm]
Flanschelle für Leistungsabnahme MaK-Zchng. 1.70.7-63.40.01-03		29,97
Motor:		
M/Johne Schwingungsdämpfer MaK-Zchng.		
Reduzierte Länge zwischen Dämpfer und letztem Zylinder ..		6,13
Massenträgheitsmoment eines Triebwerkes (Alu/CG-Kolben) θ_{all}		1082
Reduzierte Länge zwischen zwei Triebwerken l_{211}		6,75
Mit/ohne Gegengewichte an Zyl. 1,3,4,6 MaK-Zchng. 1.70.7-25.20.01-02		246
Reduzierte Länge zwischen Zyl. 1 und Schwungrad		7,46
Schwungrad: 1825 ⁰ x 120 mm breit MaK-Zchng. 1.70.6-73.10.01-26		6120
Geislinger-Kupplung Typ BC 90/20/13 an das Schwungrad angeflanscht		
Schwingmoment Außenteile $GD^2 = 659,6 \text{ kgm}^2$		1682
Statische Drehfedersteife $Cst. = 26 \times 10^6 \text{ kgcm/rad}$		385
Die dynamische Drehfedersteife C_{dyn} ist frequenzabhängig und wird in der Berechnung berücksichtigt		
Schwingmoment Innenteile $GD^2 = 65,37 \text{ kgm}^2$		166,7
Lohmann & Stolterfoht Doppeluntersetzungsgetriebe Type GVQ		
2030 ü = 3,5102 : 1 mit außenliegenden Schaltkupplungen Pneumaster		
NUG 370		
Drehschwingungsschema nach L.u.St.Zchng. 2/4448/5002/1		
Erläuterung: Die Drehsteifigkeiten von Wellen sind auf $G \cdot I_{po} = 10^{10} \text{ kgcm}^2$ bezogen. Dieses entspricht einer Reduktion auf eine Stahlwelle von 187,3 mm Φ mit einem Schubmodul von $G = 830\,000 \text{ kg/cm}^2$.		
Es ist also: $l_{red} = \frac{(G \cdot I_{po})_{red}}{G \cdot I_{po}} \cdot l = \frac{10^{10}}{G \cdot I_{po}} \cdot l = \frac{10^{10}}{C} [cm]$ wobei $C = \frac{G \cdot I_{po}}{l} [kgcm/Rad]$ Drehsteifigkeit		
Die Massen sind nicht auf einen bestimmten Radius bezogen (Kurbelradius), sondern es wird mit Massenträgheitsmomenten [kgcm ²] gerechnet. $\theta [kgcm^2] = m \cdot r^2 = 2,55 \cdot GD^2 [kgm^2]$		
Bei einem zwischengeschalteten Untersetzungsgetriebe sind die Massenträgheitsmomente und elastischen Längen aller Anlagenteile, die nicht mit Motordrehzahl umlaufen, auf Motordrehzahl reduziert.		

MAK

MAK Maschinenbau Kiel
GmbH
Abteilung für
Schwungradberechnung

Reduktion der Massen und Längen

Ktr. Nr.:

232026/027/028/029

Motor Nr.:

66034-041

Schwungmoment Innenteile der Pneumastar
 $GD^2 = 299,2 \text{ kpm}^2$ eingeschaltet
 $GD^2 = 1043,9 \text{ kpm}^2$ ausgeschaltet

Dyn. Drenfedersteife $C_{dyn} = 190,6 \times 10^6 \text{ kpm/rad}$ nur im eingekuppelten Zustand

Schwungmoment Außenteile der Pneumastar

$GD^2 = 1767,8 \text{ kpm}^2$ eingeschaltet

$GD^2 = 1023,1 \text{ kpm}^2$ ausgeschaltet

Wellenleitung nach Ka Me Wa-Zchnng. Nr. 588080
Zwischenwelle

d	l	l/l	l_{red}
730/180	12,0	0,00434	0,052
500/180	318,3	0,01997	6,356
510/180	100,0	0,01843	1,843
500/180	66,5	0,01997	1,328
980/180	12,5	0,00133	0,017

$9,596 \times 10^2$

Schwungmoment des Flansches (Zwischenwelle) sowie Flanschkupp-
lung (Propellerwelle) $GD^2 = 1950 \text{ kpm}^2$
Propellerwelle

540/180	77,0	$0,04/0,7$	0,01462	0,643
540/180	27,5		0,01462	0,402
555/540/180	10,0	$1,061 \times 0,01308$	0,01308	0,139
555/180	380,0		0,01308	4,970
610/555/180	20,0	$1,237 \times 0,00859$	0,00859	0,213
610/180	160,0		0,00859	1,374

$7,741 \times 10^2$

Verstellpropeller: $D = 5450 \text{ mm } \emptyset$, 4 Flügel, $GD^2 = 120904 \text{ kpm}^2$
in Luft
Wasserzuschlag 29 %

32282

Erläuterung: Die Drehsteifigkeiten von Wellen sind auf $G \cdot l_{po} = 10^{10} \text{ kgcm}^2$ bezogen. Dieses entspricht einer Reduktion auf eine Stahlwelle von 187,3 mm \emptyset mit einem Schubmodul von $G = 830\,000 \text{ kg/cm}^2$.

Es ist also: $l_{red} = \frac{(G \cdot l_{po})_{red}}{G \cdot l_{po}} \cdot l = \frac{10^{10}}{G \cdot l_{po}} \cdot l = \frac{10^{10}}{C} \text{ [cm]}$ wobei $C = \frac{G \cdot l_{po}}{l} \text{ [kgcm/Rad]}$ Drehsteifigkeit

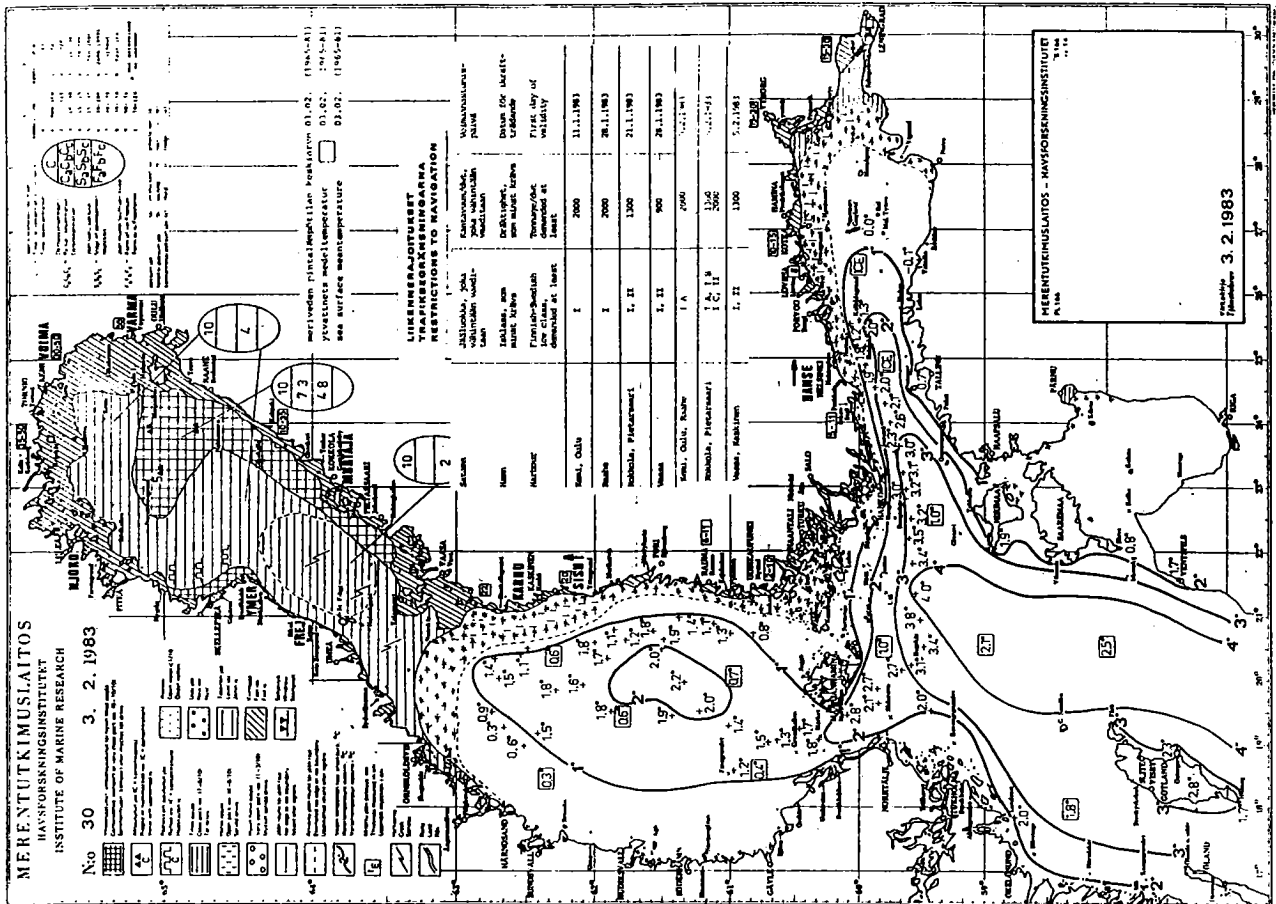
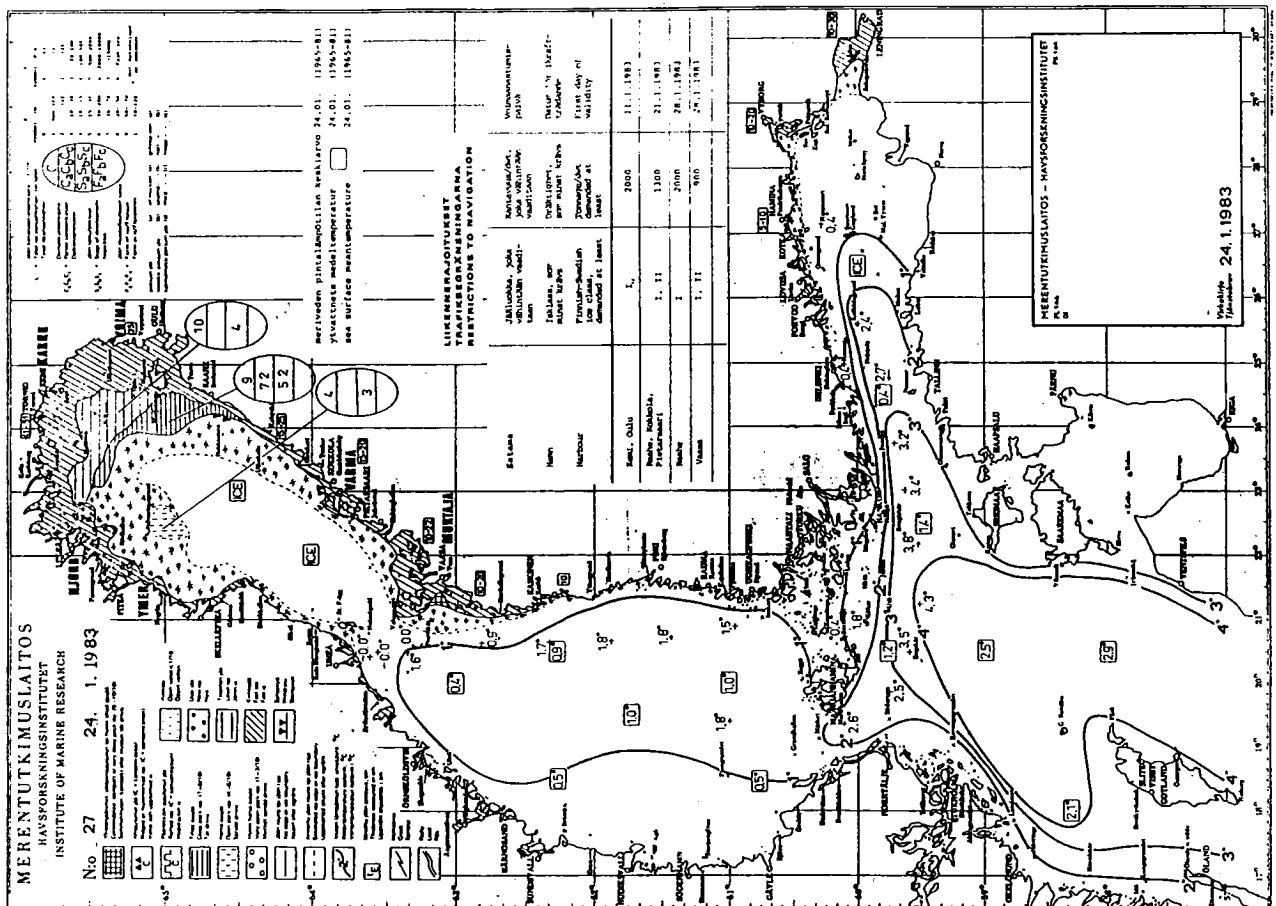
Die Massen sind nicht auf einen bestimmten Radius bezogen (Kurbelradius), sondern es wird mit Massenträgheitsmomenten $[kgcm^2]$ gerechnet. $H \text{ [kgcm}^2] = m \cdot r^2 = 2,55 \cdot GD^2 \text{ [kpm}^2]$

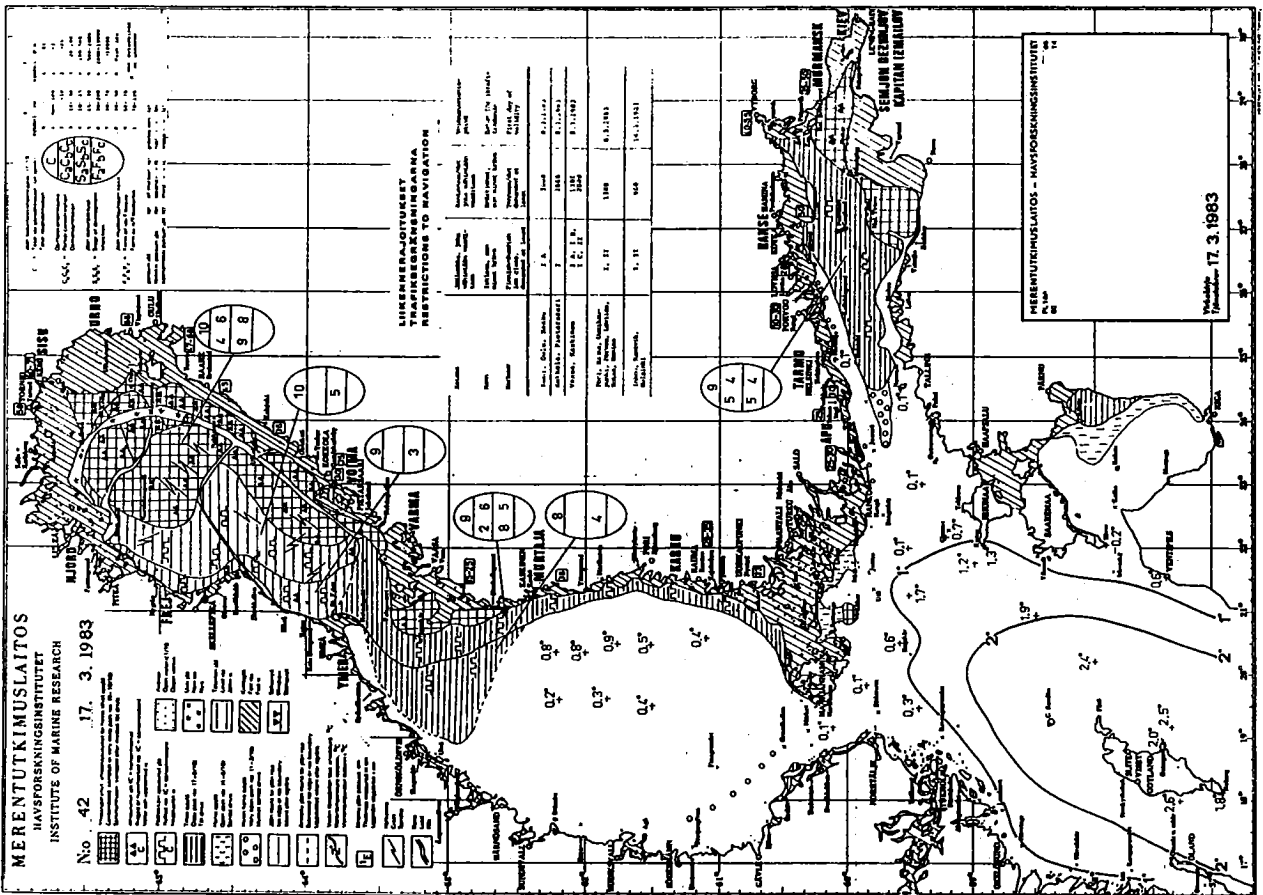
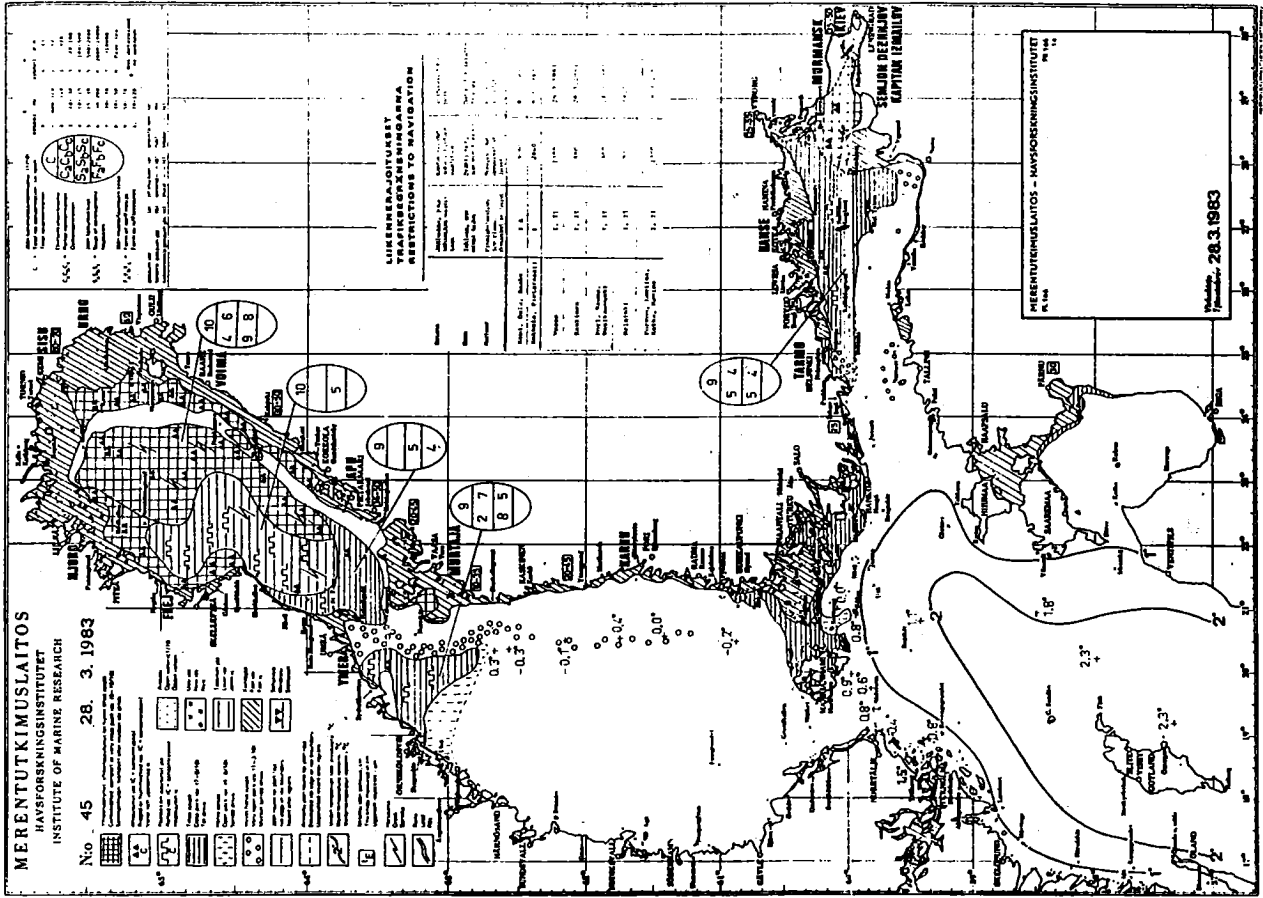
Bei einem zwischengeschalteten Untersetzungsgetriebe sind die Massenträgheitsmomente und elastischen Längen aller Anlagenteile, die nicht mit Motordrehzahl umlaufen, auf Motordrehzahl reduziert.

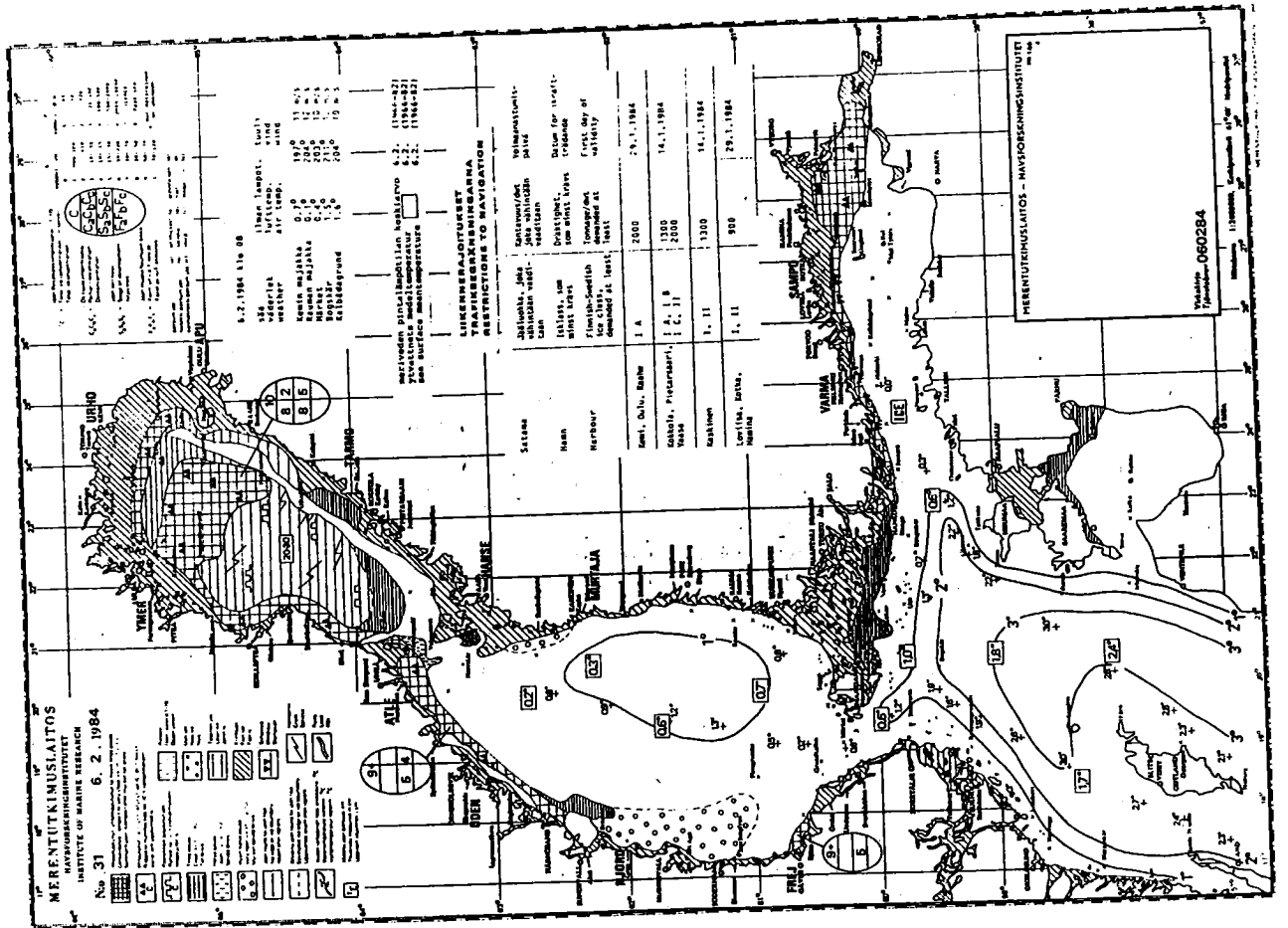
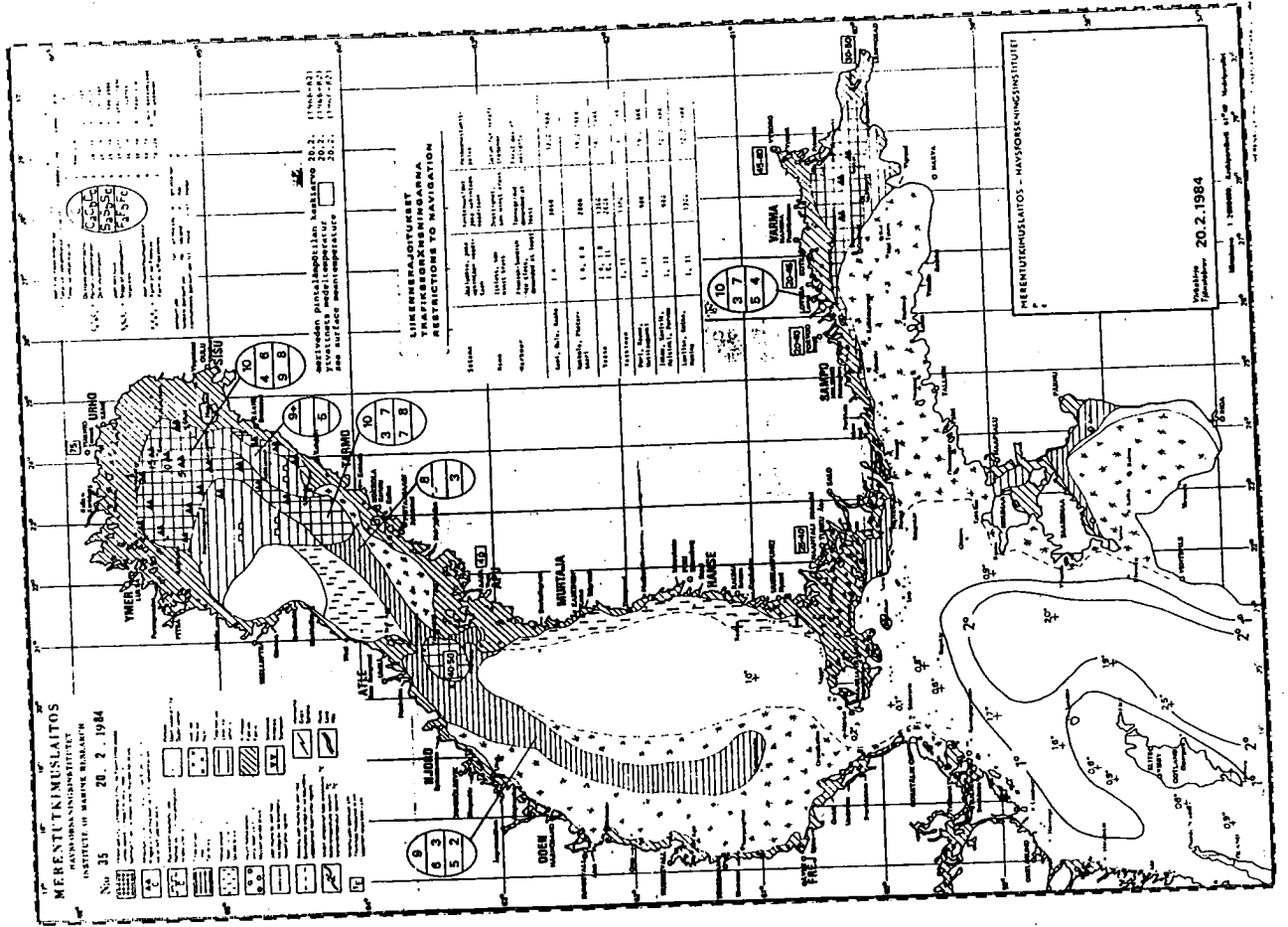
APPENDIX II (6 pages)

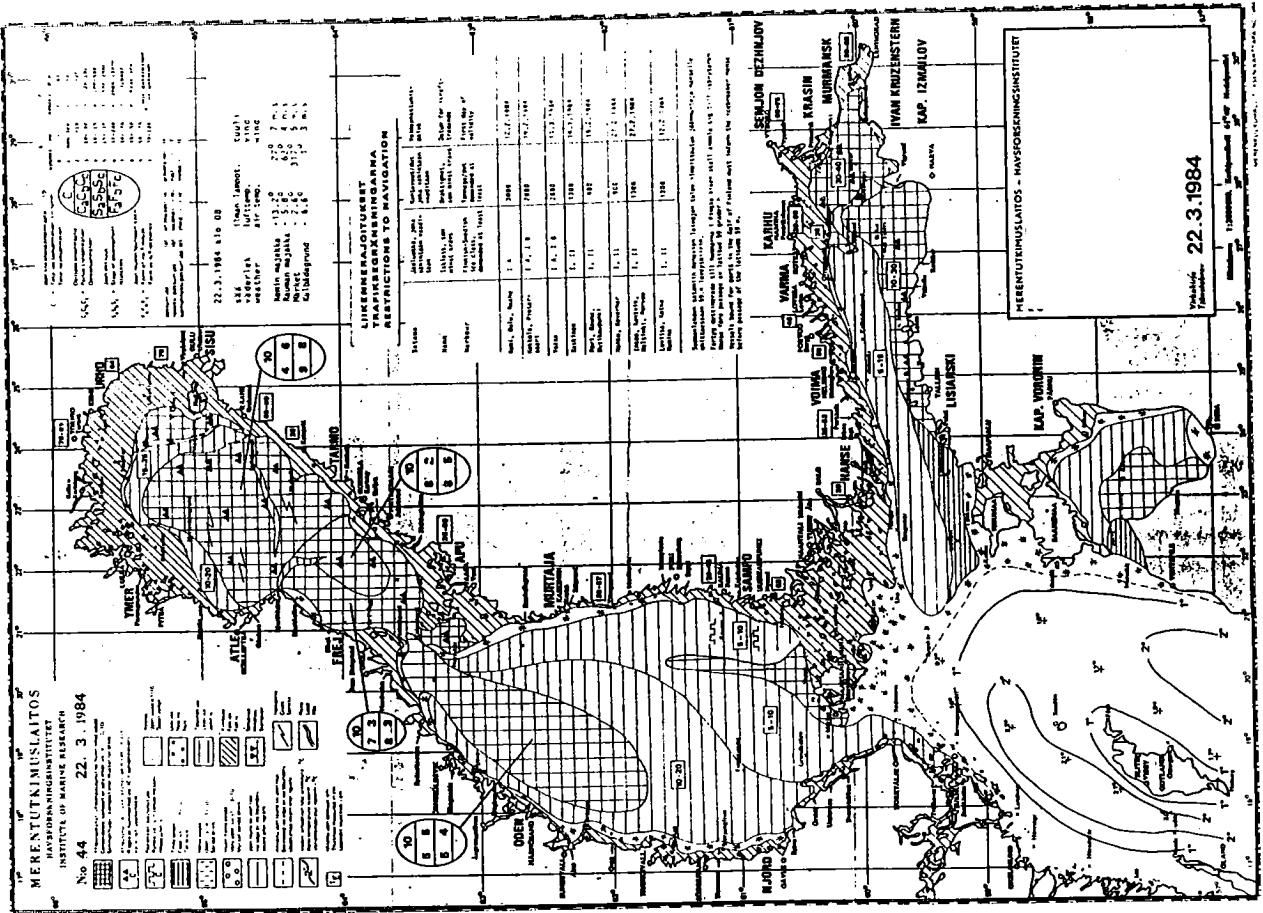
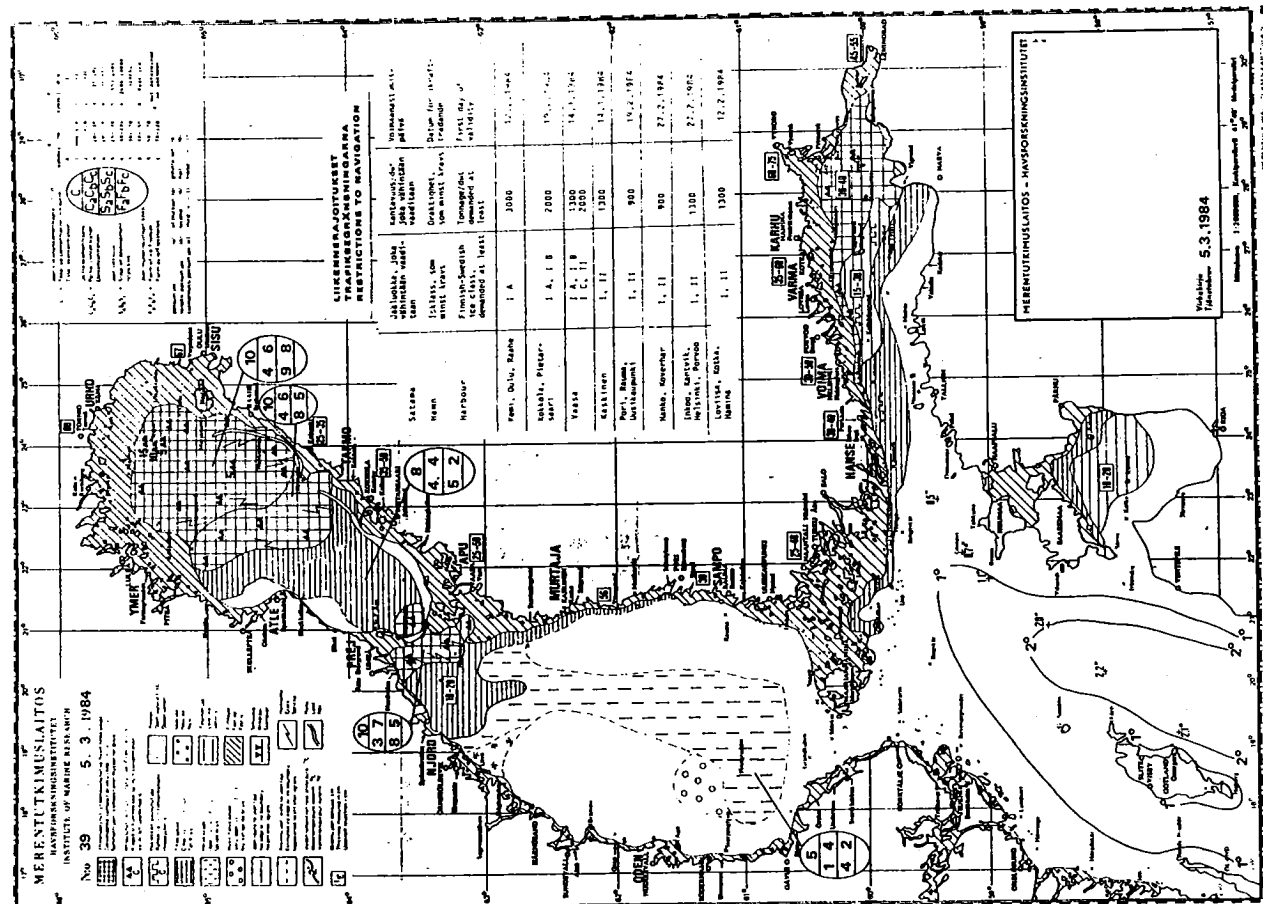
ICE CONDITIONS DURING THE LONG-TERM MEASUREMENTS

	page
Ice charts: 24.1.1983	1
3.2.1983	1
17.2.1983	2
3.3.1983	2
17.3.1983	3
28.3.1983	3
6.2.1984	4
20.2.1984	4
5.3.1984	5
22.3.1984	5
2.4.1984	6
19.4.1984	6









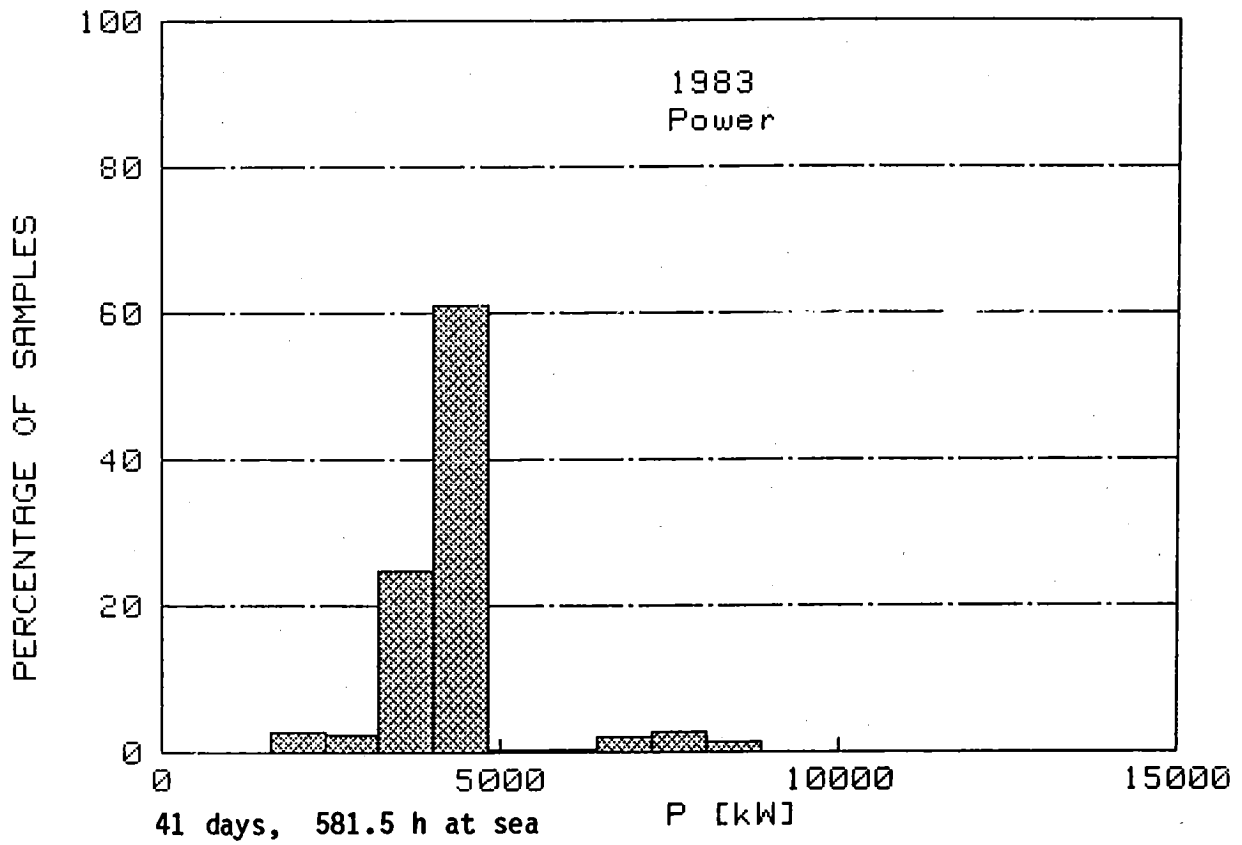
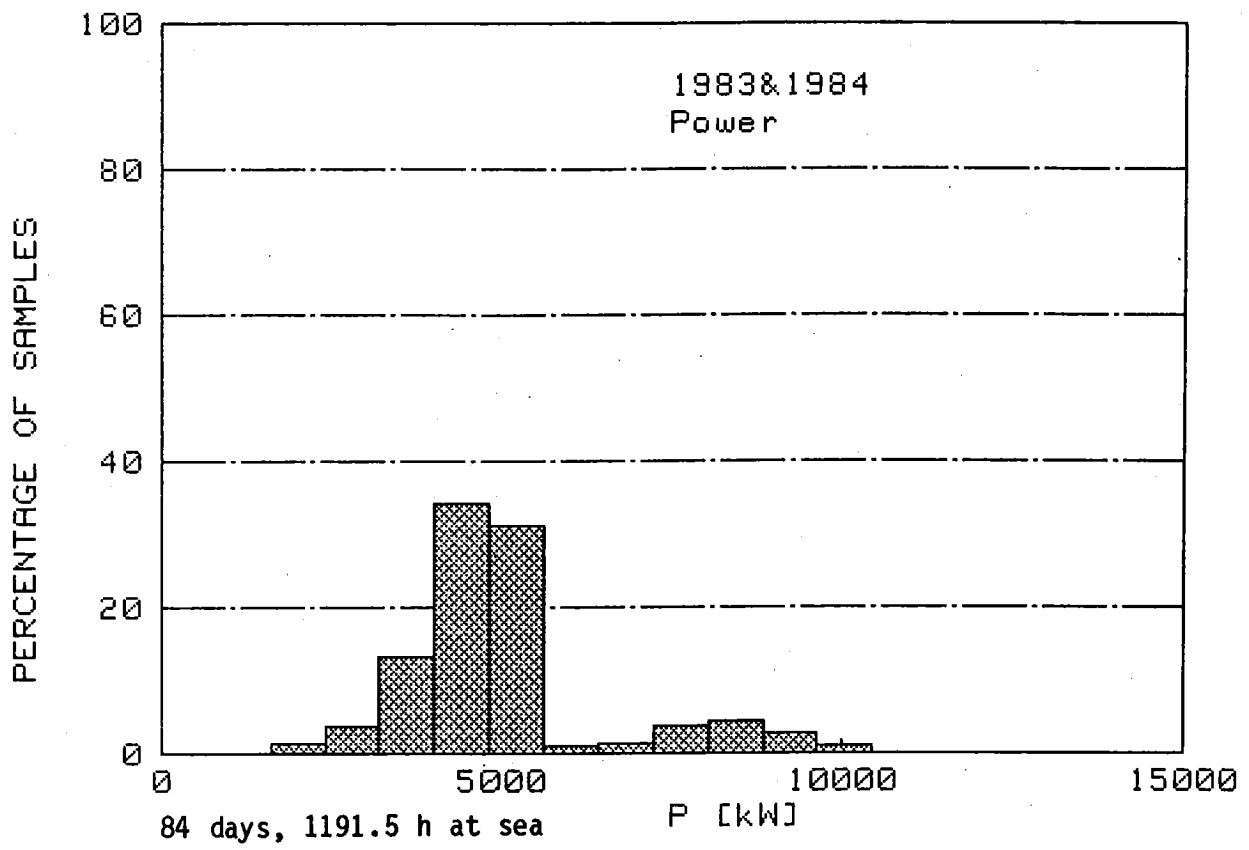
APPENDIX III (12 pages)

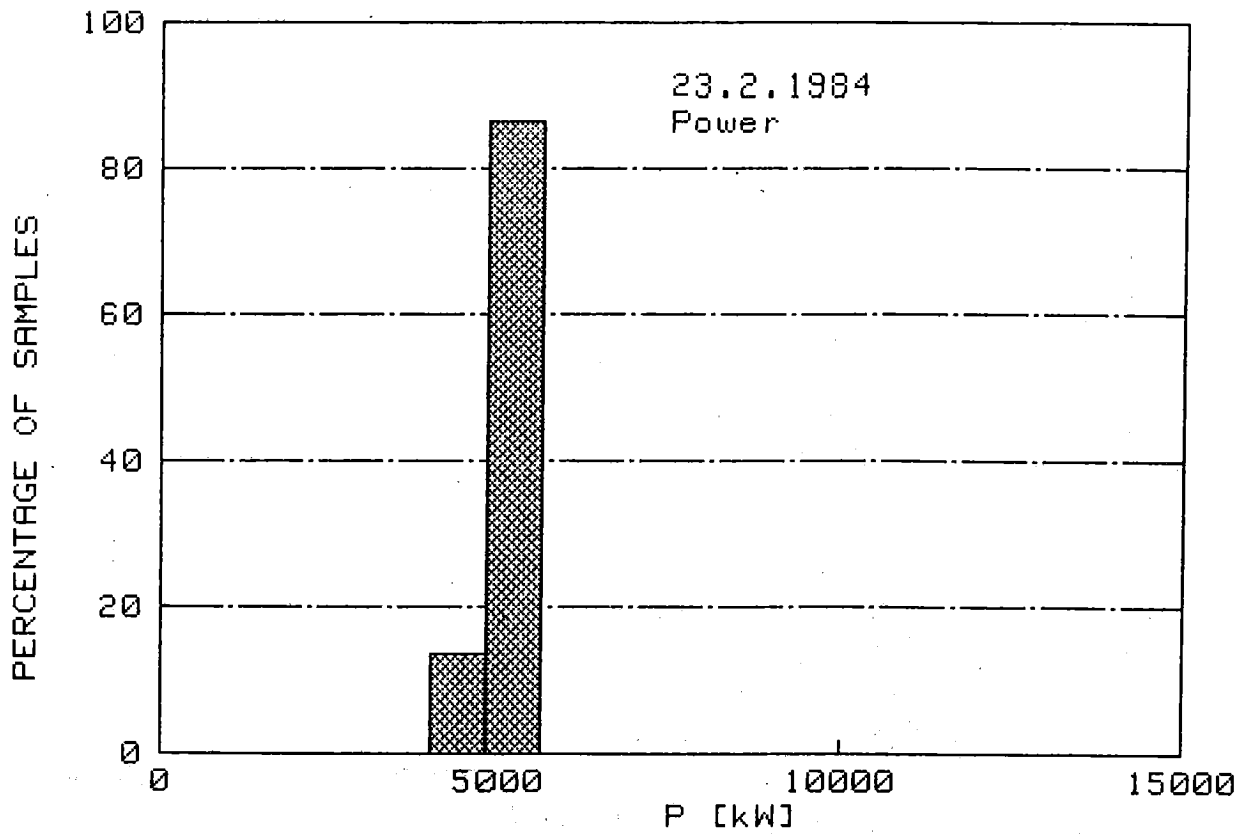
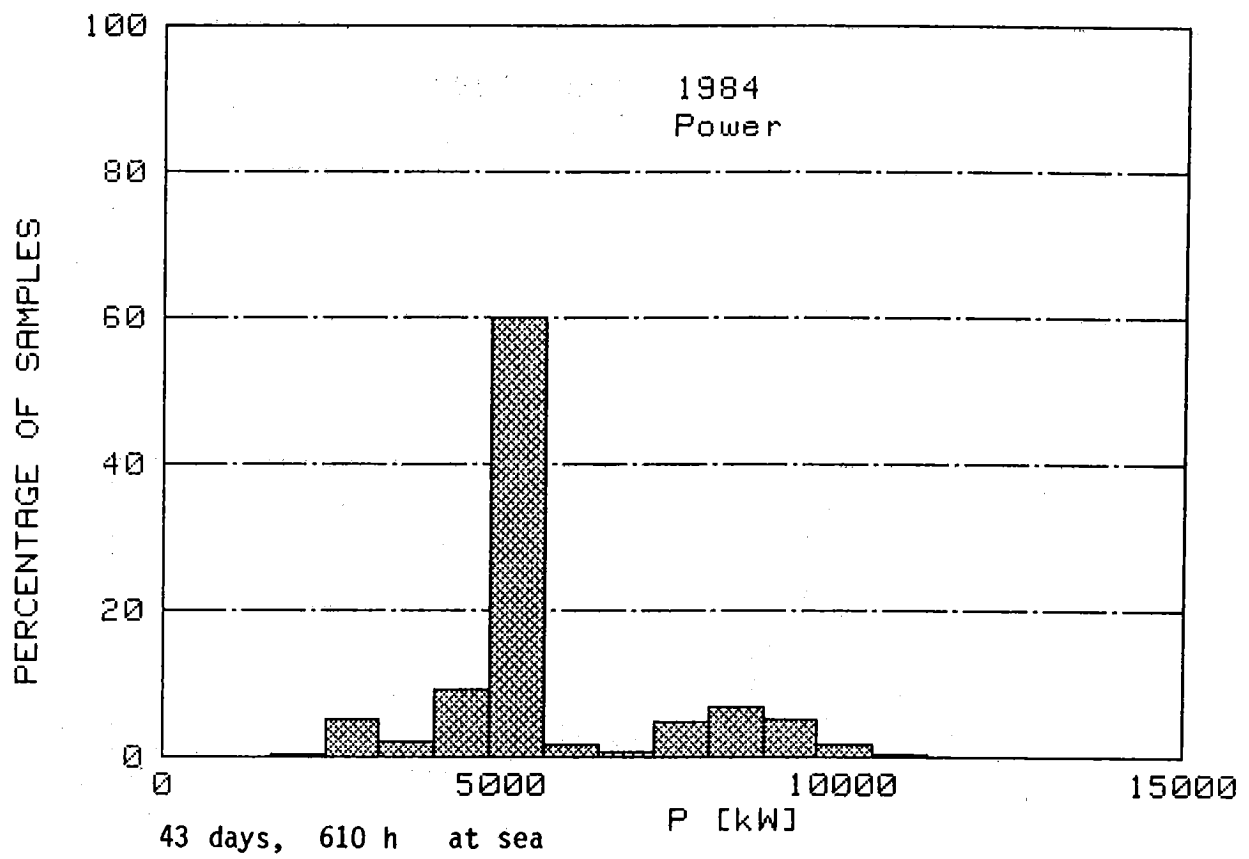
DISTRIBUTION HISTOGRAMS OF THE LONG-TERM MEASUREMENTS

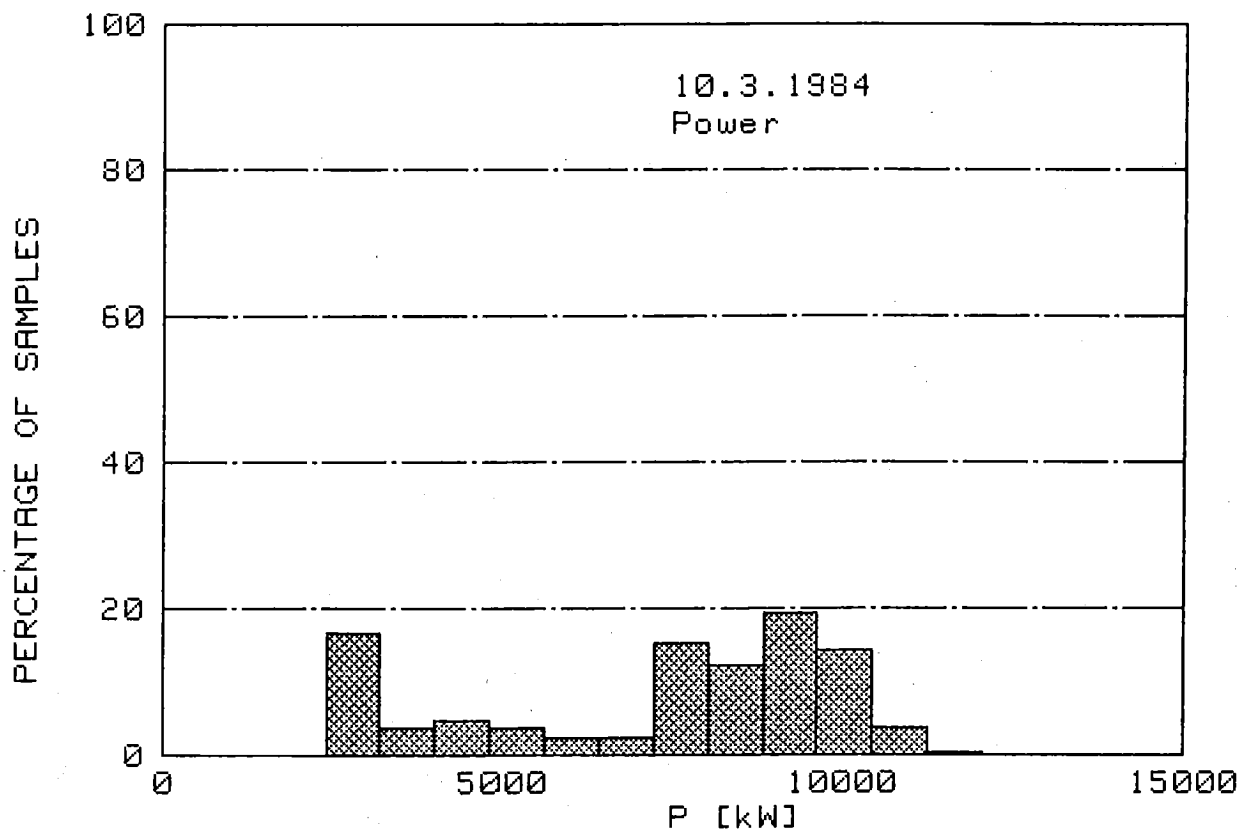
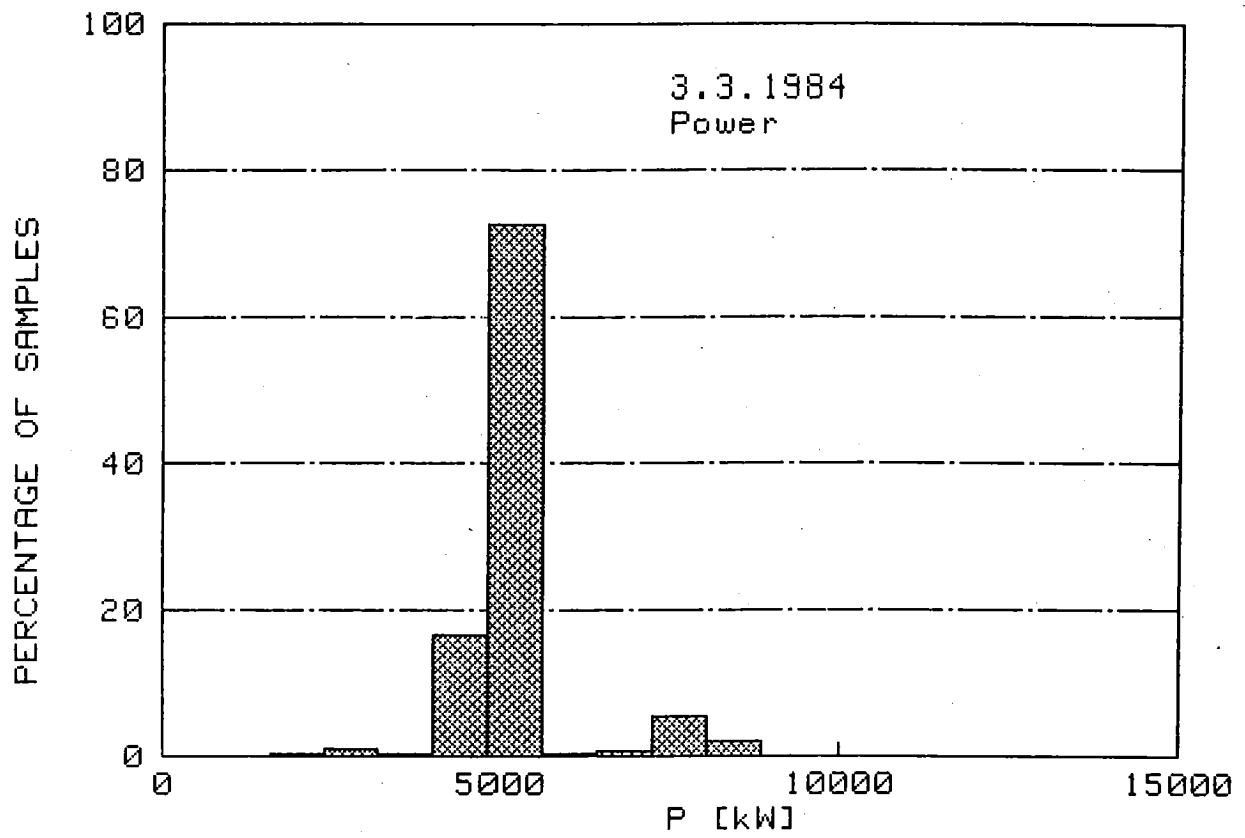
	page
Power	1
Q (0-20 Hz)	5
RQ	9

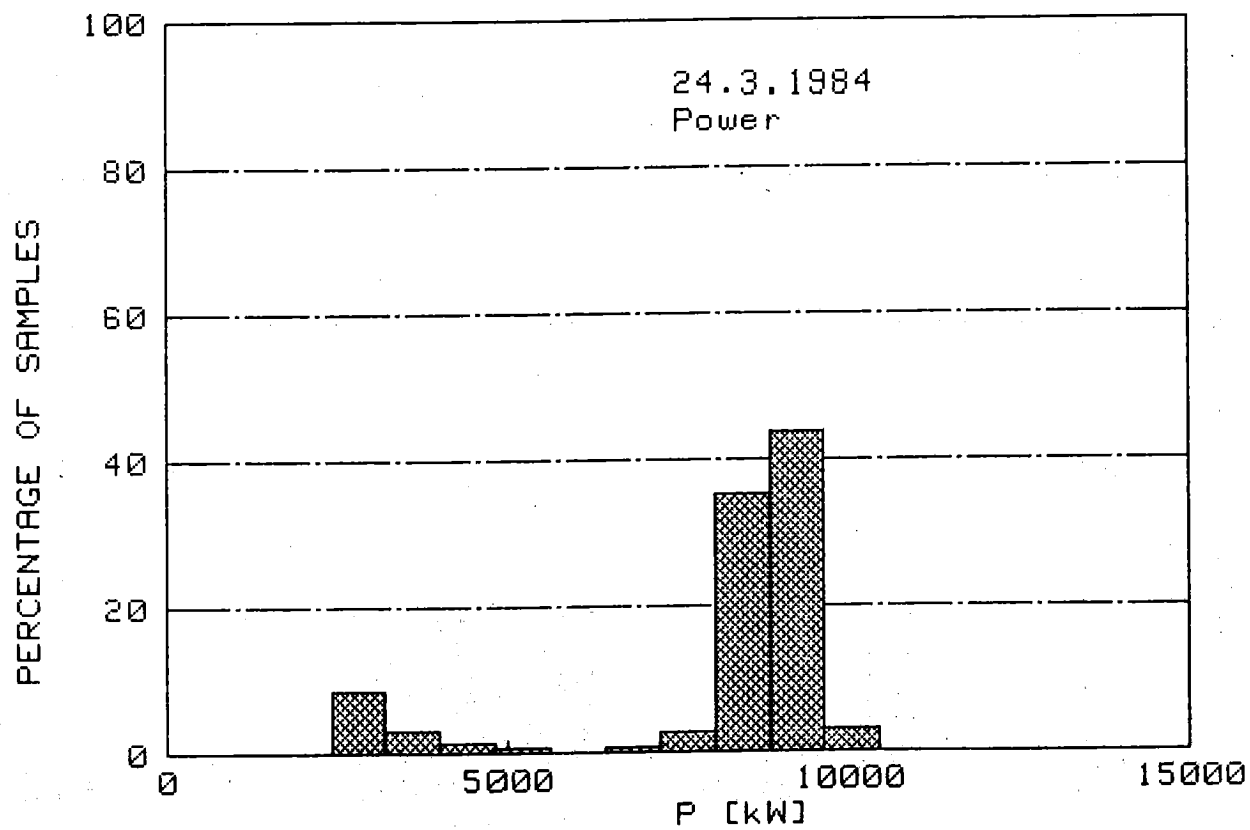
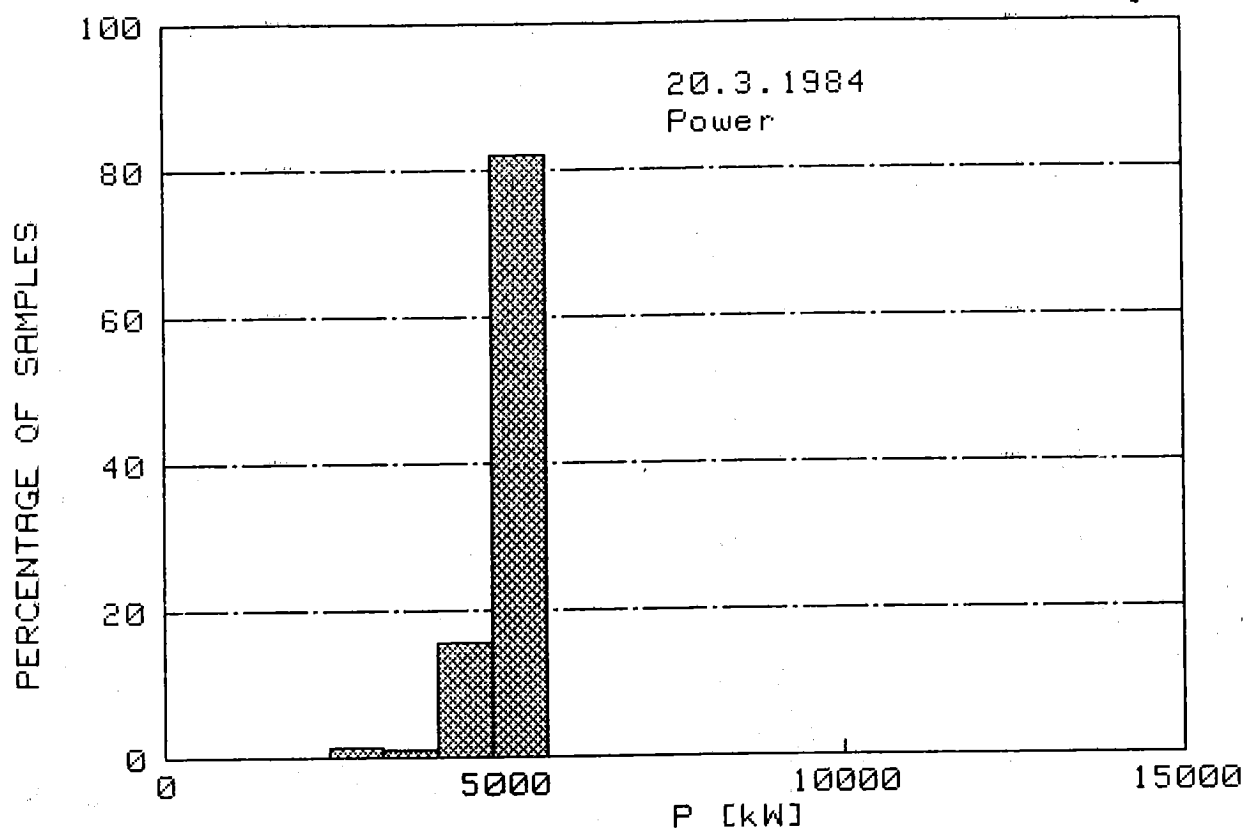
Examples of daily distributions:

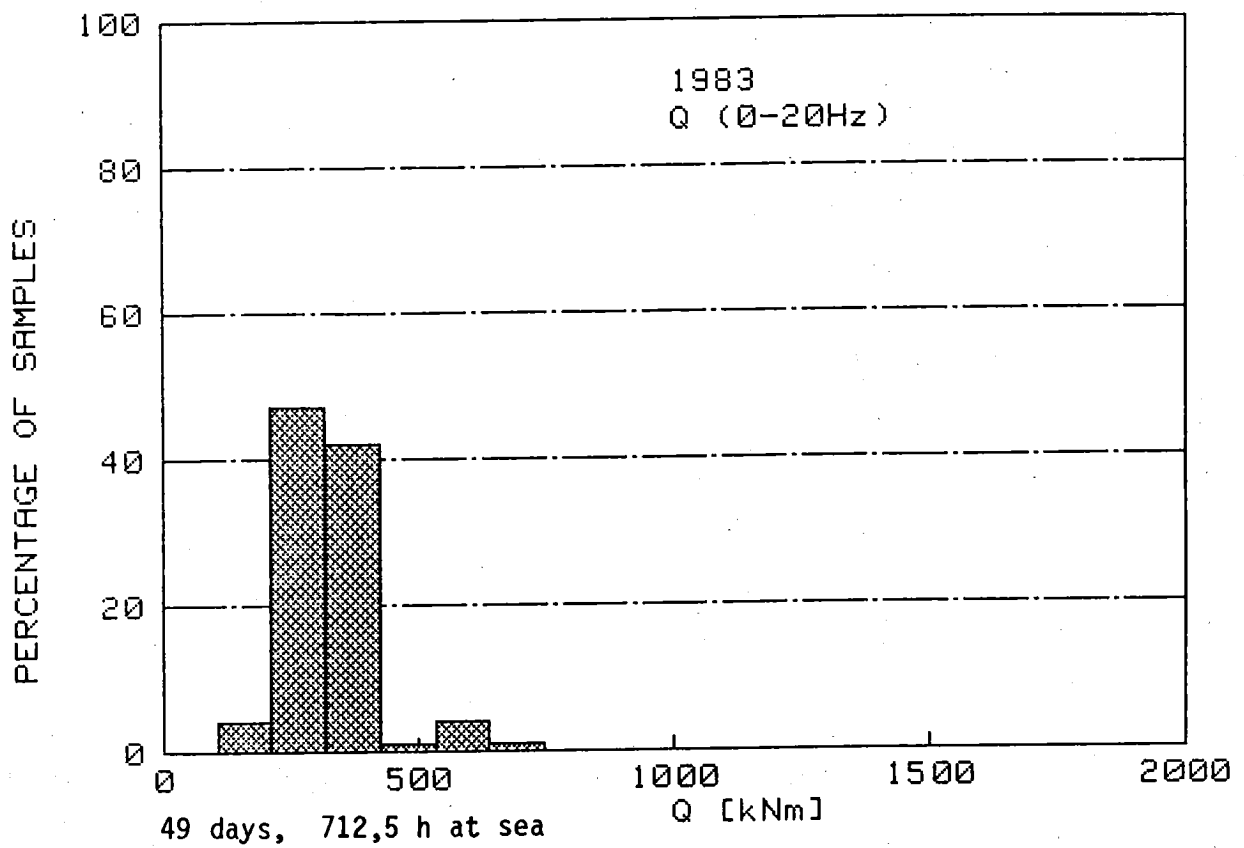
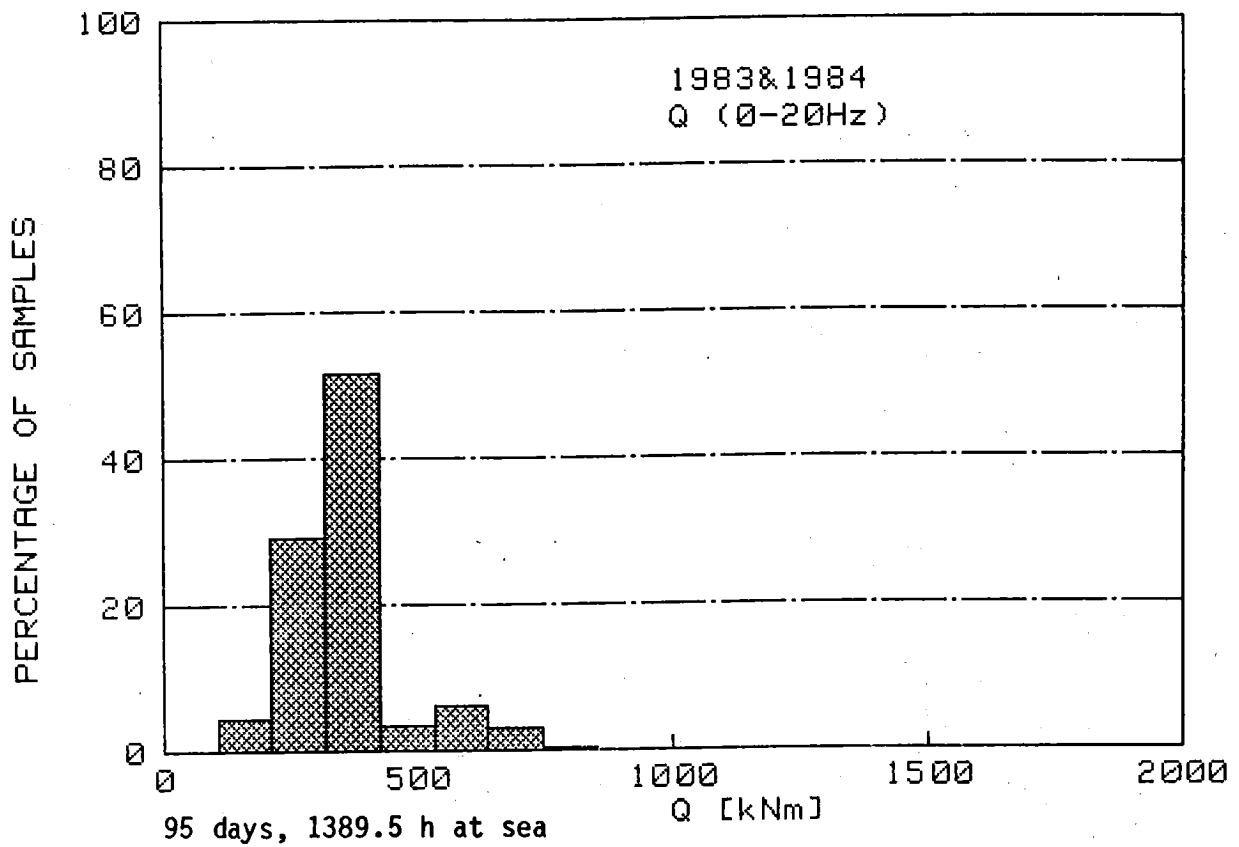
- 23.2.1984 (open sea)
at sea 24 h
draught 9.80 m
Dep. 22.2.1984 2020 Porvoo - Arr. 25.2.1984 1210 Göteborg
- 3.3.1984
at sea 19 h 45 min, in harbour 4 h 15 min
draught 9.70 m
Dep. 3.3.1984 0415 Porvoo - Arr. 5.3.1984 0905 Kemi
- 10.3.1984
at sea 18 h 50 min, engines stopped at sea 5 h 10 min
draught 9.70 m
Dep. 8.3.1984 0840 Naantali - Arr. 13.3.1984 0500 Kemi
Ice trials in the Gulf of Bothnia 9.- 12.3.1984
- 20.3.1984
at sea 12 h 30 min, in harbour 11 h 30 min
draught 6.65 m
Dep. 20.3.1984 1130 Pori - Arr. 21.3.1984 1900 Porvoo
- 24.3.1984
at sea 16 h 5 min, in harbour 7 h 55 min
draught 9.70 m
Dep. 22.3.1984 0830 Porvoo - Arr. 24.3.1984 1605 Oulu

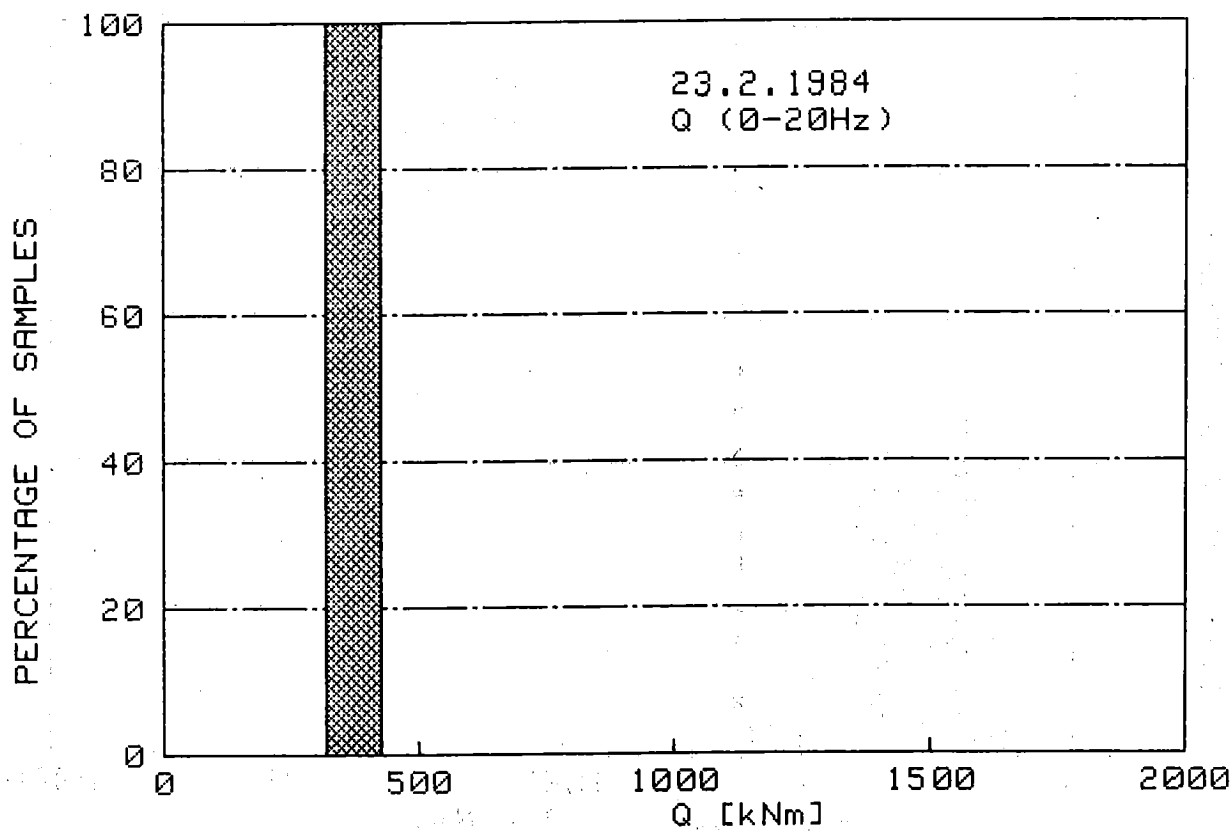
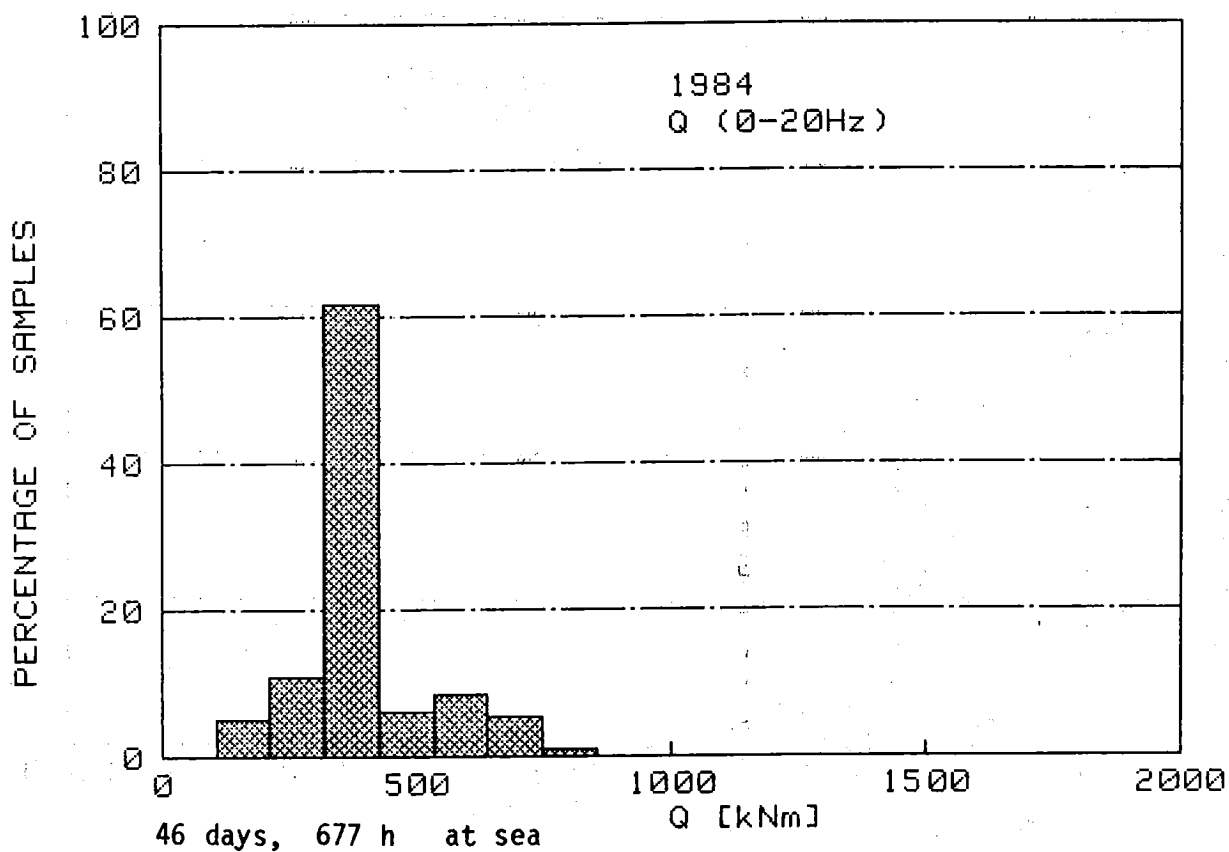


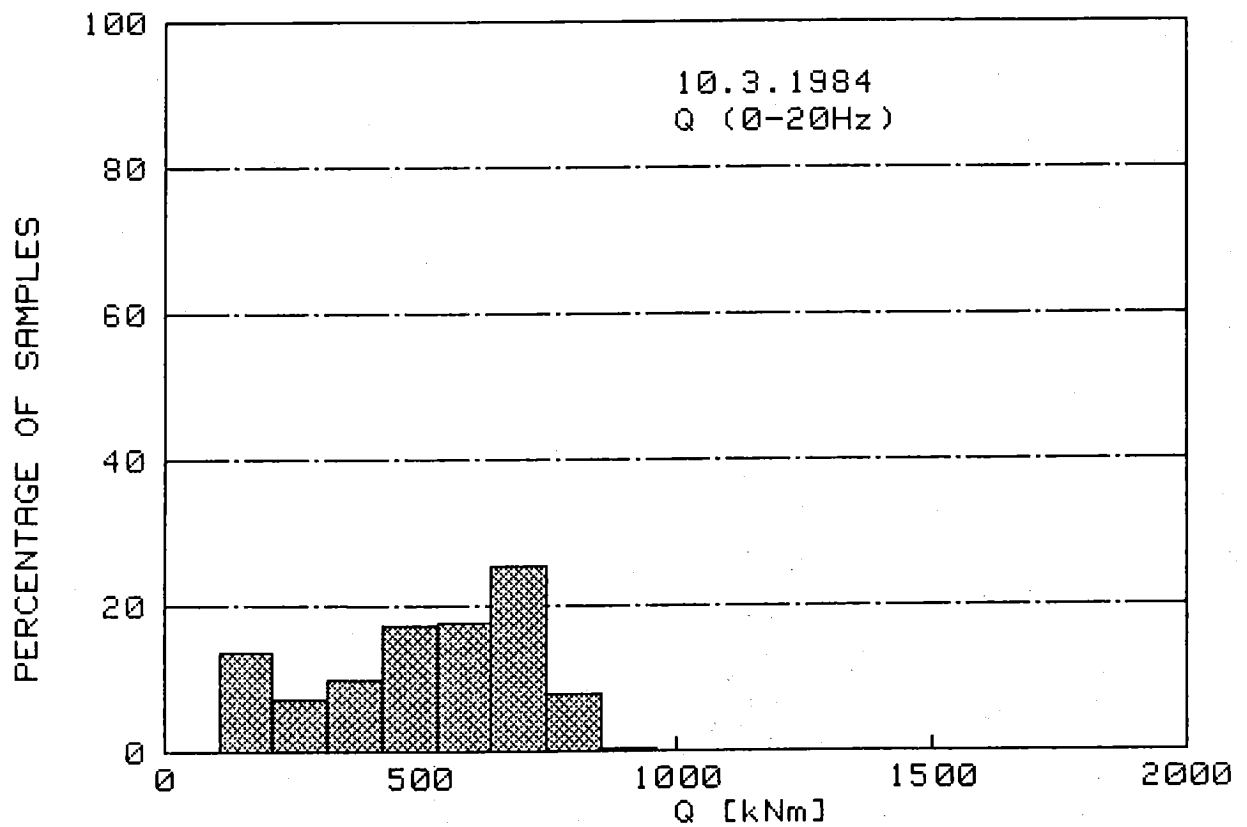
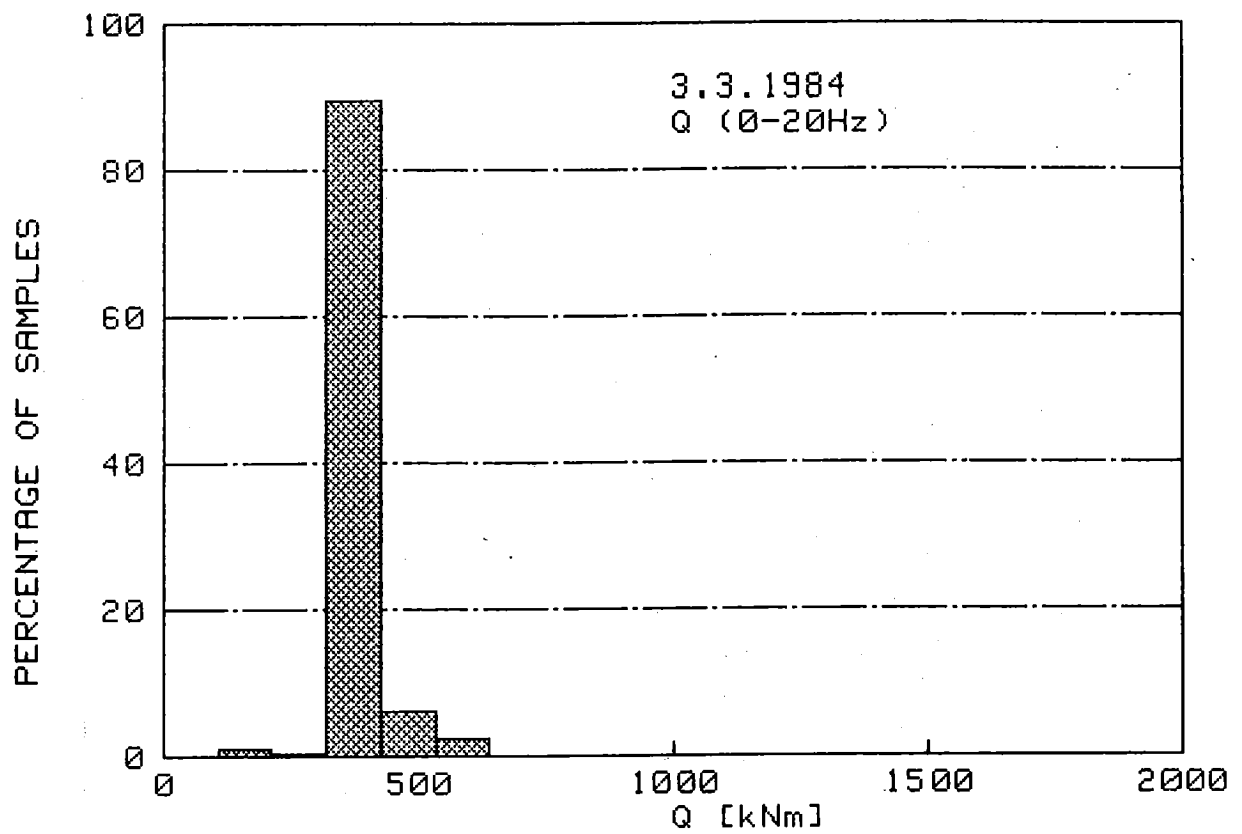


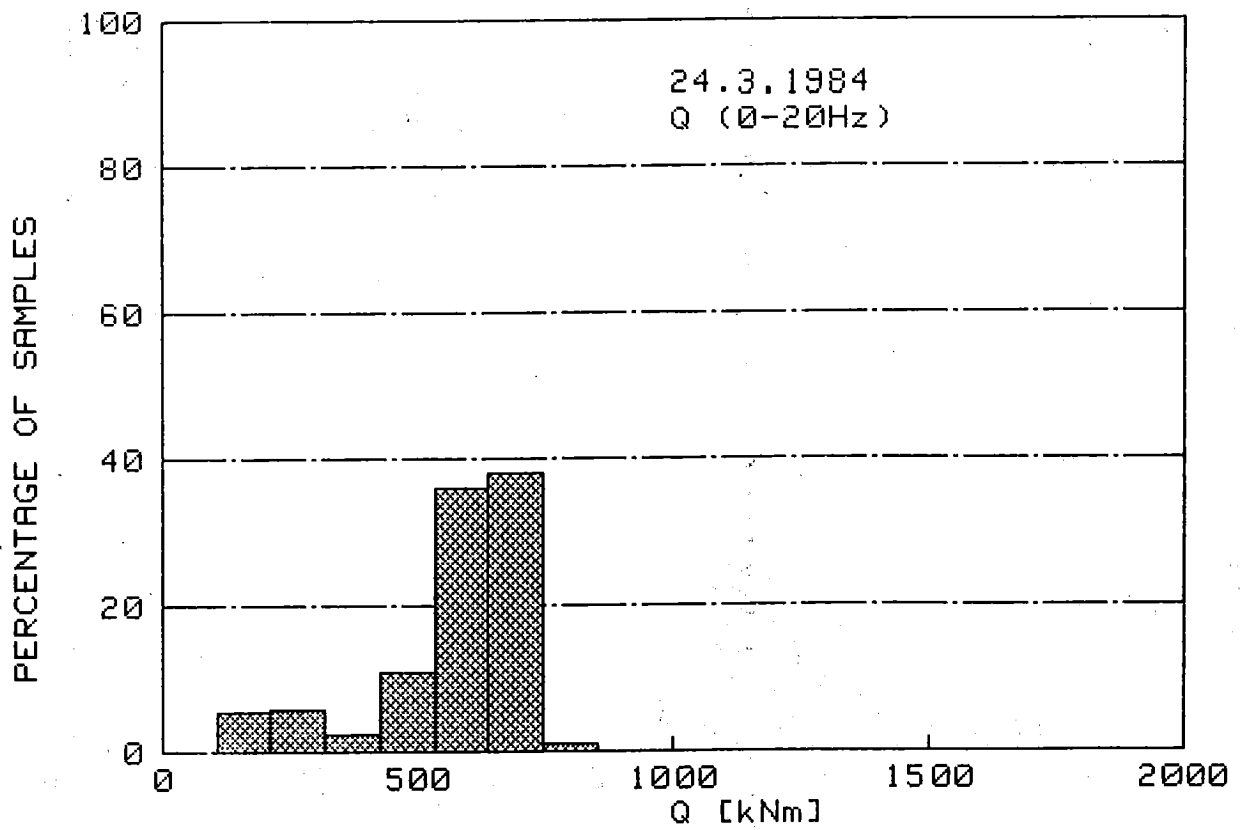
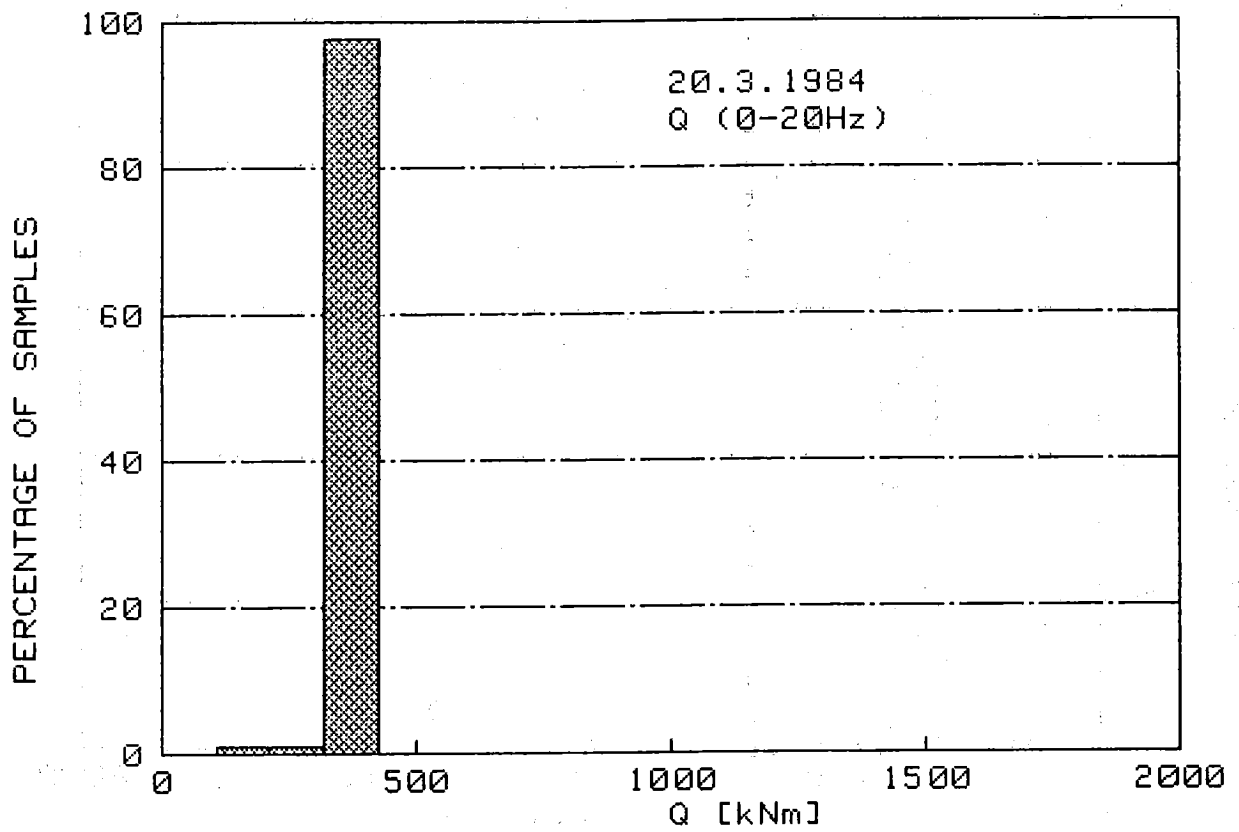


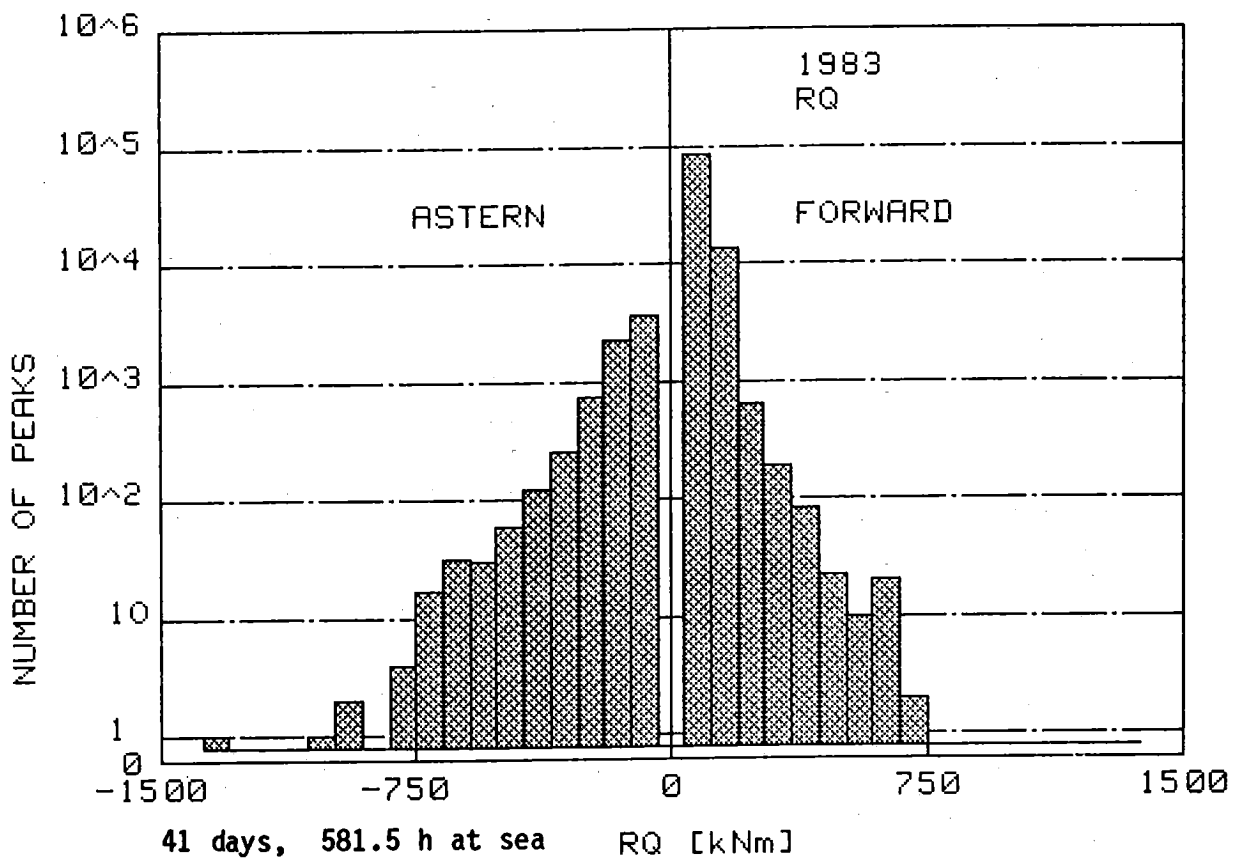
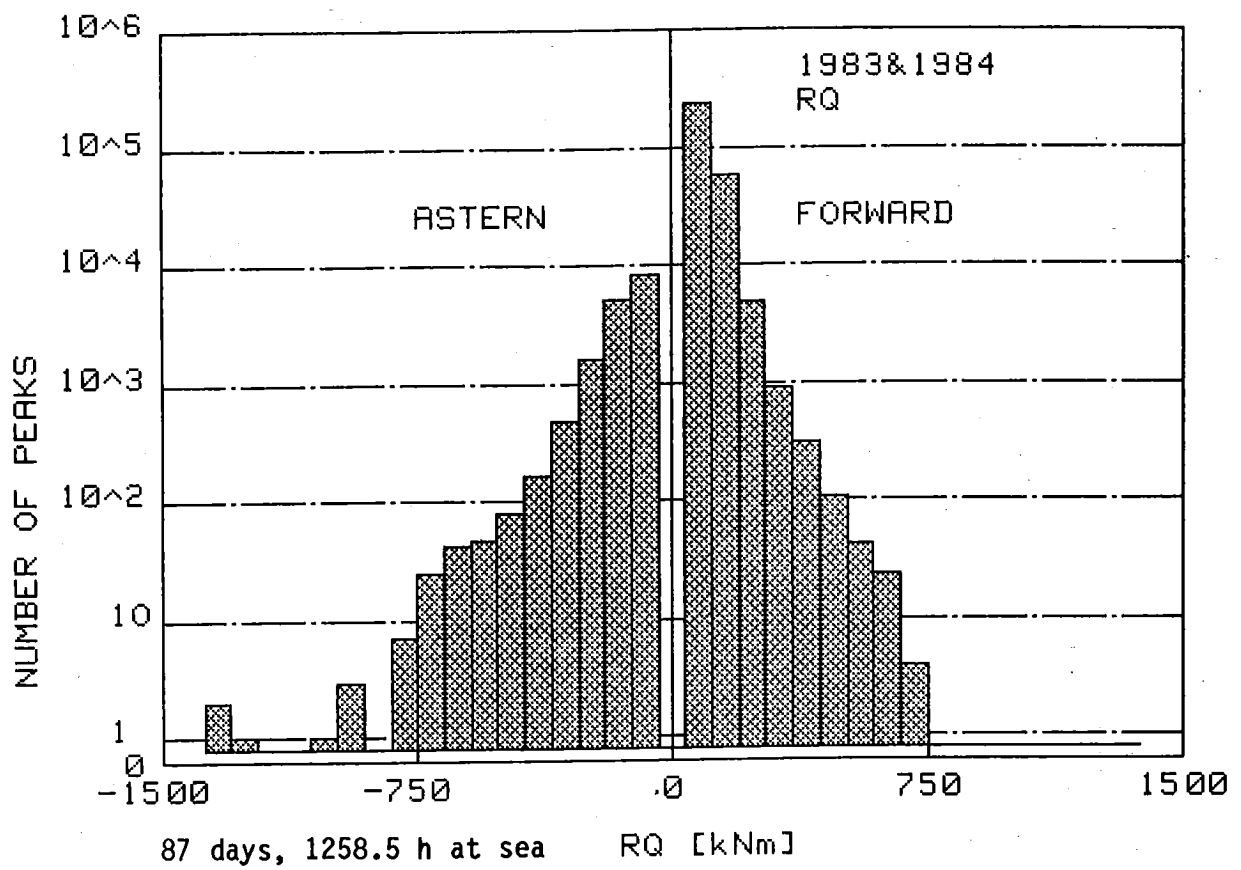


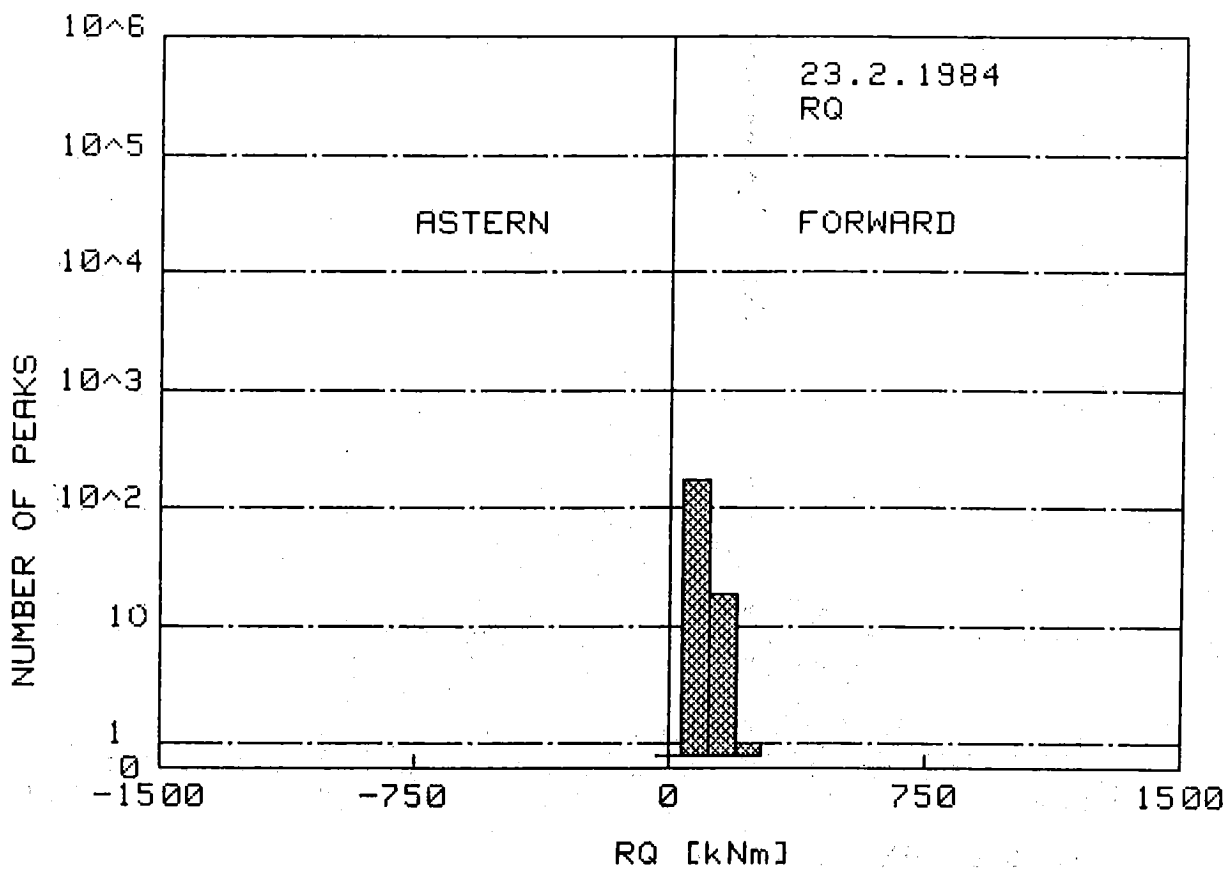
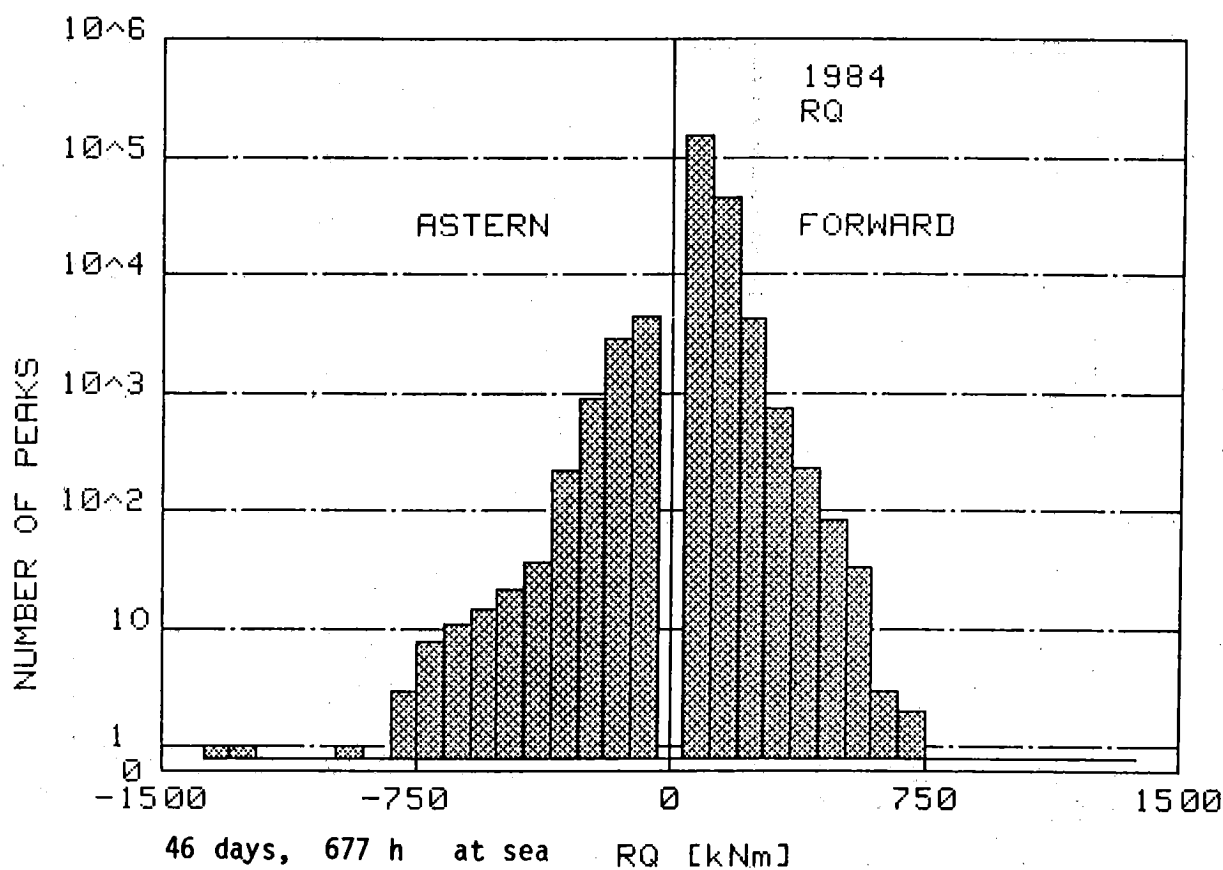


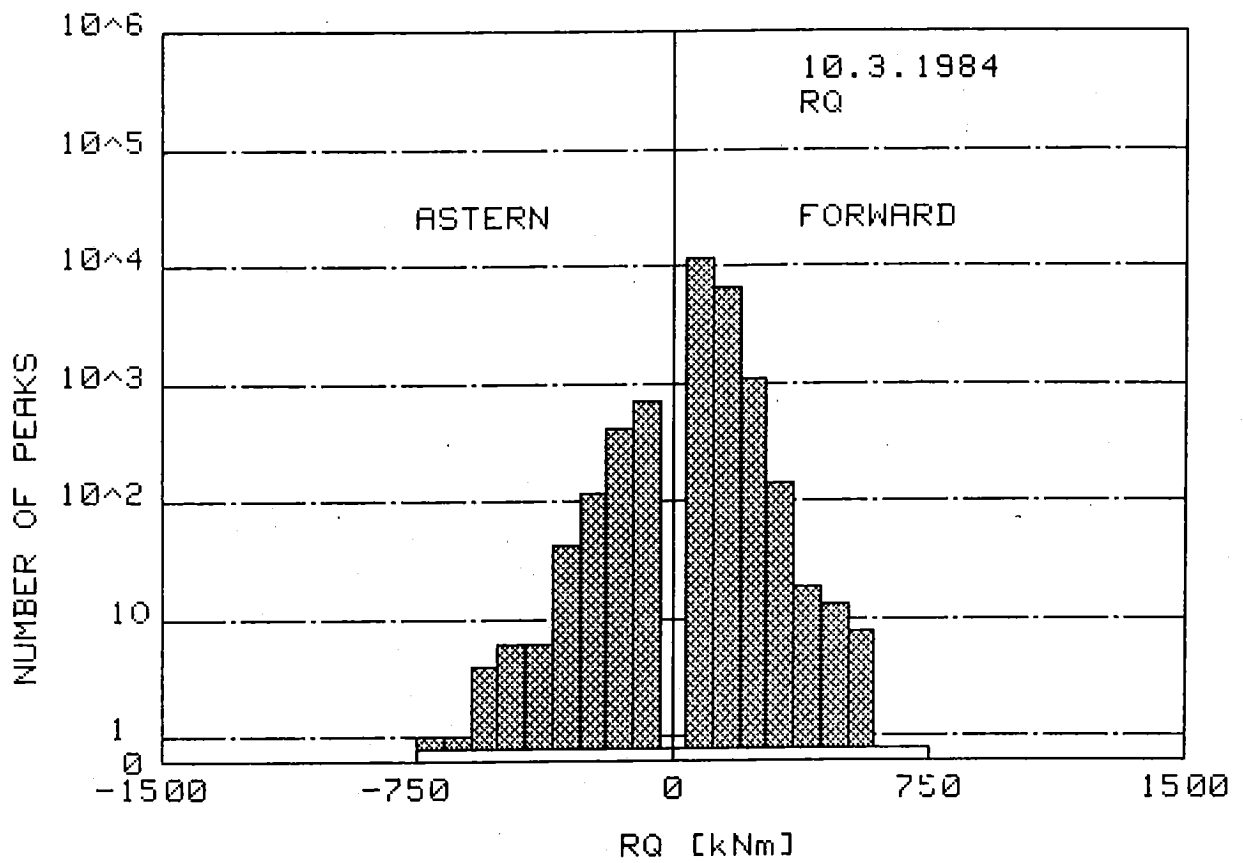
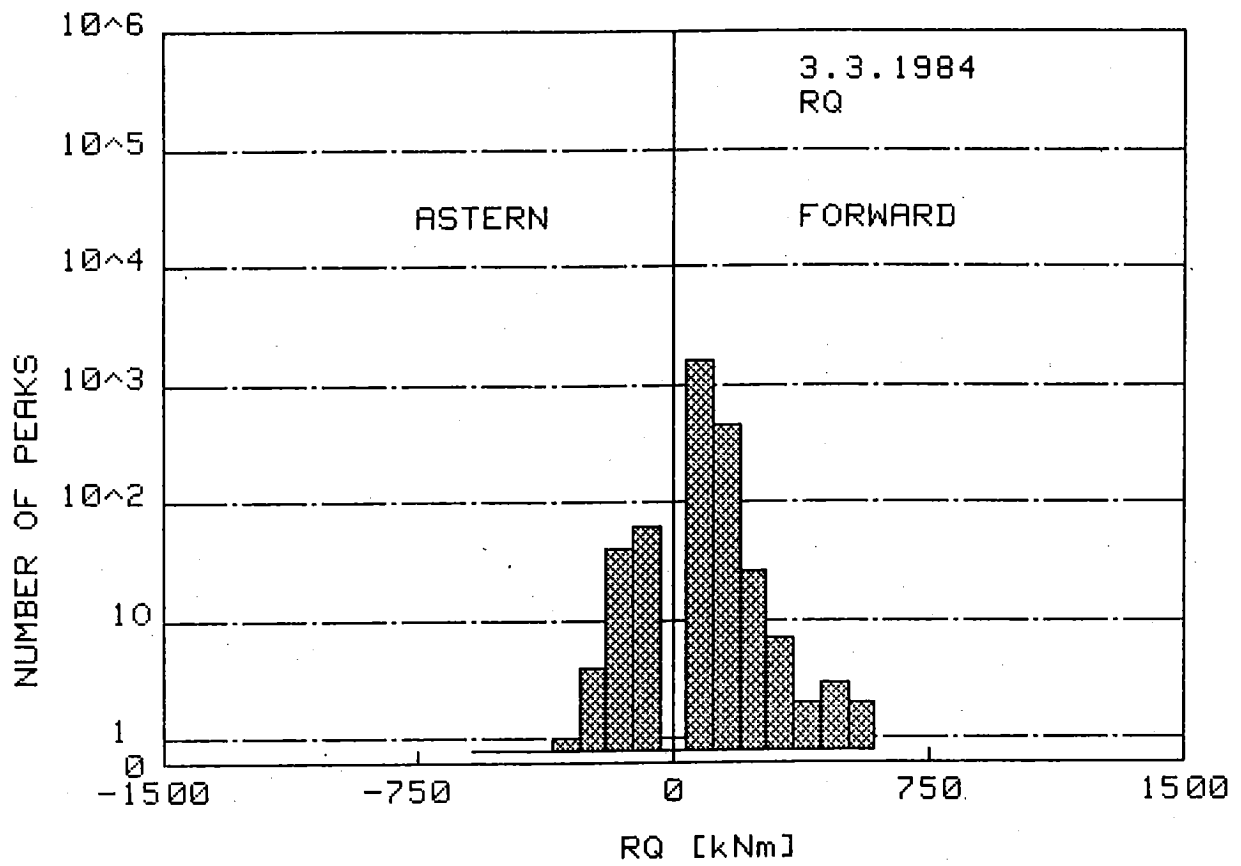


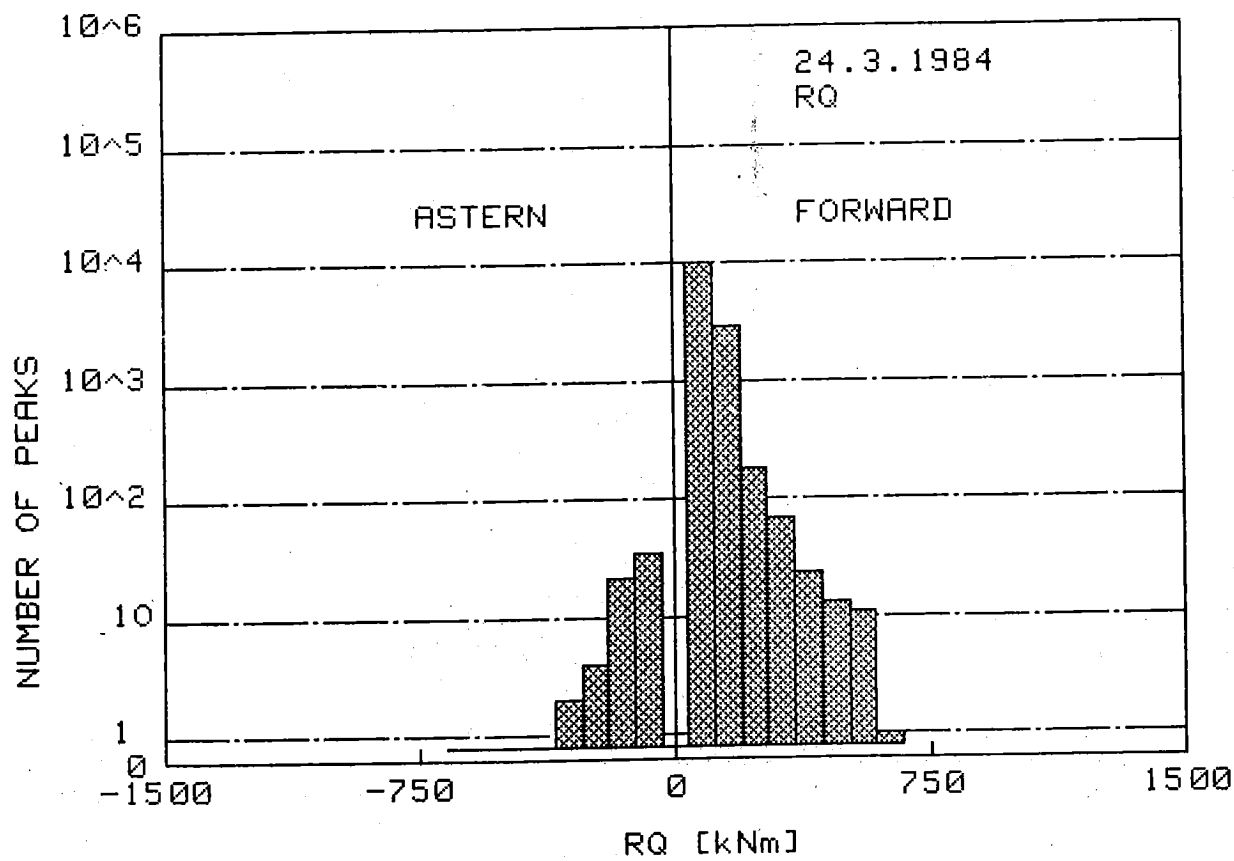
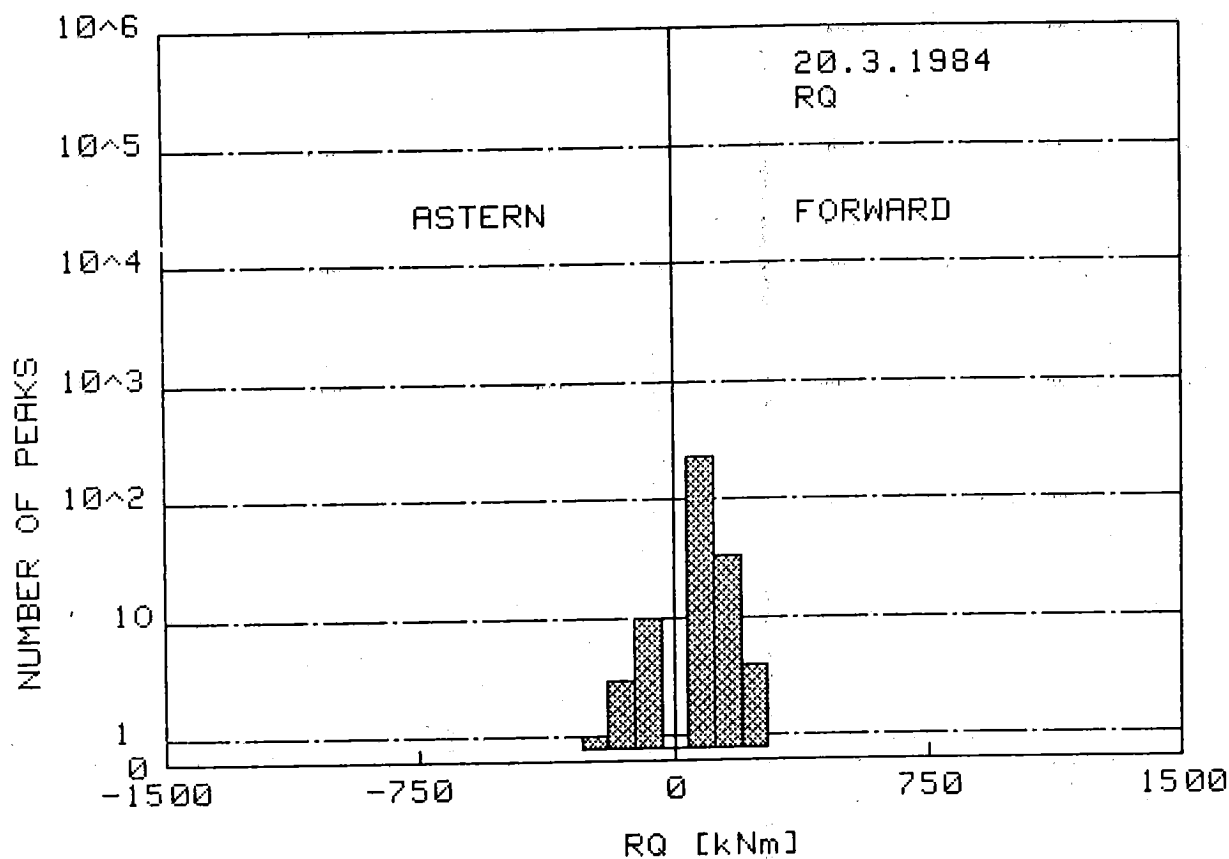












SWEDISH/FINNISH WINTER NAVIGATION

RESEARCH BOARD

R E P O R T S

- | No. | Titel |
|-----|---|
| 1. | HAVSINSKONFERENS. Protokoll (1972). |
| 2. | VINTERSJÖFART I BOTTENHAVET - Erfarenheter av SCA:s distributionssystem - L. Sjöstedt och S. Hammarsten (1972). |
| 3. | ISSKADOR PÅ FARTYG I ÖSTERSJÖN, BOTTENHAVET OCH BOTTENVIKEN. - Statistisk analys av skadefrekvenser - L. Sjöstedt och S. Hammarsten (1973). |
| 4. | PROPELLERPROBLEM. Propellerverkningsgradens beroende av bladutformningen. H. P. Loid (1973). |
| 5. | FARTYGS FRAMDRIVNINGSMOTSTÅND I IS. E. Enkvist (1974). |
| 6. | VINTERSJÖFART MED STORA FARTYG I BOTTENVIKEN - Rapport av en arbetsgrupp (1974). |
| 7. | VINTERSJÖFART I BOTTENVIKEN. Symposium Luleå (1974). |
| 8. | HAVSISUNDERSÖKNINGEN I BOTTENVIKEN VINTERN 1974. A. Omstedt, T. Thompson och I. Udin (1974). |
| 9. | KARTERING AV YTVATTENTEMPERATUREN I VATTNEN RUNT SVERIGE. J-E. Lundqvist, A. Omstedt och I. Udin (1974). |
| 10. | EXPERIMENTS ON REMOTE SENSING OF SEA ICE USING A MICROWAVE RADIOMETER. M. Tiuri, M. Hallikainen and K. Kaski (1974). |
| 11. | BOTTENVIKENS STÅLFYRAR - HÅLLFÄLSTHETSANALYS OCH FÖRBÄTTRINGSFÖRSLAG. M. Määttänen (1974). |
| 12. | FORMATION AND STRUCTURE OF ICE RIDGES IN THE BALTIC. E. Palosuo (1975). |
| 13. | CALCULATION OF ICE DRIFT IN THE BOTHNIAN BAY AND THE QUARK. A. Valli and M. Leppäranta (1975). |

14. A. NARROW BEAM SONAR TO MEASURE THE SUBMARINE PROFILE OF AN ICE RIDGE. E. Palosuo, T. Pousi and M. Luukkala (1976).
15. THE AVERAGE SURFACE TEMPERATURE IN THE AUTUMN AND THE EARLY WINTER ON THE GULF OF BOTHNIA, THE NORTHERN BALTIC SEA AND THE GULF OF FINLAND (1966-1974). H. Grönvall and E. Palosuo (1976).
- 16:1 SEA ICE -75. Programme. Å. Blomquist, C. Pilo and T. Thompson (1975).
- 16:2 SEA ICE -75. Ground truth report. I. Udin (1976).
- 16:3 SEA ICE -75. Ice detection by SLAR. R. H. J. Morra and G. P. de Loor (1976).
- 16:4 SEA ICE -75. Analysis of SLAR data. S. Parashar (1976).
- 16:5 SEA ICE -75. FLAR, ODAR, ship's radar. J. Nilsson, T. Hagman and Y. Nilsson (1976).
- 16:6 SEA ICE -75. IR-scanner results. E. Fagerlund and G. Lundholm (1976).
- 16:7 SEA ICE -75. Radaraltimeter results. S. Axelsson (1976).
- 16:8 SEA ICE -75. Dynamical report. I. Udin and A. Omstedt (1976).
- 16:9 SEA ICE -75. Summary report. Å. Blomquist, C. Pilo and Thompson (1976).
17. THE SHAPE AND SIZE OF ICE RIDGES IN THE BALTIC ACCORDING TO MEASUREMENTS AND CALCULATIONS. Arno Keinonen (1976).
18. A NUMERICAL MODEL FOR FORECASTING THE ICE MOTION IN THE BAY AND SEA OF BOTNIA. I. Udin and A. Ullerstig (1977).
19. CREEP OF FRESH WATER ICE AT HIGH HOMOLOGOUS TEMPERATURES. E. F. M. Leppävuori (1976).
20. ECONOMICS OF WINTER NAVIGATION IN THE NORTHERN PART OF THE GULF OF BOTNIA. B. M. Johansson (1977).
21. MEASUREMENT AND ANALYSIS OF ICE-INDUCED STRESSES IN THE SHELL OF AN ICEBREAKER. P. Varsta (1977).

22. MEASUREMENTS OF PHYSICAL CHARACTERISTICS OF RIDGES ON APRIL 14 AND 15, 1977. A. Keinonen (1977).
23. ICE ACCRETION ON SHIPS WITH SPECIAL EMPHASIS ON BALTIC CONDITIONS. I-E. Lundqvist and I. Udin (1978).
24. PRESENTATION OF SEA ICE RIDGES IN GENERAL AND PHYSICAL CHARACTERISTICS OF BALTIC RIDGES FOR SHIP RESISTANCE CALCULATIONS. A. Keinonen (1978).
25. ON CONDITIONS FOR THE RISE OF SELF-EXCITED ICE-INDUCED AUTONOMOUS OSCILLATIONS IN SLENDER MARINE PILE STRUCTURES. M. Määttänen (1978).
26. SOME RESULTS FROM A JOINT SWEDISH-FINNISH SEA ICE EXPERIMENT, MARCH 1977. A. Omstedt and J. Sohlberg (1978).
27. ON PLASTIC DESIGN OF AN ICE-STRENGTHENED FRAME. P. Varsta, I.V. Droumev and M. Hakala (1978).
28. LONG TERM MEASUREMENTS OF ICE PRESSURE AND ICE-INDUCED STRESSES ON THE ICE BREAKER SISU IN WINTER 1978. J. Vuorio, K. Riska, P. Varsta (1979).
29. ON THE DRIFT AND DEFORMATION OF SEA ICE FIELDS IN THE BOTHNIAN BAY. M. Leppäranta (1980).
30. A SENSITIVITY ANALYSIS OF STEADY FREE FLOATING ICE. A. Omstedt (1980).
31. A STUDY OF THE LARGE SCALE COOLING IN THE BAY OF BOTHNIA. J. Sahlberg and H. Törnevik (1980).
32. STATISTICAL FEATURES OF SEA ICE RIDGING IN THE GULF OF BOTHNIA. M. Leppäranta (1980).
33. PERFORMANCE OF MARINE PROPELLERS IN ICE-CLOGGED CHANNELS. V. Kostilainen (1981)

34. BASIS. A DATABANK FOR BALTIC SEA ICE AND SEA SURFACE TEMPERATURES. I. Udin, J. Sahlberg, J-E Lundqvist, S. Uusitalo, A. Seinä, M. Leppäranta (1981)
35. VERTICAL MIXING AND RESTRATIFICATION IN THE BAY OF BOTHNIA DURING COOLING. A. Omstedt and J. Sahlberg (1982)
36. FORMATION, THICKNESS AND STABILITY OF FAST ICE ALONG THE FINNISH COAST. E. Palosuo, M. Leppäranta and A. Seinä (1982)
37. DYNAMIC LOADS AND RESPONSE OF ICEBREAKER SISU DURING CONTINUOUS ICEBREAKING. J. Matusiak (1982)
38. Undersökning av skrovformens inverkan på propellerns isbelastning samt rännans renhetsgrad genom modellförsök i is. Wadam, Wärtsilä (1982)
39. A forecasting model for water cooling in the Gulf of Bothnia and Lake Vänern. Anders Omstedt (1984).
40. The atmospheric boundary layer over the Bothnian Bay: A review of work on momentum transfer and wind structure. Sylvain Joffre (1984).
41. An investigation of the crystal structure of sea ice in the Bothnian Bay. Anders Omstedt (1985).

